

TG
416
.A241
1997
v. 2

A CONTINUOUS SPAN ALUMINUM GIRDER CONCRETE DECK BRIDGE

FINAL REPORT

PART 2 OF 2:
FATIGUE TESTS OF ALUMINUM GIRDERS

MAY 1997



*Center for Transportation
Research and Education*

IOWA STATE UNIVERSITY

A CONTINUOUS SPAN ALUMINUM GIRDER CONCRETE DECK BRIDGE

FINAL REPORT PART II

FATIGUE TESTS OF ALUMINUM GIRDERS

by

R. E. Abendroth
W. W. Sanders
S. Hansz

TRANSPORT

OCT 22 1998

MISSISSIPPI BRANCH

Bridge Engineering Center
Iowa State University

through the
Center for Transportation Research and Education

with funding by the
Iowa Department of Transportation and the
Federal Highway Administration

May 1997

The opinions, findings and conclusions expressed herein are those of the authors and not necessarily those of the Iowa Department of Transportation, nor the United States Department of Transportation, Federal highway Administration.

TABLE OF CONTENTS

	Page
LIST OF FIGURES	v
LIST OF TABLES	ix
NOMENCLATURE	xi
PREFACE	xiii
ABSTRACT	xv
CHAPTER 1. INTRODUCTION	1
1.1. General Background	1
1.2. Need for Study	5
1.3. Research Program	6
1.4. Literature Review	7
CHAPTER 2. LABORATORY TESTS	19
2.1. Test Specimens	19
2.1.1. Girder removal from bridge	19
2.1.2. Girder material composition	19
2.1.3. Long girder specimens	22
2.1.4. Short girder specimens	28
2.1.5. Welding procedure for the new plates	32
2.1.6. Weld detail categories	33
2.2. Instrumentation and Test Apparatus	35
2.2.1. Test frame and load actuators	35
2.2.2. Instrumentation	38
2.3. Test Methods	44
2.3.1. Test parameters	44
2.3.2. Data acquisition	45
2.3.3. Test procedure	46
2.3.4. Fatigue fractures	47
2.3.5. Fatigue fracture reinforcement	49
CHAPTER 3. EXPERIMENTAL AND ANALYTICAL RESULTS	53
3.1. Stress Ranges and Events	53
3.2. Category E Weld Detail Fractures	58
3.2.1. Original midspan bottom flange splice	58
3.2.2. Original I-shaped diaphragm connections	63

TABLE OF CONTENTS (Cont'd)

	Page
3.2.3. New bottom flange cover plates	68
3.2.4. New horizontal web plate attachments	74
3.3. Weldments Not Tested for Fatigue Strength	79
3.4. Fatigue Fractures at Holes	80
3.5. Section Properties and Bending Strains	81
3.5.1. Neutral axis and moment of inertia	81
3.5.2. Strain ranges	83
3.6. SN-Relationships	83
3.6.1. Specimen fatigue strengths	83
3.6.2. SN-curve comparisons	90
 CHAPTER 4. EPILOGUE	 97
4.1. Summary	97
4.2. Conclusions	103
4.3. Recommendations	104
 REFERENCES	 107
 ACKNOWLEDGMENTS	 111
 APPENDIX A. TEST SPECIMEN FATIGUE LIFE HISTORY	 113
 APPENDIX B. TEST SPECIMEN STRESS HISTORY DATA	 131

LIST OF FIGURES

		Page
Figure 1.1.	Original Clive Road Bridge: (a) West elevation, (b) Cross section looking north	3
Figure 2.1.	Elevation of the long girder specimens	23
Figure 2.2.	Midspan flange splice detail: (a) Partial elevation; (b) Underside of the bottom flange	25
Figure 2.3.	Cross-sectional views of the long girder specimens (all dimensions in inches): (a) Interior girder segment along the abutment side of the splice; (b) Interior girder segment along the pier side of the splice; (c) Exterior girder segment along the abutment side of the splice; (d) Exterior girder segment along the pier side of splice	26
Figure 2.4.	Diaphragm connections on the long girder specimens (all dimensions in inches): (a) Front elevation of an exterior girder; (b) Rear elevation of an exterior girder; (c) Front elevation of an interior girder; (d) Rear elevation of an interior girder	27
Figure 2.5.	Shear connectors: (a) Plan view; (b) Elevation; (c) Side view	29
Figure 2.6.	Shear connector locations: (a) Long exterior girder specimens; (b) Long interior girder specimens; (c) Short exterior girder specimens; (d) Short interior girder specimens	30
Figure 2.7.	Elevation of the short girder specimens	31
Figure 2.8.	Cross-sectional views of the short girder specimens (all dimensions in inches): (a) Exterior girder (b) Interior girder	31
Figure 2.9.	Test frame and apparatus for the long girder specimens	36
Figure 2.10.	Test frame and apparatus for the short girder specimens	37
Figure 2.11.	Strain gauge locations on the long girder specimens	39
Figure 2.12.	Strain gauge locations on the short girder specimens	41
Figure 2.13.	DCDT locations on the long girder specimens	42

LIST OF FIGURES (cont'd)

	Page
Figure 2.14. DCDT locations on the short girder specimens	43
Figure 2.15. Cover-plate repair detail no. 1	50
Figure 2.16. Cover-plate repair detail no. 2	50
Figure 2.17. Web plate repair detail	50
Figure 2.18. Web plate brace for the long girder specimens	51
Figure 2.19. Long girder specimen with a portion of the bottom flange and web plate removed	51
Figure 2.20. Web plate brace at load points	51
Figure 3.1. Strain history near the flange cover plate no. 2 on the long exterior girder specimen no. 1	55
Figure 3.2. Strain readings for strain gauge no. 15 on the long exterior specimen no. 1	57
Figure 3.3. Fatigue fracture at the original bottom flange splice in the long exterior girder specimen no. 1: (a) Partial elevation; (b) Underside of the bottom flange	60
Figure 3.4. Photograph of the fatigue fracture at the original bottom flange splice in the long exterior specimen no. 2	61
Figure 3.5. Photograph of the fracture surface at the original bottom flange splice in the long exterior girder specimen no. 2	62
Figure 3.6. Fatigue fracture at the tip of the bottom flange of the I-shaped diaphragm connection on the long exterior girder specimen no. 1: (a) Front elevation; (b) Back elevation	64
Figure 3.7. Fatigue fracture at the diaphragm connection on the long interior girder specimen no. 1: (a) Front elevation; (b) Back elevation	65
Figure 3.8. Fatigue fracture at the new bottom flange cover plate no. 2 on the short exterior girder specimen no. 1: (a) Partial elevation; (b) Underside of the bottom flange	69

LIST OF FIGURES (cont'd)

	Page
Figure 3.9. Photograph of the fatigue fracture at the new bottom flange cover plate no. 2 on the short exterior girder specimen no. 1	70
Figure 3.10. Photograph of the fracture surface at the new bottom flange cover plate no. 2 on the short exterior girder specimen no. 1	72
Figure 3.11. Fatigue fracture at the new horizontal web plate attachment no. 1 on the long exterior girder specimen no. 2: (a) Front elevation; (b) Back elevation	75
Figure 3.12. Photograph of the fatigue fracture at the new horizontal web plate attachment no. 1 on the front face of the long exterior girder specimen no. 2	77
Figure 3.13. Photograph of the fatigue fracture at the new horizontal web plate attachment no. 1 on the back face of the long exterior girder specimen no. 2	78
Figure 3.14. Nominal SN-curves for Category E details	87
Figure 3.15. Experimental SN-curves for Category E details	88
Figure 3.16. SN-curves for transverse-fillet welds on full-size specimens	91
Figure 3.17. SN-curves for small and full-size Category E weldments (R varies)	93
Figure 3.18. Aluminum Association and ECCS SN-curves for Category E details	95

LIST OF TABLES

	Page
Table 2.1. Chemical composition of aluminum alloy plates and welding wire (% wt.)	21
Table 2.2. Yield and ultimate strengths of 5083-H113 aluminum alloy	22
Table 2.3. Welding parameters	33
Table 3.1. Original midspan bottom flange splice fatigue fractures	63
Table 3.2. Original I-shaped diaphragm connection fatigue fractures	67
Table 3.3. New bottom flange cover-plate fatigue fractures	71
Table 3.4. New horizontal web plate attachment fatigue fractures	76
Table 3.5. Section properties for the test specimens	82
Table 3.6. Theoretical and experimental strain ranges for the test specimens	84
Table 3.7. Category E weldments with fatigue fractures	86
Table 3.8. Category E weldments without fatigue fractures	86
Table A.1. Life history of the long exterior girder specimen no. 1	114
Table A.2. Life history of the long exterior girder specimen no. 2	118
Table A.3. Life history of the long interior girder specimen no. 1	120
Table A.4. Life history of the long interior girder specimen no. 2	123
Table A.5. Life history of the short exterior girder specimen no. 1	124
Table A.6. Life history of the short interior girder specimen no. 1	126
Table A.7. Life history of the short interior girder specimen no. 2	128
Table B.1. Stress-range data for the long exterior girder specimen no. 1	132
Table B.2. Stress-range data for the long exterior girder specimen no. 2	135

LIST OF TABLES (Cont'd)

	Page
Table B.3. Stress-range data for the long interior girder specimen no. 1	137
Table B.4. Stress-range data for the long interior girder specimen no. 2	139
Table B.5. Stress-range data for the short exterior girder specimen no. 1	140
Table B.6. Stress-range data for the short interior girder specimen no. 1	141
Table B.7. Stress-range data for the short interior girder specimen no. 2	143

NOMENCLATURE

- A = stress range (y-axis) intercept at $N = 1$ for the SN-curve, for Category E details by the Aluminum Association: $A = 160$ ksi, and for a F3-Classification by ECCS: $A = 574.9$ MPa (83.4 ksi);
- C_1, C_2 = constants associated with the linear-regression line that is soecufued by the AASHTO-LRFD aluminum fatigue design provisions, for Category E details: $C_1 = 36.0 \times 10^8$ and $C_2 = 0.237$;
- E = modulus of elasticity;
- F_u = ultimate tensile stress;
- F_y = yield stress;
- I_{ex} = experimental moment of inertia with respect to the neutral axis (x-axis) of the girder specimen;
- I_{tx} = theoretical moment of inertia with respect to the neutral axis (x-axis) of the girder specimen;
- M = calculated girder bending moment at a strain gauge position;
- m = absolute value of the slope of the linear-regression line for the SN-relationship, for Category E details by the Aluminum Association: $m = 3.45$ ksi, and for a F3-Classification by ECCS: $m = 4.32$ MPa (also 4.32 ksi);
- N = number of load cycles;
- P_{max} = maximum cyclic load;
- P_{min} = minimum cyclic load;
- R = stress ratio;
- SR = stress range;
- s_{ra} = induced, service level, nominal-stress range at a weldment;
- s_{rd} = allowable, fatigue strength, stress range;
- y_{en} = experimental neutral-axis location, measured from the underside of the bottom flange of the girder;

NOMENCLATURE (Cont'd)

- y_{tn} = theoretical neutral-axis location, measured from the underside of the bottom flange of the girder;
- y_1, y_2 = heights to strain gauges;
- $(\Delta F)_n$ = nominal-stress range fatigue resistance;
- $(\Delta F)_{th}$ = constant-amplitude fatigue threshold specified by the AASHTO-LRFD aluminum fatigue design provisions, for Category E details: $(\Delta F)_{th} = 2.0$ ksi at 10-million load cycles;
- ϵ_1, ϵ_2 = experimental bending strain at the strain gauges that were at heights y_1 and y_2 , respectively, from the bottom of the girder;
- σ_m = mean flexural stress;
- σ_{max} = maximum flexural stress; and
- σ_{min} = minimum flexural stress.

PREFACE

The final report entitled "A Continuous Span Aluminum Girder Concrete Deck Bridge" is published in two parts: Part I - "Field Test Performance and Evaluation" and Part II - "Fatigue Tests of Aluminum Girders". Part I of the final report addresses the field testing and analysis of those results to establish the behavior of the original Clive Road Bridge that carried highway traffic over Interstate 80 (I-80) in the northwest region of Des Moines, Iowa. The bridge was load tested in 1959, shortly after its construction and in 1993, just prior to its demolition. Part I of the final report presents some of the results from both field tests, finite element predictions of the behavior of the aluminum bridge girders, and load distribution studies. Part II of the final report addresses the laboratory fatigue testing and analysis of those results to establish the behavior of aluminum girders that were removed from the original Clive Road Bridge. The fatigue strength of the weld details that existed in the original bridge girders and the weld details that are common in welded girders and that were added to the aluminum girders are presented in this part of the final report.

ABSTRACT

Aluminum alloys have been used to a limited extent in bridge construction. Only nine aluminum girder bridges have been built in the continental United States. Recently however, renewed interest in using aluminum alloys for bridges has occurred. Aluminum has a low weight to strength ratio and has a natural resistance to corrosion. To improve current specification provisions for structural application of aluminum, research on the behavior of full-size aluminum members needs to be conducted.

In 1957, the Iowa State Highway Commission, with financial assistance from the aluminum industry, constructed a 220-ft long, four-span continuous, aluminum girder bridge to carry traffic on Clive Road (86th Street) over Interstate 80 near Des Moines, Iowa. The bridge had four, welded I-shape girders that were fabricated in pairs with welded diaphragms between an exterior and an interior girder. The interior diaphragms between the girder pairs were bolted to girder brackets. A composite, reinforced concrete deck served as the roadway surface. The bridge, which had performed successfully for about 35 years of service, was removed in the fall of 1993 to make way for an interchange at the same location.

Prior to the bridge demolition, load tests were conducted to monitor girder and diaphragm bending strains and deflections in the northern end span. Fatigue testing of the aluminum girders that were removed from the end spans were conducted by applying constant-amplitude, cyclic loads. These tests established the fatigue strength of an existing, welded, flange-splice detail and added, welded, flange-cover plates and horizontal web plate attachment details.

This part of the final report focuses on the fatigue tests of the aluminum girder sections that were removed from the bridge and on the analysis of the experimental data to establish the fatigue strength of full-size specimens. Seventeen fatigue fractures that were classified as Category E weld details developed in the seven girder test specimens. Linear-regression analyses of the fatigue test results established both nominal and experimental stress-range versus load cycle relationships (SN-curves) for the fatigue strength of fillet-welded connections. The nominal strength SN-curve obtained by this research essentially matched the SN-curve for Category E aluminum weldments given in the AASHTO-LRFD specifications. All of the Category E fatigue fractures that developed in the girder test specimens satisfied the allowable SN-relationship specified by the fatigue provisions of the Aluminum Association. The lower-bound strength line that was set at two standard deviations below the least-squares regression line through the fatigue fracture data points related well with the Aluminum Association SN-curve. The results from the experimental tests of this research have provided additional information regarding behavioral characteristics of full-size, aluminum members and have confirmed that aluminum has the strength properties needed for highway bridge girders.

CHAPTER 1. INTRODUCTION

1.1. General Background

Aluminum has proven to be an economical choice in structural applications beyond those in the aerospace industry. The use of aluminum in the building and construction industry has grown to possess an annual 15-billion dollar market share [21]. The applications in which aluminum has been used are quite diverse. Curtain walls and skylight framing, roof sheeting, storage vessels, and long span domed roofs have been commonly made from aluminum alloys. In the transportation structures sector, aluminum has been used for signs, sign structures, light poles, guardrails, bridge girders, and bridge decks.

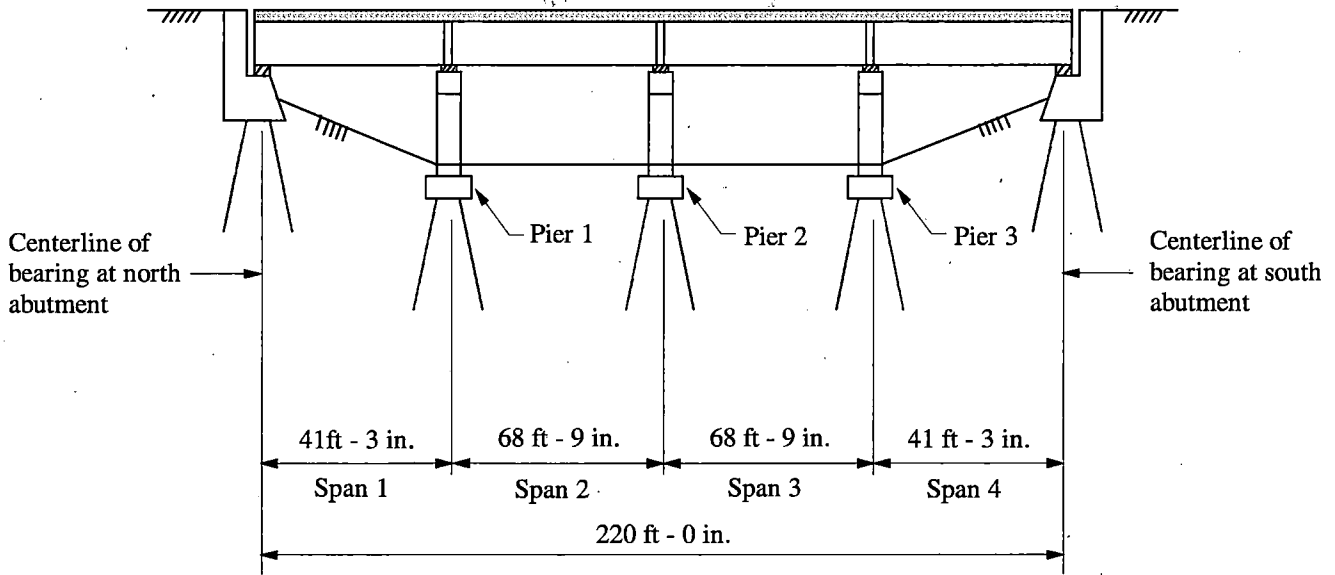
Since connections between aluminum members can be bolted, welded, and riveted, the breadth of applications for this metal are comparable to those for structural steel [34]. Aluminum alloys possess a natural resistance to corrosion and have yield strengths comparable to commonly used carbon steels as A36 or high strength steels A572 Grades 42 and 50. One of the most significant advantages of aluminum compared to steel is its strength-to-weight ratio. Aluminum is particularly attractive where dead load is a primary concern, since aluminum weighs about one-third the weight of an equivalent volume of structural steel. Aluminum is available in cast, forged, rolled, extruded, and sheet forms; therefore, aluminum is as commercially versatile as structural steel. Design specifications for aluminum have been developed to provide structural engineers with design requirements for this material. Due to the ease of erecting aluminum structures and the trend of decreasing costs in the production of aluminum [21], the utilization of aluminum in structural applications will continue to develop.

As of 1996, only nine bridges that used aluminum for the major components were built [3] in the United States of America (USA). One of these bridges [15,16,39,56] was built in 1957 to

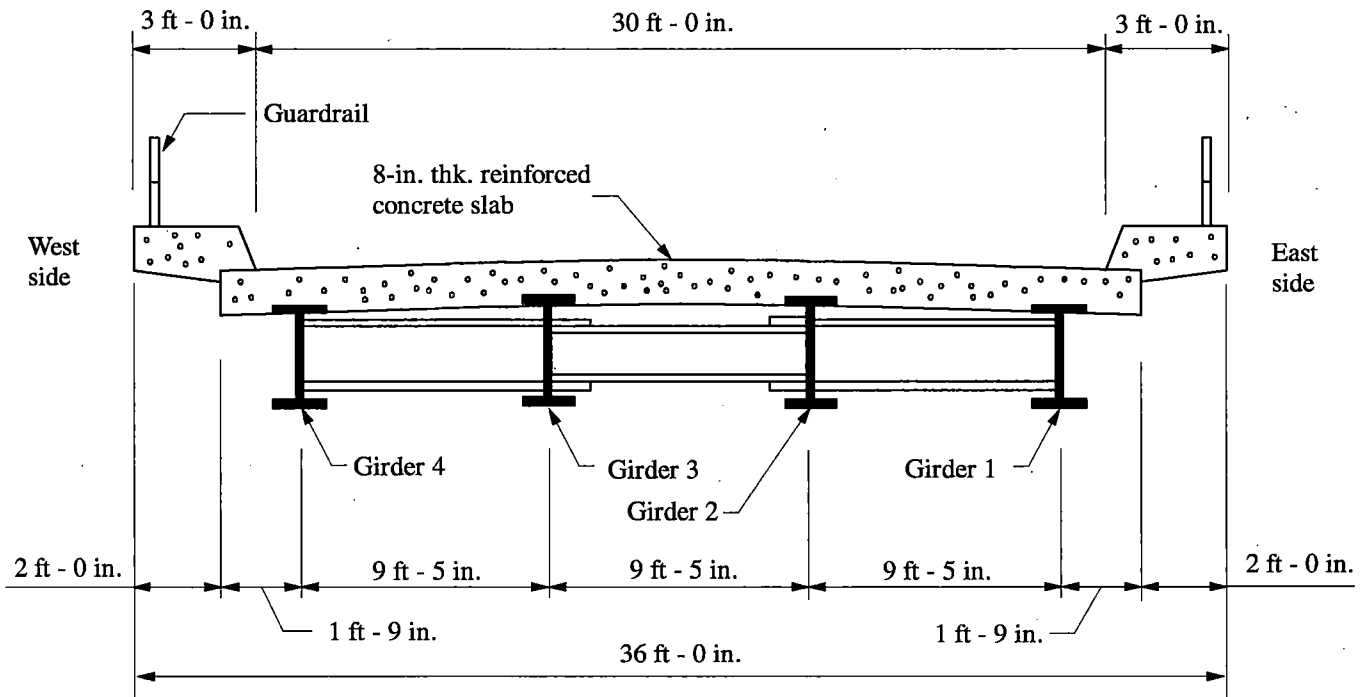
carry Clive Road (86th Street) traffic over Interstate 80 (I-80). The original Clive Road Bridge was located in Polk County near the northwest side of Des Moines, Iowa. This bridge, which was constructed with the partial financial support from the aluminum industry during a period of time when structural steel was not readily available, was the only welded, I-shaped, aluminum girder bridge ever built in the USA. The bridge had four continuous spans, an overall length of 220 ft, and a width of 36 ft. Figure 1.1 shows an elevation and a cross section of the bridge. The roadway width was equal to 30 ft and a 3-ft wide curb existed along both the east and west sides of the bridge. Four aluminum girders were spaced at 9.50 ft on center across spans of 41.25, 68.75, 68.75, and 41.25 ft. The girders acted compositely with an 8-in. thick, reinforced concrete slab through the use of shear connectors.

The depth of the interior girders was approximately 38 in. and that of the exterior girders was about 36 in. The flange widths ranged from 12 to 18 in. A total of six different girder cross sections (three for each interior girder and three for each exterior girder) were used along the length of the bridge. For each line of girders, one field-bolted and five shop-welded connections were used to splice the girders at the points where the cross section of a girder changed.

The continuous aluminum girders were connected to each other by welded, I-shaped, aluminum diaphragms that were uniformly spaced at 13.75 ft along the length of the bridge. The plate material for the diaphragms was the same as that for the girders. Six sizes of diaphragms were used in the bridge. The diaphragm connections between an exterior girder and an interior girder were shop welded, while those between the interior girders were field bolted. This type of construction permitted the shop fabrication and field erection of the girders in pairs. The structural members were fabricated from 5083-H113 aluminum plates. This alloy series is a non-heat-



(a)



(b)

Figure 1.1. Original Clive Road Bridge: West elevation; (b) Cross section looking north

treatable, structural aluminum alloy that has suitable properties for welding. Over 76,000 lb of aluminum were required for the bridge superstructure and expansion joints at the ends of the bridge.

The bridge had performed successfully during its 35 years of service, as evidenced by a review of the inspection reports that were periodically written throughout the life of the bridge. These reports revealed that the girders in the second and third spans had been struck in 1978 by overheight vehicles. The major notches that occurred in the bottom flanges of the impacted girders had been ground smooth. Also, the inspection reports noted that cracks had developed in four of the welded joints between the intermediate diaphragms and the girder webs in span 3 (the third span south of the north abutment). Some of these cracks may have been caused by the major vehicle impacts and/or induced by fatigue loading. Even though many years of useful life remained for this bridge, it was removed during September and October of 1993 as part of an interchange and roadway widening construction project.

Just prior to the start of the bridge demolition, static-load tests of the bridge were conducted by researchers at Iowa State University (ISU) [2,42]. The strain results measured during the 1993 field tests, predicted responses obtained from a finite element model of the bridge, and load distribution behavior for this bridge were presented in Part 1 of the final report [1] for this research, in the thesis by Mahadevan [33], and in a paper by Abendroth, Sanders, and Mahadevan [2]. During the demolition of the bridge, the girder end spans were retained to examine the fatigue behavior of these aluminum girder sections when they were subjected to constant-amplitude cyclic loads. The bending stress versus load-cycle responses for the girders and discussions of the induced fatigue fractures are presented in this part (Part 2) of the final report for this research. A historical discussion that addressed the construction and the 1959 static and dynamic-load field testing of the

bridge is given in Ref. 2 and 30. A discussion of the potential redesign of the bridge based on current European codes is contained in Ref. 31.

1.2. Need for Study

Design specifications for aluminum girder highway bridges [11] have been available for a number of years. The recent American Association of State Highway and Transportation Officials (AASHTO) Load and Resistance Factor Design (LRFD) Bridge Specifications [12] includes a section for the design of aluminum bridges. However, in many instances, the design criteria for aluminum girder bridges have been taken directly from or modified from those for steel girder bridges [10,12]. Specific studies are needed to develop distinct criteria for aluminum girder bridges or to confirm the applicability of the steel girder criteria to aluminum girder bridges.

Various fatigue strength studies of aluminum welds have accumulated vast amounts of data that have been used to produce design criterion. However, the majority of this data has been obtained from testing small-size specimens. The relevance of data obtained from small-size specimens compared to that obtained from full-size specimens has been questioned [41]. Fatigue testing of full-size commonly used aluminum weldments is essential in order to justify and improve the specification criteria for fatigue design [43]. Only a limited number of large, welded aluminum members have become available for laboratory fatigue testing.

Several years ago, the Iowa Department of Transportation (Iowa DOT) and Polk County engineers determined that the Clive Road Bridge needed to be redesigned as a full-interchange. The removal of the original bridge provided a unique opportunity to obtain experimental data for both the static-load behavior of an aluminum girder bridge and the fatigue strength behavior of full-size aluminum components. One of the objectives of the fatigue study was to affirm the validity of current fatigue design criteria for Category E weld details for aluminum girder elements. Another

objective was to increase the state of knowledge on the fatigue behavior of full-size aluminum specimens. This part of the final report is limited to the discussion of the fatigue testing of the aluminum girder segments. As noted earlier, details concerning the field testing and finite-element modeling of the original aluminum girder bridge are compiled in Part 1 of the Final Report [1], and in the works of Mahadevan [33], and Abendroth, Sanders, and Mahadevan [2].

1.3. Research Program

The overall research program consists of four parts: inspection; static-load, field tests and analyses of the original bridge; and laboratory fatigue tests of aluminum girder sections. The inspection of the bridge superstructure, particularly the aluminum girders, was done by a team consisting of ISU staff, Lehigh University staff, and personnel from the Iowa DOT.

The 1993 field tests consisted of loading the bridge with an overloaded truck that was driven to various points on the bridge. The load points complied with the critical AASHTO Bridge Design Specifications [10] loading positions. Instrumentation consisted of electrical-resistance strain gauges and direct-current displacement transducers. The test results provided data on load distribution and on general static-load behavior.

Laboratory fatigue tests were conducted on the girders that were removed from the end spans of the original bridge. The girder sections were modified by welding plate attachments that reflect the type of connections that are used in present construction techniques for which additional fatigue data is needed. The beams were also tested to establish their remaining fatigue life. Other objectives of the research program were to provide information on the effects of 35 years of service of an aluminum girder bridge and to establish load-distribution factors for the composite concrete deck-aluminum girder bridge.

1.4. Literature Review

A short description of the aluminum bridges that were constructed in the USA and Canada and the literature review associated with the field testing of the Clive Road Bridge is given in the first part of this final report [1]. The literature review presented here will address only fatigue strength studies of aluminum.

In 1947, Hartmann, Holt, and Zambocky [29] investigated the fatigue behavior of welded joints for aluminum alloys. These researchers used several welding techniques. They concluded that the inert-gas welding procedure produced the best fatigue strength. Prior to this time, the aerospace industry had performed fatigue tests [40] of high-strength aluminum alloy plates that were connected by rivets. By 1960, inert-gas welding methods essentially replaced the use of metal fusing techniques such as oxy-acetylene welding, metal-arc welding, and brazing in structural aluminum applications [51]. Two inert-gas methods are commonly used: Gas-Metal-Arc Welding (GMAW, formerly known as Inert-Gas-Metal-Arc Welding (MIG)) and Gas-Tungsten-Arc Welding (GTAW, formerly known as Inert-Gas-Tungsten-Arc Welding (TIG)) [38]. GMAW is generally more popular than GTAW, since the former can be performed at a high rate of speed and at any weld position. However, GTAW is reputed [5,51] to provide a superior weld bead and to produce a wider heat-affected-zone due to its slower welding rate than GMAW. The best inert-gas welding results are produced by a Helium and Argon gas mixture ratio of 4 to 1, respectively [9].

When welding is used for connections, only certain alloys are recommended for the aluminum members. The heat generated during the welding process reduces the strength of aluminum alloys that attained their strength by heat treatment or cold working [21]. Heat-treatable alloys [47] are classified as the 2000, 6000, and 7000 aluminum alloy series, for which the main alloying elements are copper, magnesium and silicon, and zinc, respectively. The ultimate strength,

yield strength, and ductility characteristics for these alloys can be reduced by as much as 60% in the vicinity of the welded connections [38]. Reheat treatment after welding can be performed to restore the yield and ultimate strengths; however, a reduction in the ductility of the metal will occur. Such characteristics make heat-treatable, aluminum alloys less suitable for use in structures that will be subjected to dynamic loading conditions.

Non-heat-treatable, weldable, aluminum alloys [47] are exclusive to the 3000 and 5000 aluminum alloy series as designated by the Aluminum Association [4]. The 5000-series, aluminum alloys are used for structural applications, since their tensile strengths and ductility are higher than that for the 3000-series, aluminum alloys. Magnesium is the primary alloying element for the 5000 series. Moderate to high-strength alloys are produced by controlling the magnesium content. Aluminum alloys with a 4-6% magnesium content have yield strengths comparable to A36 steel. A significant amount of research has been conducted with welded, 5000-series, aluminum alloys for shipbuilding and storage vessel applications [38,41]. The majority of the fatigue tests of aluminum specimens have been performed on the 5000 series (or foreign equivalent) alloys [43].

Most welded-aluminum, fatigue-test programs have involved axial stress testing. The investigations by Hartmann, Holt, and Zambocky [29] utilized a mechanically driven testing machine. Their tests were performed at 3.5 cycles per second (hz) with maximum stresses as great as 30 ksi. Gunn and McLester [22] performed constant-amplitude, axial-stress tests on various specimens containing fillet welds at rates as great as 216 hz. This fast testing rate was possible due to the small size of their specimens and the low magnitudes of load.

Full-sized structures and structural components are usually tested by bending methods using servo-controlled, electro-hydraulic, direct-stress cycling machines [34]. Sutherland [52] performed bending tests of various geometries of butt welds on extruded, 7-in. deep by 4-in. wide, I-beams that

were between 4 and 10 ft in length. Gurney [25] investigated the fatigue strength of vertical web stiffeners in regions of combined moment and shear and in regions of pure moment, using 11-in. deep by 5-ft long beams. Gurney concluded that stiffeners in combined stress regions failed at a lower principal-stress range than stiffeners in constant-moment regions.

Fatigue testing is usually performed by constant-amplitude, stress cycling. The loading cycle is defined by the minimum and maximum stresses in the cycle (σ_{\min} and σ_{\max} , respectively). The mean stress, σ_m , stress range, SR, and stress ratio, R, are defined as:

$$\sigma_m = (\sigma_{\min} + \sigma_{\max})/2 \quad (1.1)$$

$$SR = (\sigma_{\max} - \sigma_{\min}) \quad (1.2)$$

$$R = (\sigma_{\min}/\sigma_{\max}) \quad (1.3)$$

Laboratory data gathered through testing similar specimens are usually reported in terms of a graph of the nominal-stress range versus the number of load cycles, N, that produce a fatigue fracture [43]. These plots of the fatigue data are referred to as SN-curves. A nominal stress is considered to be a stress that is calculated by applying engineering mechanics principles. Nominal-stress values are normally used because the actual stress at the point of fracture is difficult to determine to an acceptable degree of accuracy.

SN-curves are normally plotted using logarithmic scales for both axes, since a linear-regression analysis of the fatigue data can be presented by straight-line relationships [13]. The basic linear-regression line that is established from a statistical analysis of the fatigue data represents a 50% survival line. Lines that are drawn at two standard deviations above and below the basic regression line represents the 5% and 95% survival lines, respectively. Guidelines and recommendations for the statistical analysis of linearized, stress-life, fatigue data can be found in ASTM E739-80 [13].

SN-curves are usually characterized by either two or three behavioral regions [34]. The first region contains fatigue failures that occur at less than 10,000 load cycles. These fatigue strengths usually coincide with the static-load strength of the member [51]. When σ_{\max} is decreased from the static-strength level and when the SR versus N relationship is plotted on a log-log scale, the number of load cycles needed to induce a fatigue failure essentially increases linearly. This linear relationship is associated with the second region of fatigue behavior. For constant-amplitude cyclic loading, a third region exists. This region is characterized by a threshold stress or endurance limit (constant-stress range level). For this region of behavior, fatigue failure will not occur if SR does not exceed the endurance limit, regardless of the number of load applications. The number of load cycles that corresponds to the endurance limit is a function of the geometry of the detail and is always in excess of one-million load cycles.

For variable-amplitude, cyclic loading an endurance limit is assumed not to exist. Instead, either a "knee point" may occur in the SR versus N relationship that signifies the start of a third region of fatigue behavior, where the slope of the SN-curve is flatter than that in the second region, or a "knee point" might not occur, and the second region of SR versus N relationship is assumed to extend indefinitely. For this latter model of variable-amplitude loading, a third region of fatigue behavior does not exist. More variable-amplitude fatigue research, involving very large numbers of load cycles, is needed to resolve which model of fatigue behavior is correct. During variable-amplitude loading, researchers [21,34] suspect that fatigue damage induced by the largest stress ranges permits the low-stress cycles to also cause fatigue damage. For a particular detail category, the initial portion of the SN-curves for variable-amplitude load cases is the same as that for constant-amplitude load cases. American aluminum-alloy fatigue provisions [8,12] for variable-amplitude loading specify SN-curves with a continuation of the constant-amplitude slope that occurs in region

two of the SR versus N relationship beyond the constant-amplitude, threshold stress, while a European standard [20] specifies a reduced slope beyond the constant-amplitude, threshold stress.

Extensive research has been performed on the fatigue behavior of aluminum weldments. In the past 50 years, research programs have examined the fatigue strength of various joint configurations and the influence of weld-related parameters, such as post-weld treatments, magnitude of residual stresses, and size of components. Motivation for this research concerns the development of design criteria for aluminum alloys comparable to those for structural steel. The earliest research programs investigating the fatigue behavior of aluminum weldments established the weld geometry as the prime factor influencing the fatigue life of a specimen. Hartmann, Holt, and Zambocky [29] examined the fatigue lives of 15 weld configurations representing typical butt and fillet-welded details in 3/8-in. thick plates. The researchers concluded that a butt weld with the reinforcement ground flush with the connected plates had the greatest fatigue strength. This conclusion was confirmed by the works of Hartmann, Holt and Eaton [28], and Mindlin [35]. The geometrical effects of butt welds in steel were further examined by Sanders, Derecho, and Munse [44]. They determined that the presence of weld reinforcement increases the static strength of a member; however, the reinforcement could reduce the fatigue strength by as much as 50%.

Gunn and McLester [22] tested specimens with joints characterized by strong configurations (such as longitudinal, butt-welded plates with the reinforcement removed) and weak configurations (such as single, fillet-welded tee-joints) of various alloys and treatments in order to obtain data for the development of aluminum, fatigue-design rules. They determined that fatigue fractures occurring beyond the application of 10,000 load cycles for an aluminum weld detail is independent of the specimen alloy. Person [38] investigated the relative strengths of butt and fillet welds involving six configurations. He tested butt, lap, and tee-welded joints for 5052 and 6061 aluminum

alloy plates that were 3/16 to 3/8-in. thick. Person concluded that the weakest joints tested were tee joints that had a single-fillet weld. These joints had strengths equal to about 25% of the strength of double-fillet-welded tee joints and about 15% of the strength of full-penetration, groove-welded, tee joints with the reinforcement removed.

Tomlinson and Wood [55] discussed the metallurgical, geometrical, and physical factors that affect the fatigue strength of welded joints. After reviewing aluminum fatigue data, they concluded that a symmetrical joint configuration is important to improve the fatigue strength of a welded connection; fatigue failures in specimens with sound butt, lap, or fillet-welded joints occur at the junction of the weld bead and the parent metal; and relief of residual-tensile stresses improve the fatigue performance of a detail.

Gurney [25,26], demonstrated the influence of externally induced residual stresses on the fatigue strength of steel and aluminum specimens. He used spot heating and the application of local compression to induce compressive-residual stresses near fillet welds on 1/2-in. thick, axial-test specimens. Gurney determined that these methods increased the fatigue strength of non-load carrying fillet welds by as much as 100% at two-million load cycles. Another method that can be used to improve the fatigue performance of welded aluminum joints involves peening of the weld to induce residual-compressive stresses in the material. Brosilow [18] stated that hammer, needle and shot peening are post-weld treatments that substantially improve the fatigue life of a weld when implemented properly. Montemarano and Wells [37] tested brush-shot peened, butt and fillet welds on 1/4 and 5/8-in. thick, 5086 aluminum alloy plates. They determined that post-weld, brush-shot peening improved the fatigue performance of butt welds to that associated with an unwelded aluminum plate and that the fatigue strength of fillet welds increased from a stress range of 2.75 ksi to 5.0 ksi at 10-million load cycles.

In 1969, the Aluminum Alloys Committee of the Welding Research Council (WRC) began a review of fatigue research regarding aluminum weldments. Studies from worldwide private and government laboratories were analyzed to determine the state-of-knowledge and to outline areas that needed further research. A computerized data bank of fatigue-test results was developed to be used for statistical analyses that would establish factors affecting fatigue behavior. Sanders [41] recommended further studies on the influence of joint configurations and the effect of loading history. As a result of this extensive review, additional studies concerning the fatigue behavior of butt-welded, 5000-series, aluminum alloy members were undertaken by Sanders and Gannon [45] and Sanders and McDowell [46]. These studies examined weld geometry and the effects of corrosive environments on the fatigue behavior of these connections.

In 1983, a second survey that addressed the state-of-the-art of fatigue behavior in aluminum weldments was published by Sanders and Day [43]. Even though a computer data bank that was sponsored by the Committee for Aluminum Fatigue Data Exchange and Evaluation (CAFDEE) contains the results from over 1,000 fatigue-test series involving nearly 12,000 individual tests, Sanders and Day recommended the need for additional fatigue testing of fillet-welded joints. They also noted that most of the fatigue data was associated with small-size, butt-welded specimens that were loaded in axial tension. They urged the testing of full-size members and welded joints in order to justify the continued use of fatigue-test data obtained from small-size test specimens for the development of design criteria.

In recent years, an increase in the fatigue testing of full-size aluminum components has begun; however, the results are limited [34]. A paper published by Taylor [54] describes the fatigue testing of a 28-in. diameter, welded, pressure vessel that was fabricated from 3/4-in. thick, 5083 aluminum alloy plates. Sharp and Nordmark [48] investigated the fatigue strength of a 3-ft high by

25.5-ft long, welded tubular truss. The extruded-tube truss members were 6061-T6 aluminum. The primary concern of their study was to determine the influence of welding and erection-residual stresses on the fatigue strength of the truss. They conclude that residual stresses did not appear to influence the fatigue performance of the welded connections and that the fatigue behavior of the truss related well to that established from small-size specimen data involving similar connections. However, Mazzolani [34] noted that the fatigue strength of welded specimens decreases as the component size increases. A possible explanation for size effects relates to the phenomenon that residual stress magnitudes increase as the plate thickness increases. Gurney [23] concluded that the fatigue strength of transverse, non-load carrying, fillet-welded joints depends on the thickness of the stressed member, as well as the toe-to-toe length of the attachment.

Extensive laboratory testing of structural aluminum weldments has been conducted at the Technical University of Munich in Munich, Germany. Under the direction of Kosteas [19], fatigue tests were performed at various stress ratios on 52 beams that were fabricated from 5083 and 7020 aluminum alloy plates. The beams contained ten weld configurations that are commonly incorporated into structures. These fatigue test results were compared to those obtained from existing, small-size, specimen data, involving similar weld configurations. With respect to non-load carrying transverse welds, they concluded that a reduction in fatigue strength exists for full-size specimens compared to that for small-size specimens. Erickson and Kosteas [19] noted that relating small-size specimen fatigue data to the behavior of large-size specimen weldments was difficult. They stated that the compilation of fatigue data for full-size specimens is crucial in order to properly establish the relationship between the existing small-size specimen data and that for realistic sizes of structural components. In a textbook by Sharp, Nordmark, and Menzemer [49], the authors

briefly discuss the effect of specimen size on the fatigue strength. They comment that full-size specimens will have lower fatigue strengths than comparable small-size specimens.

Provisions for fatigue design of welded-aluminum connections have been presented in several national codes. Beginning in the early 1980's, efforts began in the USA, Canada, and Europe to bring the specifications for structural use of aluminum into compatibility with those of other structural materials and to develop more realistic criteria. Both CAFDEE in the United States, and the Aluminum Fatigue Behavior Evaluation and Testing (ALFABET) project in Germany, under the direction of Kosteas of the Technical University of Munich, maintained aluminum fatigue data bases to assist in the expansion of knowledge and in the organization of information. More recently, the Munich data base has become the primary data base. Each international fatigue strength criteria reflects the philosophies and traditions of those involved with their inception [34]; therefore, each criteria is inherently different. The differences in the national fatigue design criterion concerns the selection of the specified materials, classification of detail categories, and strength parameters.

Sanders and McDowell [46] noted that the first USA design provision for the fatigue strength of aluminum components was developed in 1962 by the American Society of Civil Engineers (ASCE). This document pertained only to 6061-T6 and 6062-T6 aluminum alloys, which are magnesium-silicon alloys that are artificially aged by immersion in a chemical solution. The fatigue provisions only addressed riveted and bolted connections. The specification states that mechanically fastened members, which are designed in accordance with the specification and which are free of re-entrant corners or other stress raisers, can withstand at least 100,000 cycles of maximum live load without experiencing a fatigue failure. For load applications greater than 100,000 cycles, allowable stress equations are provided for two categories of stress ratio ($R \leq 0.5$ and $R > 0.5$). Although limited in topics, the ASCE aluminum fatigue design recommendations were used worldwide until the early 1980's [34].

Aluminum structural design specifications for the USA are published by the Aluminum Association. Prior to the fifth (1986) edition of Specifications for Aluminum Structures [7], the fatigue design provisions were actually the 1962 ASCE Specification. The third edition of the Specifications for Aluminum Structures [6] and the two previous editions permitted the effects of fatigue to be neglected when 20,000 or fewer repetitions of the maximum load occurred. This approach was consistent with the results of prior research, which concluded that the low-cycle fatigue strength of a connection was essentially the same as the static strength. When more than 20,000 load cycles exist, the specifications suggested that prototypes of the specific detail in question should be tested to establish the fatigue strength. In addition, these specifications suggested implementing variable-amplitude, loading techniques to better approximate the actual loading history. Since such testing is difficult and costly to conduct, the first three editions of these specifications essentially discouraged the use of aluminum welding for dynamic load applications.

The fifth edition of the Specification for Aluminum Structures [7] adopted the same methodology that was used for the fatigue design of steel weldments. Allowable-stress ranges are specified for detail categories that correspond to particular weld details. Twenty weld details are illustrated for six detail categories. The sixth edition of the Specification for Aluminum Structures [8] reflects the progress made in the organization and analysis of aluminum fatigue data. This specification addresses constant and variable-amplitude loading. The detail category definitions are the same as those in the fifth edition of the specification.

The British BS 8118 Standard [17] devotes a chapter to the design of welded aluminum structures that are subjected to fatigue conditions. These specifications mention the usage of 3000, 5000, 6000 and 7000-series aluminum alloys in welding; however, the specification does not apply different criteria to these alloys. Twenty-nine classes of joints that are divided into three groups are mentioned: Non-welded details (7 classes); welded details on the surface of loaded members (11

classes); and welded details at end connections (11 classes). Each class of joint has an SN-curve that relates the maximum stress range to the number of load cycles. The BS 8118 Standard does not address the influence of the stress ratio on the fatigue performance of a joint class.

The European Convention for Construction Steelwork (ECCS) presented the European Recommendations for Aluminum Alloy Structures (ERAAS) Fatigue Design document [20], which was the product of years of research, analysis, and international collaboration. The document specifies 32 joint details that belong to six classes based on their mechanical and geometrical features. SN-curves that relate the nominal, allowable-stress range to the number of load cycles are provided for each detail. The stress ratio is incorporated into the SN-curves by providing factors for the various joint types. Variable-amplitude, cyclic-load cases are evaluated through the use of the Palmgren-Miner Rule [36]. The approach provides for a sloped continuation of the SN-curve beyond the constant-amplitude, endurance limit that was set at 5-million load cycles. This third region of the SN-relationship continues until 100-million load cycles, after which an assumed variable-amplitude, endurance limit is reached. Effects of residual stress and stress concentrations are considered for each detail. The ERAAS document provides for a fatigue strength reduction when plate thickness are greater than 1 in. In recent years, the development of a European standard for design has been initiated through Eurocode. This development is still underway.

CHAPTER 2. LABORATORY TESTS

2.1. Test Specimens

2.1.1. Girder removal from bridge

Eight girder segments were obtained when the original Clive Road Bridge was removed to allow for the construction of a new interchange. As the bridge was being disassembled, the four girder sections in each of the 41.25-ft long end spans were salvaged. Each of the girder sections was flame cut in the adjacent span just beyond the girder bearing point at the bridge pier. The 8-in. thick reinforced concrete slab was saw cut parallel to the girder length in order to retain a portion of the concrete deck. The exterior and interior girder sections retained deck widths of approximately 18 and 24 in., respectively. Four girders were used to obtain specimens for constant-amplitude, fatigue testing; and the four remaining girders were saved for possible future variable-amplitude, fatigue testing. The girders that were designated for the constant-amplitude, fatigue testing were cut into two sections. An approximately 26-ft long section was cut from the end of the girder that was closest to the original bridge pier location. The remaining approximately 15-ft long section was the portion of the girder that was closest to the original bridge abutment location.

2.1.2. Girder material composition

The girders had been fabricated in 1958 by the Pullman Standard Car Company of Chicago, Illinois. The Aluminum Company of America (Alcoa), Kaiser Aluminum and Chemical Corporation, and Reynolds Metal Company manufactured the 5083-H113 aluminum alloy plates for the girders. The H113 designation refers to the temper for this wrought alloy. The notation H1 indicates that only strain hardening was used to obtain the specified strengths for this alloy, and the number 13 refers to the degree of strain hardening [47]. The chemical composition (expressed as a % by weight) for each element in this aluminum alloy as produced by the three manufacturers and

as published by the Aluminum Association is listed in Table 2.1. This table also lists the chemical composition for the 5183 aluminum alloy metal for the welding wire. Magnesium is the primary alloying element in this material. The 5000-series aluminum alloys possess moderately high strength and they are not heat treated.

The average values for the ultimate tensile stress, F_u , and yield stress, F_y , for the 5083 aluminum alloy that were obtained from the 1958 mill reports for the aluminum plates, are currently published as typical values by the Aluminum Association, and were determined from tension test coupons taken from the girder specimens are listed in Table 2.2.

The rectangular-shaped, aluminum, tension-test coupons were cut from an original girder web plate at a location that was several feet away from a flame-cut scar or region that experienced effects of fabrication during specimen preparation. The long dimension for the tension coupons was parallel to the rolling direction of the girder web plate. The test coupons were prepared and tested in accordance with the American Society for Testing and Materials (ASTM) Standard E8 [14]. The aluminum used in the tension-test coupons had been in service for over 35 years. The modulus of elasticity, E , for the aluminum plates was determined to be equal to 10,300 ksi from the tension-test coupons. This measured E -value was in agreement with published magnitudes for this parameter.

New, 5083-H321 aluminum alloy, bottom flange, cover plates; horizontal web plate attachments; and vertical web stiffener plates were welded to the girder test specimens. This alloy differs from the original, 5083-H113 aluminum alloy only by the temper. Both alloys are strain hardened to attain a desired strength, but the 5083-H321 aluminum alloy is also stabilized by a chemical aging process to improve the ductility of the metal. The Aluminum Association specifies that for 1/8-in. to 1 1/2-in. thick plates in this alloy, the range in F_u and F_y should be between 44.0 and 56.0 ksi and 31.0 and 43.0 ksi, respectively. The welding wire for the original and the new welds

Table 2.1. Chemical composition of aluminum alloy plates and welding wire (% wt.)

Item	Alcoa	Kaiser Aluminum	Kaiser Aluminum	Reynolds Metals	Aluminum Association
Alloy	5083-H113	5083-H113	5183	5083-H113	5083
Material	½-in. thick web plates	1 & 1 3/4-in. thick plates	0.063-in. diameter welding wire	3/8, 3/4, and 1 1/4-in. thick plates	plates
Copper (max.)	0.10	0.05	0.10	0.10	0.10
Iron (max.)	0.40	0.25	0.40	0.40	0.40
Silicon (max.)	0.40	0.25	0.40	0.40	0.40
Manganese (max.)	1.00	0.80	1.00	1.00	1.00
Manganese (min.)	0.50	0.50	0.50	0.50	0.40
Magnesium (max.)	4.90	4.90	5.20	4.90	4.90
Magnesium (min.)	4.00	4.40	4.30	4.00	4.00
Zinc (max.)	0.25	0.20	0.25	0.25	0.25
Chromium (max.)	0.25	0.18	0.25	0.25	0.25
Chromium (min.)	---	0.07	---	---	---
Titanium (max.)	0.15	0.10	0.15	0.15	0.05
Beryllium	---	---	0.0005	---	---
Others (each)	0.05	0.05	0.05	0.05	0.05
Others (total)	0.15	0.15	0.15	0.15	0.15
Aluminum	remainder	remainder	remainder	remainder	remainder

Table 2.2. Yield and ultimate strengths of 5083-H113 aluminum alloy

Source	F _u (ksi)		F _y (ksi)	
	max.	min.	max.	min.
½-in. thick web plates (1958 mill reports)	48.7	47.0	37.6	36.8
¾-in. thick flange plates (1958 mill reports)	51.0	44.0	---	31.0
1-in. thick flange plates (1958 mill reports)	46.4	45.4	34.0	32.8
1 ¼-in. thick flange plates (1958 mill reports)	51.0	44.0	---	31.0
1 ¾-in. thick flange plates (1958 mill reports)	44.8	44.2	35.2	31.7
Aluminum Association	---	44.0	---	28.0
Tension coupon (1996 test)	---	46.9	---	30.5

on the girders was 5183 and 5356 aluminum alloy, respectively..

The original design of the bridge specified a minimum, concrete compressive strength of 3,000 psi for the bridge deck. However, since the concrete in the bridge deck was over 35 years old and since the diameter of the aggregate was as large as 1.25 in., the concrete compressive strength was assumed to be at least equal to 5,000 psi when the fatigue tests were conducted. The compressive strength was used to calculate the concrete modulus of elasticity for the composite girder specimens.

2.1.3. Long girder specimens

Four long girder specimens were prepared for the constant-amplitude, fatigue testing. Two of the specimens were obtained from the exterior girders and the other two specimens were obtained from the interior girders of the original bridge. The simple span length of the four specimens was equal to 25 ft-2 in. These specimens extended approximately 1 ft-6 in. beyond the roller support, but this overhang was assumed to not influence the fatigue behavior of the weld details that were located well within the span of these specimens. As shown in Fig. 2.1, each of these specimens had a portion of the reinforced concrete deck attached to its top flange. The pinned support was the pier

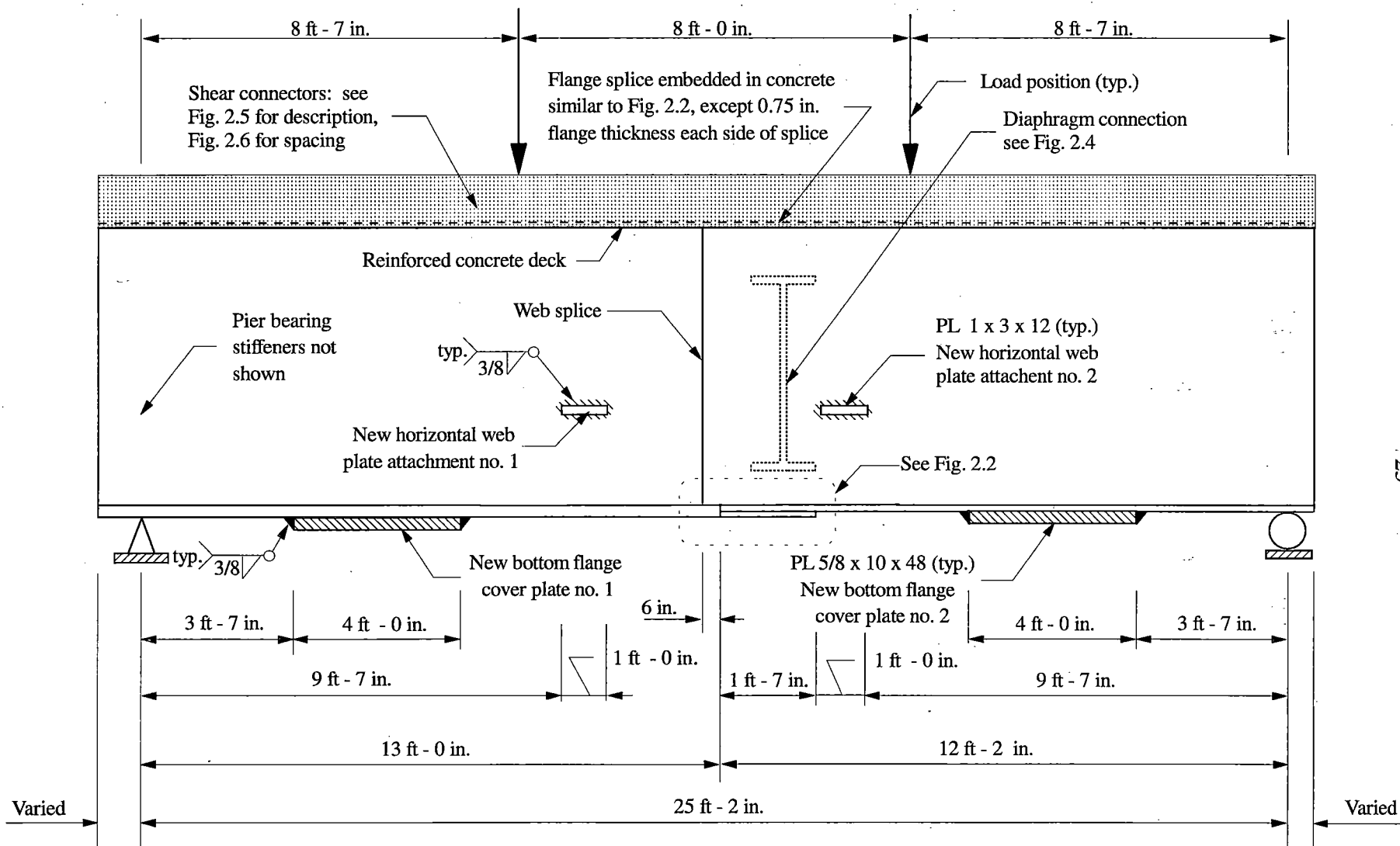
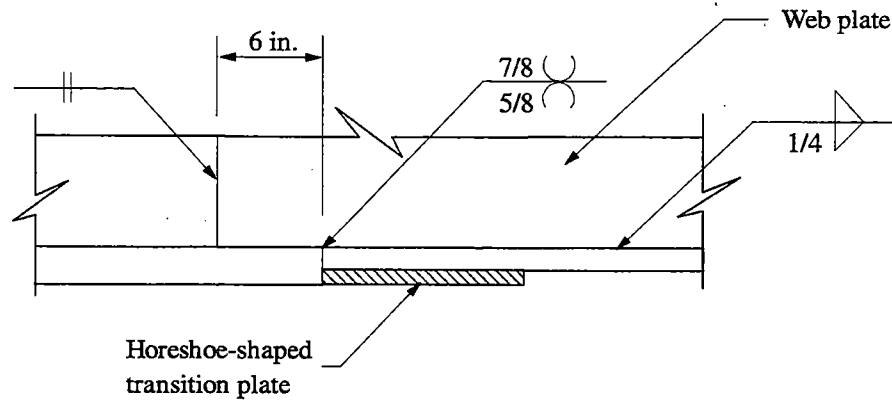


Figure 2.1. Elevation of the long girder specimens

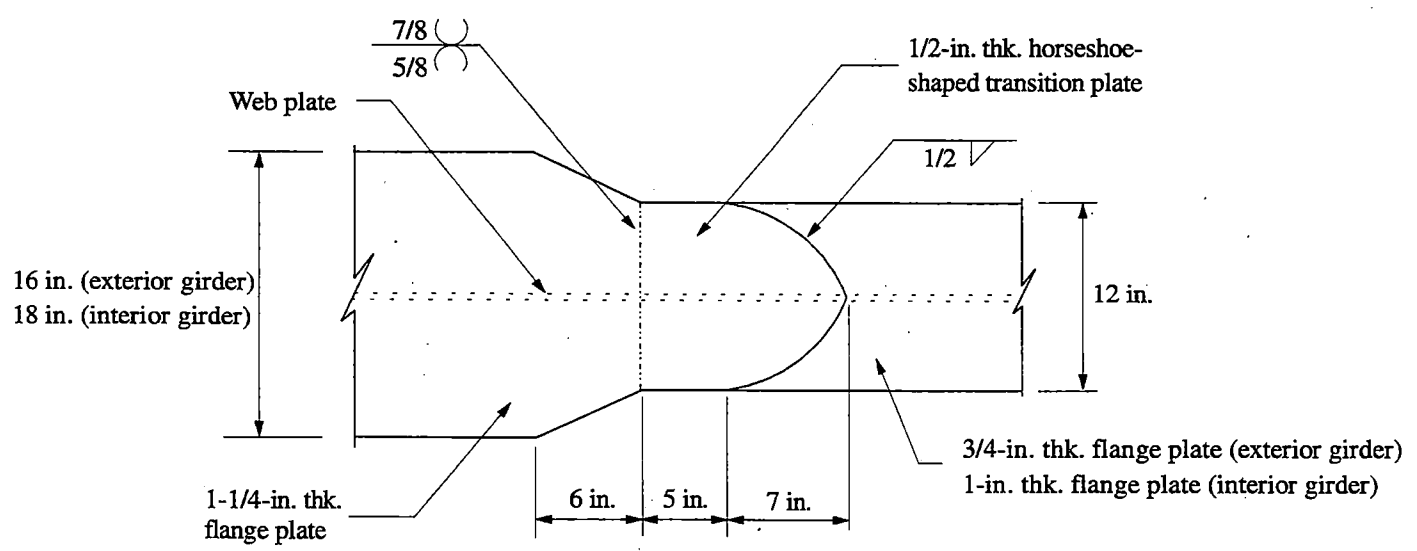
reaction point for the original bridge girder. A bearing stiffener (not shown in Fig. 2.1) occurred at this location. Two distinguishing features that were present on the original bridge girders were incorporated into the long girder specimens. The first feature involved a horseshoe-shaped, transition plate that was located at the bottom flange splice near the midspan of these girder sections. Figure 2.2 shows the geometrical configuration of the original girder, bottom flange splice. At this location the cross section of the girder changed. The smaller cross section was used along the portion of the girder length that was closest to the original bridge abutment. Cross-sectional views for the girder sections near the pier and abutment ends of the long girder specimens are shown in Fig. 2.3. The web plate for the interior girder sections was 2 in. deeper and the bottom flange plate was larger than those plates used for the exterior girders.

The second feature involved the diaphragm connections in the original bridge. Both the exterior and interior girder specimens had a segment of an I-shaped diaphragm that was fillet welded to one side of the girder web plate, as shown in Fig. 2.4. An interior girder diaphragm connection (Fig. 2.4c) consisted of separate rectangular plates that passed through slots that had been cut in the girder web. These plates were fillet welded to the girder web plate and served as flange connection plates for an interior I-shaped diaphragm. The interior diaphragms had connected together the shop-fabricated girder pairs in the original bridge. The 1/2-in. thick, vertical stiffener plate shown in Fig. 2.4c was fillet welded to the bottom flange plate for the diaphragm connection and to the web and bottom flange plates of the girder.

Two types of plate attachments that were not present on the original bridge girders were added to the long girder specimens. These plate attachments represented details that are commonly used on welded plate girders. Figure 2.1 shows two, bottom flange, cover plates that were fillet welded along all four edges to the bottom flange of the girder specimen and two, horizontal, web



(a)



(b)

Figure 2.2. Midspan flange splice detail: (a) Partial elevation; (b) Underside of the bottom flange

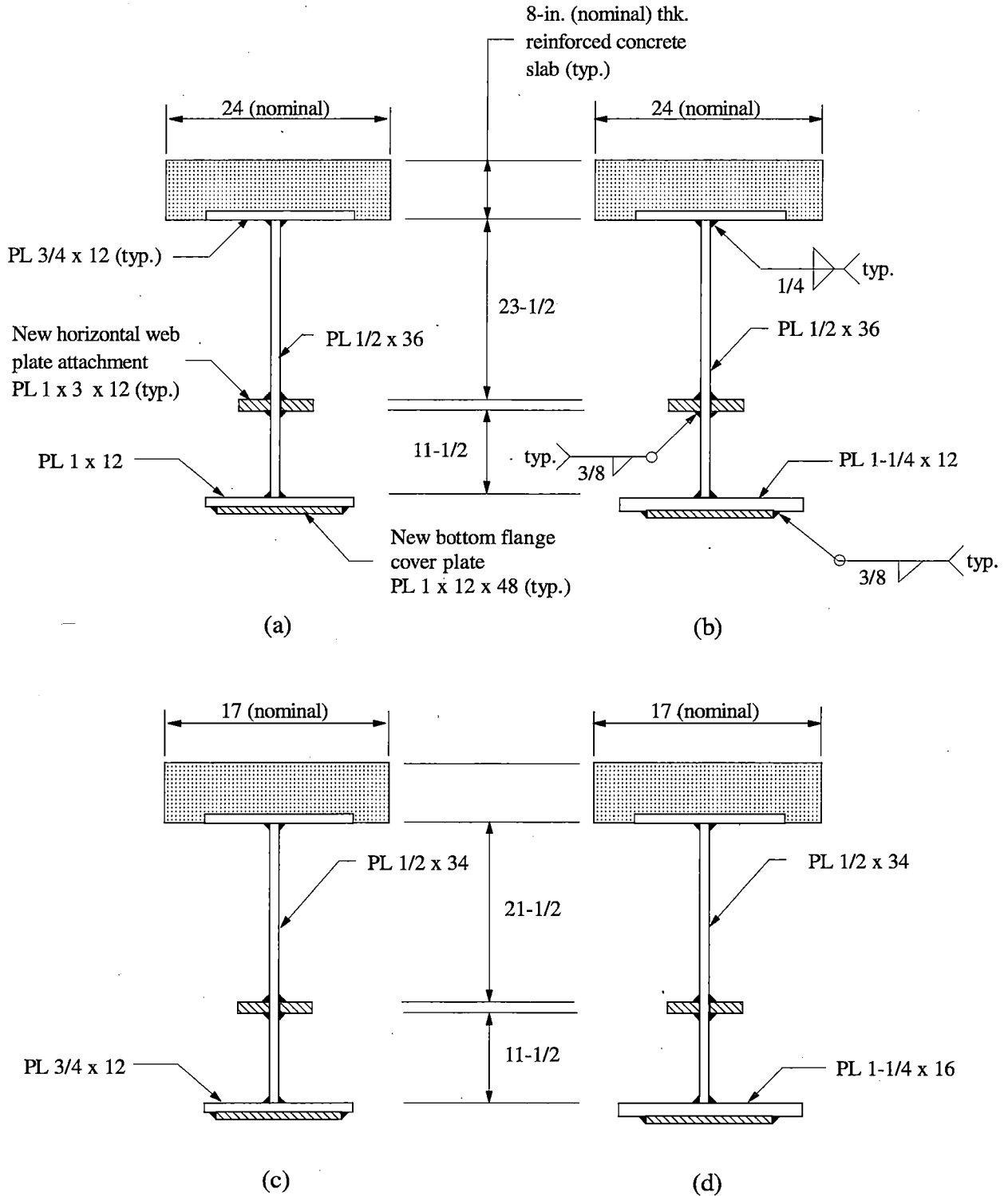


Figure 2.3. Cross-sectional views of the long girder specimens (all dimensions in inches):
 (a) Interior girder segment along the abutment side of the splice; (b) Interior girder segment along the pier side of the splice; (c) Exterior girder segment along the abutment side of the splice; (d) Exterior girder segment along the pier side of the splice

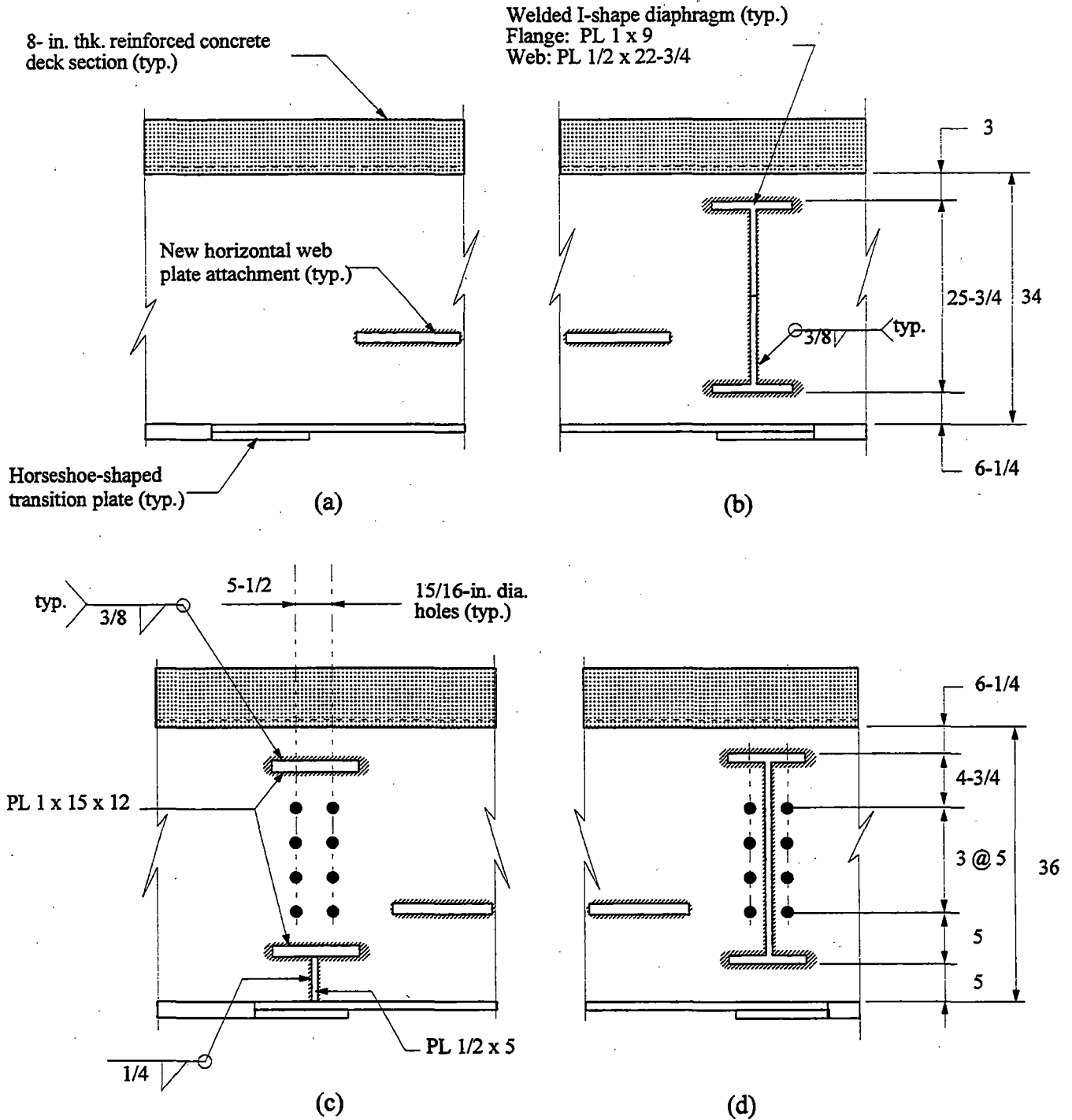


Figure 2.4. Diaphragm connections on the long girder specimens (all dimensions in inches):
 (a) Front elevation of an exterior girder; (b) Rear elevation of an exterior girder;
 (c) Front elevation of an interior girder; (d) Rear elevation of an interior girder

plate attachments that were fillet welded all around to each side of the girder web plate, as indicated in Fig. 2.4.

The interior and exterior, long girder specimens had different amounts and locations of longitudinal reinforcing bars and shear connectors in the concrete deck. An angle-shaped, shear connector is shown in Fig. 2.5. The locations of the shear connectors along the long interior and an exterior girder specimens are shown in Fig. 2.6. The long interior girder specimens had a larger number of shear connectors than that for the long exterior girder specimens.

2.1.4. Short girder specimens

Four short girder specimens were prepared for the constant-amplitude, fatigue testing. However, only three of these specimens were actually tested. The short specimens were obtained from the portion of the girders that were near the abutments of the original bridge. At this location, each girder had a uniform cross section. Figure 2.7 shows an elevation of a short girder specimen. The test span for these specimens was 13 ft-9 in. The ends of the short girder specimens had weld-plate attachments (not shown in Fig. 2.7) that were part of the original bridge construction. At the pinned support, an extensive diaphragm assembly existed that was a portion of the abutment diaphragm. At the roller support, an I-shaped, intermediate, diaphragm connection existed that was identical with the one described for the long girder specimens. The interior and exterior girders had been fabricated with different size plates. The cross sections of the short interior and exterior girder specimens are shown in Fig. 2.8.

Due to the limits on the capacity of the loading apparatus, the concrete deck was removed from each of these specimens to reduce the flexural stiffness of the specimens. To facilitate the loading of the short girder specimens, 8-in. thick by 18-in. square, concrete, load pads were cast in place at the load points on the top flange of these specimens. In order to avoid composite action

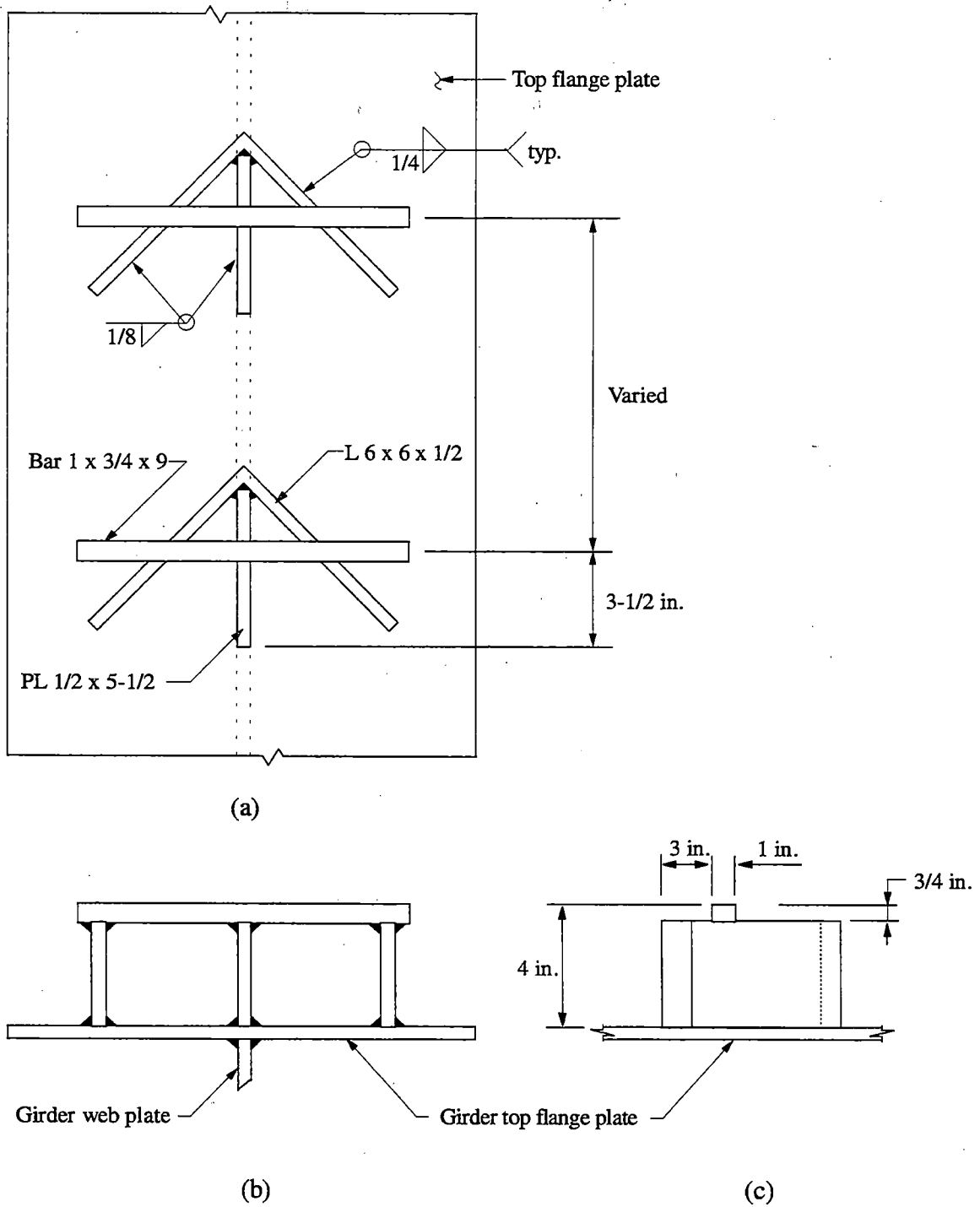
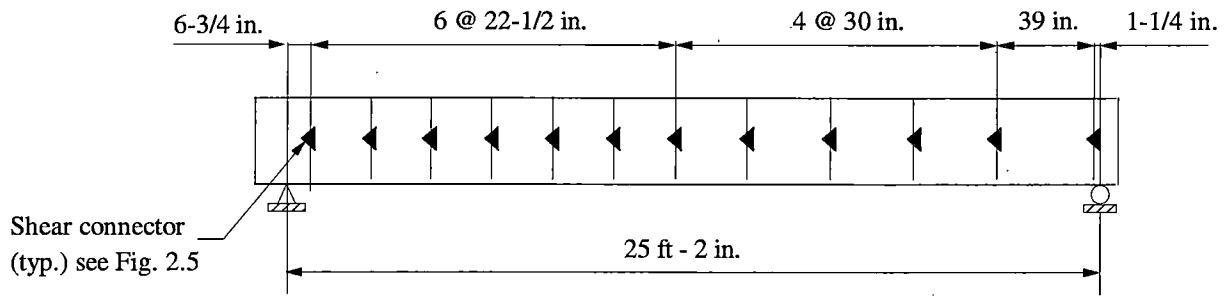
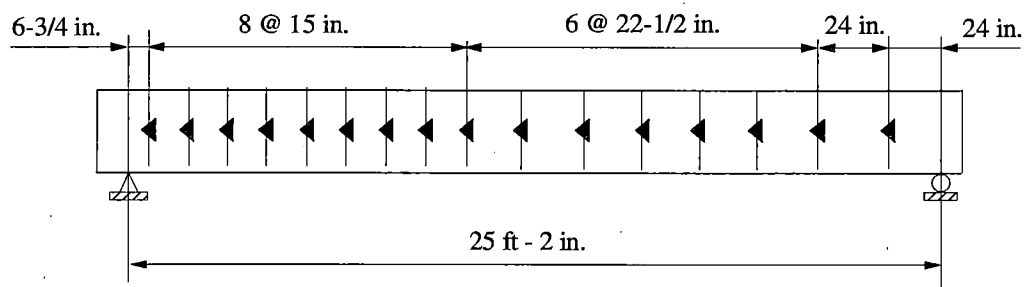


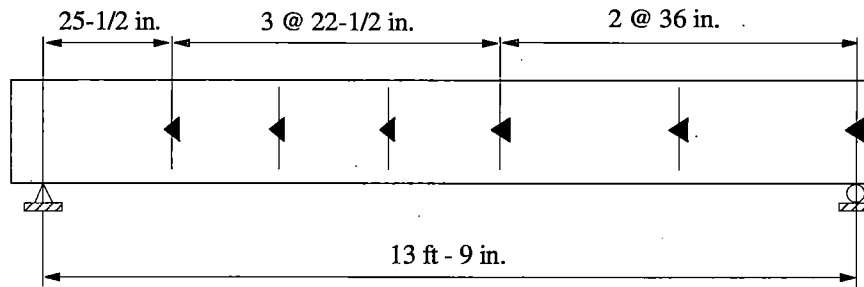
Figure 2.5 Shear connectors: (a) Plan view; (b) Elevation; (c) Side view



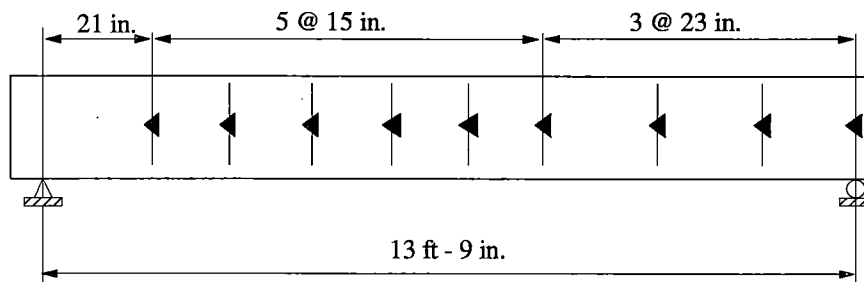
(a)



(b)



(c)



(d)

Figure 2.6. Shear connector locations: (a) Long exterior girder specimens; (b) Long interior girder specimens; (c) Short exterior girder specimens; (d) Short interior girder specimens

between the concrete pads and the aluminum girder, the top surface of the girder flange was oiled prior to casting the concrete. The angle-shaped, shear connectors within the midspan of the short girder specimens were removed to eliminate possible interference with the load pads.

Two types of plate attachments were added to the short girder specimens to represent connection details that are common to plate girders. Figure 2.7 shows two, bottom flange cover plates, similar to plates that were welded on the long girder specimens. These plates were fillet welded along all four edges to the bottom flange of a short girder specimen. This figure also shows partial-height, web stiffener plates that were fillet welded all around to the web and bottom flange plates in the central region of the short girder specimens. Figure 2.8 shows that these web stiffener plates were placed in pairs on opposite sides of the girder web plate; therefore, each short girder specimen had four partial-height, web stiffener plates.

2.1.5. Welding procedure for the new plates

The girder plate surfaces at the locations for the new plate attachments were lightly ground with a grinding wheel to expose a clean surface. Just prior to welding, a steel-wire brush was used to clean the surface. All welding was performed in the flat position. Prior to depositing the 3/8-in. fillet welds, each new plate attachment was held in position with tack welds. For the bottom flange cover plates, the tack welds were located at approximately 6 in. from each of the four corners of the plate along the length of the plate. The tack welds for the horizontal, web plate attachments were placed at each end of a stiffener across its thickness.

All fillet welds were deposited by using a single pass of the electrode. The welding of each cover plate to a girder bottom flange plate was performed in four steps. The first two steps involved welding along the plate width (across the girder flange width). These welds started at the position of one of the tack welds and extended across the end of the plate to the tack weld on the opposite

side. The last two steps involved welding along the cover plate length (along the girder flange length) between the tack weld locations. Each horizontal, web plate attachment was welded to a girder web plate with a single pass being made on each side of the stiffener. The welding parameters for the new and original welds on the girder segments are given in Table 2.3.

All new welds were visually inspected for defects by a Certified Welding Inspector. A second weld pass was performed in instances where the fillet weld leg size was not at least three-eighths of an inch. When rewelding was required, the surfaces were first scraped clean with a stainless-steel brush.

Table 2.3. Welding parameters

Welding parameter	New welds (1995)	Original welds (1958)
Filler wire alloy	5356	5183
Filler wire diameter (in.)	3/32	1/16
Voltage (volts)	26	27
Current (amp)	250	210
Wire speed (in./min.)	150	unknown
Pulse (hz)	227	unknown
Gas mixture ^a	75% He-25% Ar	75% He-25% Ar
Gas flow rate (cfm)	60	120

^aOriginal welding gases were contained in separate tanks and new welding gases were mixed in a single tank

2.1.6. Weld detail categories

The original and new welds that were used on the girder specimens produced several stress categories as defined by the Specifications for Aluminum Structures [8]. A particular stress detail category is characterized by general and specific conditions that describe a location where a fatigue fracture could occur in the base metal or weld metal. The five general conditions are plain material,

mechanically-fastened connections, fillet-weld connections, groove-weld connections, and welded attachments. The specific conditions address identified geometries. A specific detail is classified by a letter from A through F based on the degree of susceptibility that a detail possesses for a fatigue fracture. The order from the least to the most critical detail categories is A, B, C, D, F, and E. Each detail category has a specific stress-range versus load-cycle (SN) behavioral relationship.

The original, full-penetration, groove-welded, bottom flange splice shown in Fig. 2.2a is a Category C detail. However, the original fillet weld between the horseshoe-shaped, transition plate and the bottom flange of the girder involves a Category E detail in the region of the weld near the apex of the curved edge. The original, fillet-welded connection between the bottom flange plate of the diaphragm and the exterior girder web plate, shown in Fig. 2.4b, involved both Category C and E details. Figure 2.4c that shows the original, stiffened-seat, diaphragm connection on an interior girder involved complex geometry. Recall that the horizontal, 1-in. thick plates passed through slots cut in the girder web plate. The portions of the all-around, fillet-welded connection between this plate and the interior girder web plate that were similar to those on an exterior girder can not clearly be classified as Category C or E details, according to the description provided in the Specifications for Aluminum Structures [8]. Therefore, any fatigue fractions which propagated from the bottom web plate slot were not included in the statistical analysis of the other Category E details. The fillet-welded connection between the vertical stiffener plate for this diaphragm connection and the girder web and flange plates was a Category C detail. Figure 2.4c shows that the fillet-welded connection to the top surface of the girder bottom flange plate is in the same location as the fillet-welded connection between the horseshoe-shaped, transition plate and the bottom surface of the girder bottom flange plate.

The new, bottom flange, cover plate attachments shown in Figs. 2.1, 2.3, 2.7, and 2.8 involved two detail categories. The longitudinal fillet weld along the length of the cover plates was a Category B detail, while the transverse fillet weld along the width of the cover plate was a Category E detail. Figures 2.1, 2.3, and 2.4 show fillet-welded connections for the new, horizontal web plate attachments on the long girder specimens. These connections are classified as Category E details, since the length of the plates were longer than 4 in. The fillet-welded connections between the new, partial-height, web stiffener plates and the interior girder web and flange plates, shown in Figs. 2.7 and 2.8, were Category C details.

2.2. Instrumentation and Test Apparatus

2.2.1. Test frame and load actuators

The girder specimens were tested in the Structural Engineering Laboratory at Iowa State University. Figures 2.9 and 2.10 show a long and a short girder specimen, respectively, positioned in the test frame. All of the specimens were simply supported. The original pier and abutment bearing plate on a long and short girder specimen, respectively, was used as the pin support. The other end of each specimen was supported by a roller assembly that consisted of several 1-in. thick by 12-in. square, steel plates and a 3.5-in. diameter by 12-in. long, steel rod. The short girder specimens were supported on fabricated abutments made from aluminum and steel sections that were independent of the test frame. Lateral bracing for top flange of the long girder specimens was provided at the vertical supports and at the midspan. The short girder specimens were laterally supported only at the ends of the simple span.

Loads were applied by two, servo-controlled, electro-hydraulic actuators that were manufactured by MTS Systems Corporation, Material Test Systems Division. The actuators were symmetrically positioned with respect to the midspan of a specimen and the test frame. When a long

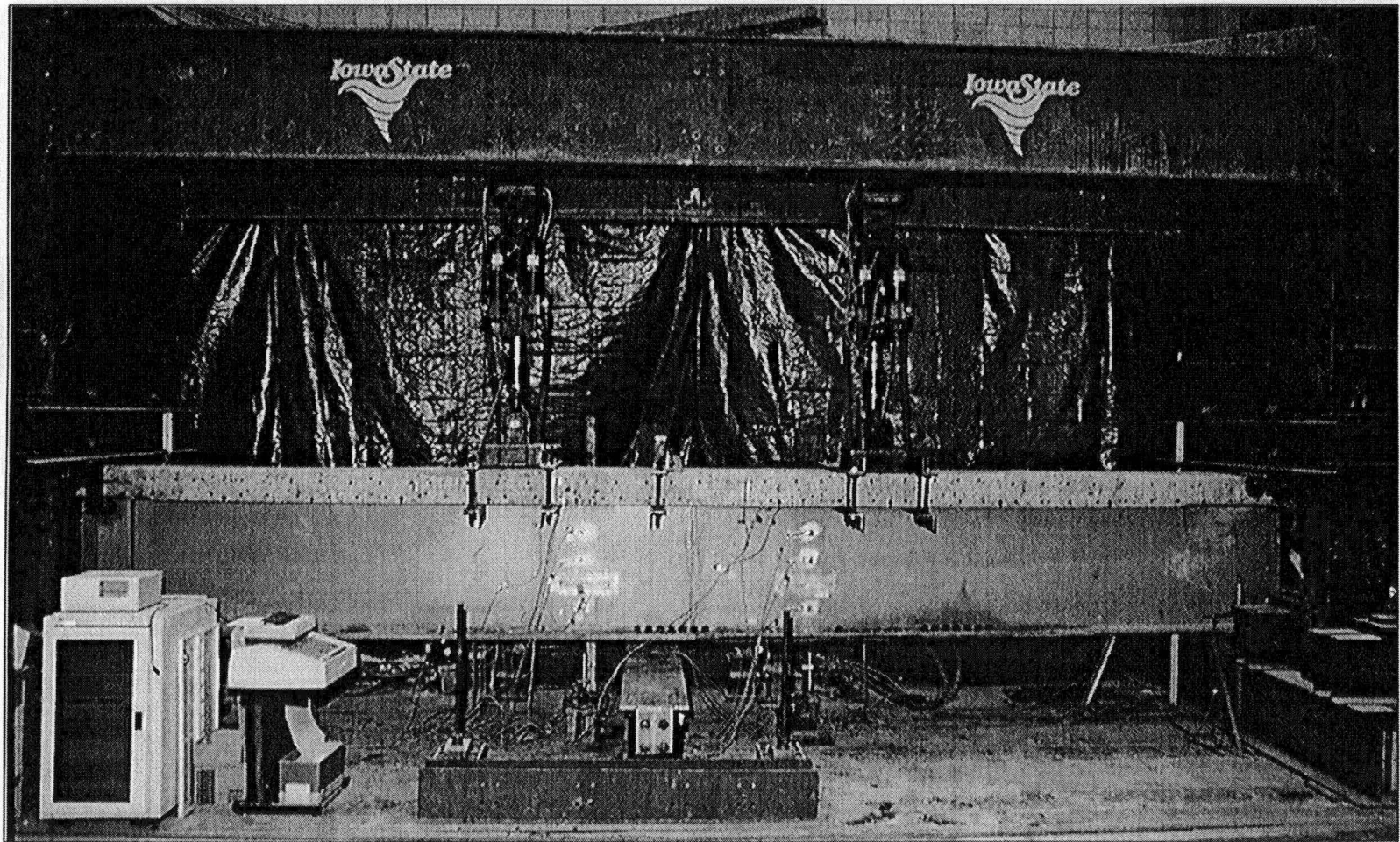


Figure 2.9. Test frame and apparatus for the long girder specimens

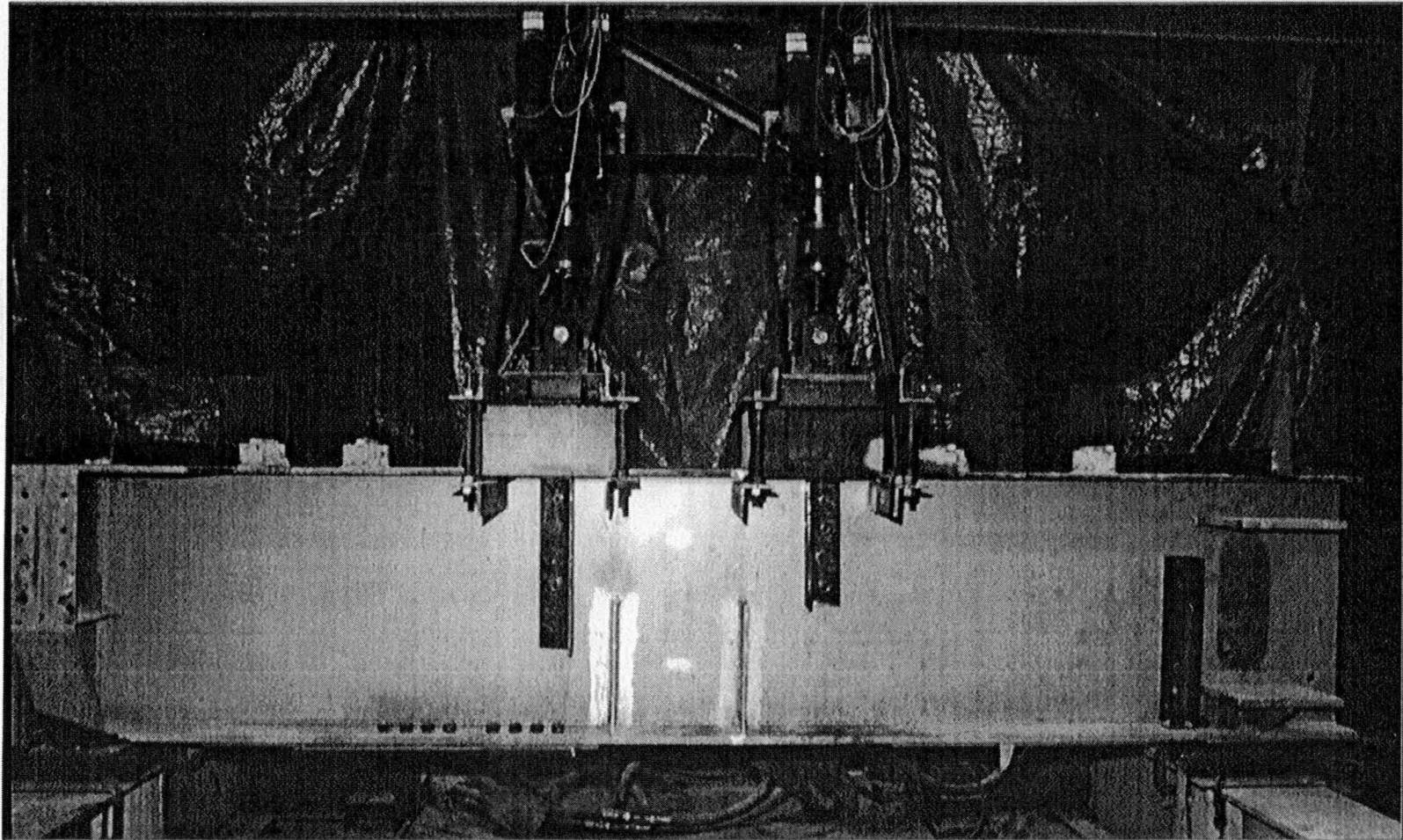


Figure 2.10. Test frame and apparatus for the short girder specimens

and a short girder specimen was tested, the actuators were spaced at 4 ft and 1.5 ft, respectively, on center. Each actuator load was distributed through a 2-in. thick by 15-in. square, steel plate and 2-in. thick, neoprene pads. The actuator plates were restrained from lateral motion by steel guides that were clamped to the top flange of a test specimen. Each actuator had a 55-kip load capacity and a 6-in. stroke range. A load cell within each actuator monitored the applied load magnitudes.

2.2.2. Instrumentation

For each specimen, electrical-resistance, strain gauges (strain gauges) and direct-current, displacement transducers (DCDTs) monitored longitudinal, flexural bending strains and horizontal and vertical displacements, respectively. This instrumentation was used to detect fatigue fracture development and to obtain experimental measurements of particular strains and deflections, which could be compared with theoretical predictions of these girder responses. Many of the strain gauges were located in close proximity to welds that were expected to fail during the fatigue tests.

The strain gauges that were attached to the aluminum girder plates and reinforced concrete deck were manufactured by Micro-Measurements of Raleigh, North Carolina. The strain gauges for the aluminum were CEA-13-250UW-120 gauges and had a 0.25 in. gauge length. The strain gauges for the concrete were EA-06-40CBY-120 gauges and had a 4.0-in. gauge length. All of the strain gauges that were used with the data acquisition equipment had an accuracy of ± 2.7 microstrains.

Each long girder specimen was instrumented with 18 strain gauges. The gauge positions are shown in Fig. 2.11. The gauges labeled "a" were attached to the top surface of the bottom flange plate, and they were positioned 3 in. from each side of the web plate. Two strain gauges were used at each of these locations. The gauges labeled "b" were attached to the web plate in vertical alignment with the center of the new, web plate attachment. One strain gauge was used at each of these locations. The gauges labeled "c" were attached to the web plate in vertical alignment with

the bottom flange tip of the original, I-shaped diaphragm. One strain gauge was used at each of these locations. The gauges labeled "d" included strain gauges that were mounted on the aluminum top flange plate and on the reinforced concrete deck. Two strain gauges were attached to the underside of the aluminum flange plate. Each of these gauges was positioned at 3 in. from each side of the web plate. Also at this location, two strain gauges were attached to the underside of the reinforced concrete deck. Each of these gauges was positioned at 6 in. from each side of the web plate. The gauges labeled "e" were attached to the top surface of the slab, and they were positioned at 6 in. from each side of the web plate. Two strain gauges were used at this location.

The strain gauge positions for the short girder specimens are shown in Fig. 2.12. Each short girder specimen was instrumented with 10 strain gauges. The gauges labeled "a" were attached to the bottom flange plate. Two strain gauges at this location were positioned the same as those for a long girder specimen. The gauges labeled "b" were attached to the web plate in vertical alignment at the midspan of a specimen. One strain gauge was placed at each of these locations. The gauges labeled "c" were attached to the underside of the aluminum top flange plate at the midspan of a specimen, and they were positioned at 3 in. from each side of the web plate. Two strain gauges were used at this location.

String-type and stem-type DCDTs were used to measure girder deflections and support motions. The girder displacements were monitored in the vertical and horizontal directions. The measurement accuracy for the DCDTs was specified to be ± 0.003 in., when a high-speed, non-integrating voltmeter was used. The locations of the DCDTs for long and short girder specimens are shown in Figs. 2.13 and 2.14, respectively. The gauges labeled "a" represent a pair of stem-type DCDTs that measured potential vertical displacement of the top surface of the bottom flange plate at the center line of the vertical supports for a specimen. The gauges labeled "b" were string-type

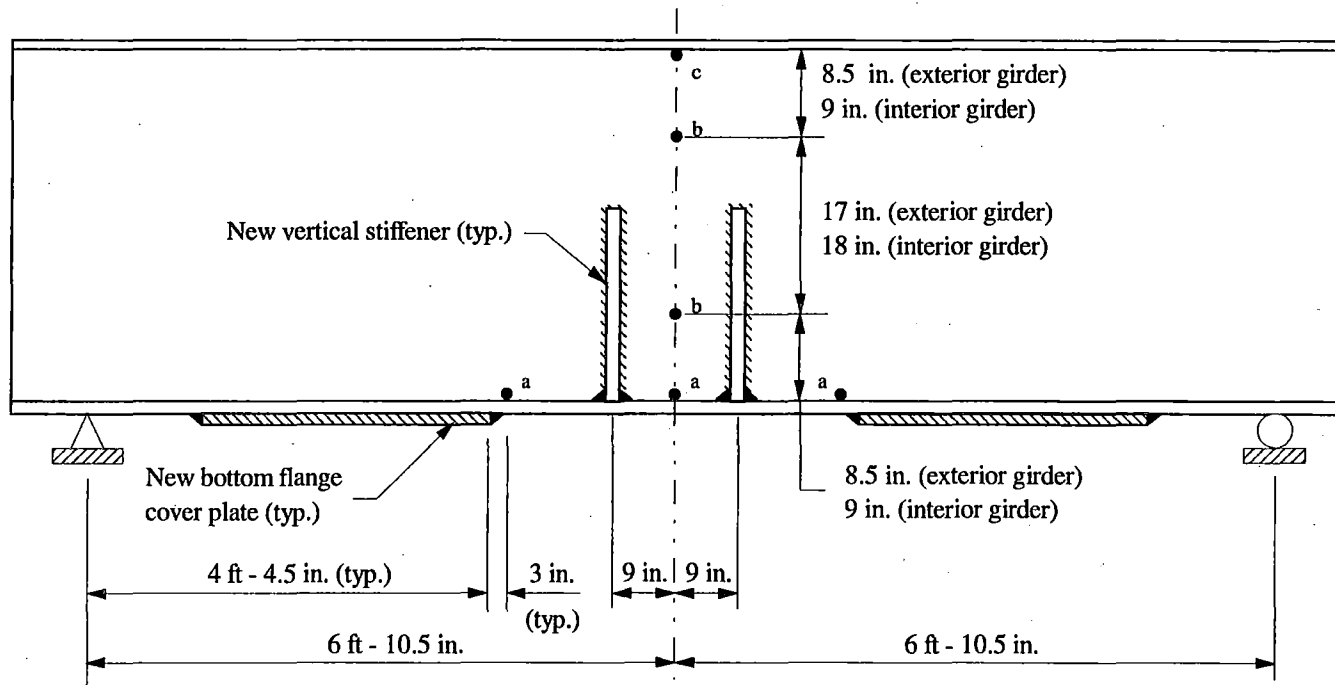


Figure 2.12. Strain gauge locations on the short girder specimens

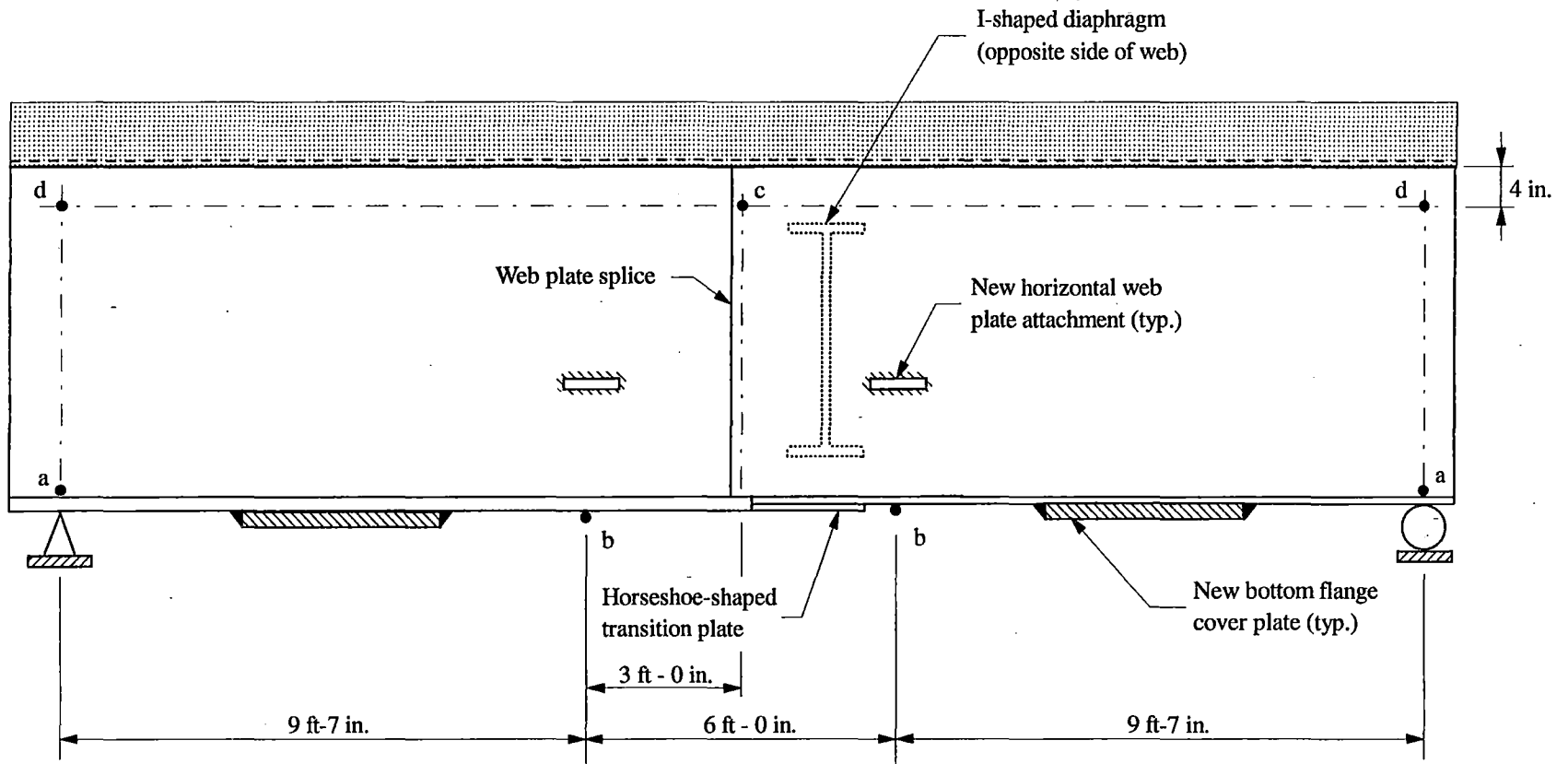


Figure 2.13. DCDT locations on the long girder specimens

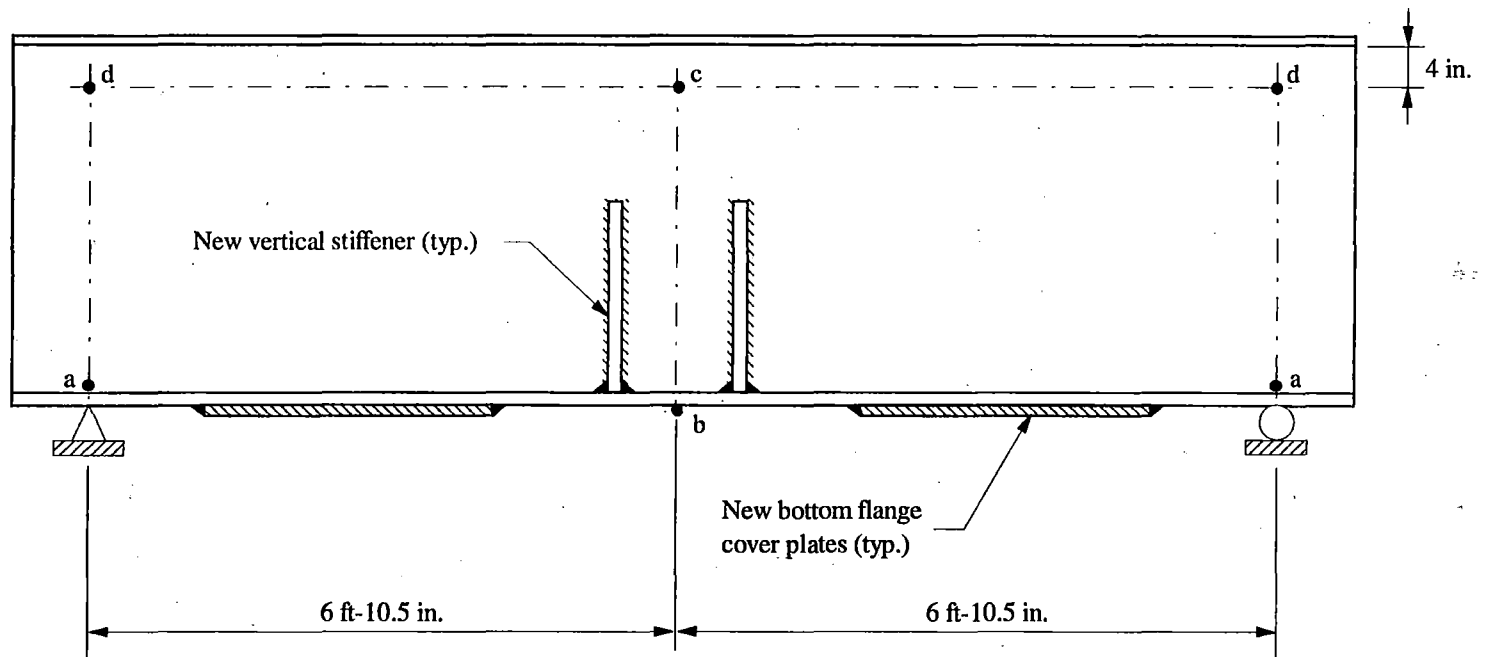


Figure 2.14. DCDT locations on the short girder specimens

DCDTs that measured the vertical displacement at the specified locations along the length of a specimen. The gauge labeled “c” was a string-type DCDT that was positioned at 4 in. below the top flange of the aluminum girder. This gauge measured the lateral displacement of a specimen at the midspan. The gauges labeled “d” were stem-type DCDTs that were positioned at 4 in. below the top flange of the aluminum girder. These gauges measured potential lateral displacement of a specimen at the vertical supports for a specimen.

2.3. Test Methods

2.3.1. Test parameters

The magnitudes of the fatigue loads that were to be initially applied to a specimen were selected after investigating the critical stress range at the location of a weldment that was considered to be the most vulnerable to fatigue damage. A desired stress range was established after reviewing past fatigue stress-range versus load-cycle relationships (SN-curves) [19], as well as appropriate sections of design specifications [8,12] for the specific weld detail. Low-stress ranges were selected in an attempt to induce fatigue fractures after two-million load cycles. The general flexure formula that is applicable for either symmetric or nonsymmetrical bending was used to obtain the minimum and maximum load magnitudes, P_{\max} and P_{\min} , respectively. The longitudinal reinforcing bars in the reinforced concrete slab were included in the determination of the geometric properties of the long girder specimens.

The specimens were positioned in the test frame for symmetrical two-point loading (Figs. 2.9 and 2.10) to induce a region of pure bending between the actuators. Each specimen was subjected to constant-amplitude, full-tension loading with a stress ratio, R , equal to 0.05. Therefore, the stress range, SR , was always 95% of the maximum tensile stress, σ_{\max} . The load frequency for a specimen was affected by the flexural stiffness of the girder and the magnitude of the maximum

load in a test cycle. The flow-rate capacity of the oil through the servo-valves in the hydraulic actuators limited the frequency of the load. The frequency of the loading on the girder specimens was between 1 and 5 hertz.

An electro-hydraulic, direct-stress, cycling system controlled the load magnitudes and frequency that were applied to a specimen. Each test was performed in a load-control mode and displacement interlocks were used to monitor the stroke of each actuator. The displacement interlocks were set to terminate the loading when an actuator stroke exceed a predetermined displacement limit. This limit was set at ± 0.015 in. with respect to the minimum and maximum displacements of the actuator during a load cycle. The minimum and maximum displacements were determined early in the loading history of a specimen, usually after an hour of dynamic loading. As fatigue cracks developed in a specimen, the actuator stroke had to be increased in order to apply the desired load. Following the reinforcement of a girder cross section at the location of a fatigue fracture, the stroke limits were adjusted for the new stroke range.

2.3.2. Data acquisition

A computer-based, data acquisition system (DAS) was used to manage the collection of test data. The software for the DAS consisted of a computer program that was written by Hansz [27] to collect strain and displacement data and to compile this data for analysis. The program permitted the voltage output from the instrumentation to be monitored by pressing a function key on the computer keyboard or at prescribed, programmed-timed intervals during the fatigue testing. The DAS collected burst-readings of the voltage outputs for the instrumentation devices. Each burst-reading lasted for about one second. During that time, voltage output from each instrument was sequentially sampled 60 times. During each of these samples, the voltage output from each instrument was monitored five times and the median value of these five readings was saved as the

test value for a particular sample. By using multiple readings for an individual measurement, the influence of erroneous data produced by electrical noise was minimized. The DAS converted the voltage readings to the appropriate units of measurement for each instrumentation device.

2.3.3. Test Procedure

After each girder specimen was symmetrically positioned and braced in the test frame, the instrumentation was installed and connected to the DAS. Prior to commencing the fatigue testing, the alignment of a specimen was verified by incrementally loading the specimen several times from the unloaded state to the maximum load that the specimen would experience in a load cycle. Strains and displacements were recorded during the incremental static loading to observe whether essentially linear, load versus strain and load versus displacement relationships were produced. This initial loading phase established whether additional shimming or repositioning of the supports for a specimen was necessary.

After the initial stability of the specimen was confirmed, the instrumentation measurements were initialized when the load from the hydraulic actuators was equal to zero. Additional measurements were recorded when the actuators applied the minimum and maximum cyclic loads (P_{\min} and P_{\max} , respectively). For these load levels, a constant load was maintained; therefore, these readings were referred to as static-load readings. Static-load readings were taken before and after a cyclic-load, test sequence was performed on a specimen.

Each specimen was visually inspected during the dynamic loading to establish whether adjustments in the load or support positions were required. Excessive support motion or twisting of the top flange plate of a specimen indicated misalignment conditions. Adjustments at the support or load points were made to minimize these motions prior to the resuming the fatigue testing. After several hundred load cycles were applied to a specimen and after the displacement responses of a

specimen had reached an essentially stable hysteretic condition, the stroke interlocks for the hydraulic rams were set to prevent over-loading of a specimen or damaging the test equipment, if a specimen became geometrically unstable.

During the dynamic loading of a specimen, instrumentation readings were automatically recorded at specific time intervals. The length of a particular time interval was a function of the load frequency and the number of anticipated load cycles that would produce a fatigue failure at a particular weld. If the cyclic loading did not produce a fatigue fracture after the number of load cycles had significantly exceeded the anticipated endurance limit for constant-amplitude, fatigue load, the stress range was increased and the cyclic loading was continued at the higher stress level. Eventually, a fatigue fracture developed at one of the stress concentration points within a specimen.

After a fatigue crack developed, the dynamic loading of a specimen was stopped, so that the crack could be documented and girder reinforcement techniques could be initiated. A girder specimen was strengthened at the location of a fatigue crack, so that further dynamic loading of the specimen could be performed in an attempt to induce a fatigue fracture at another location in the specimen. After strengthening a girder section, a static-load test was conducted at the minimum and maximum load magnitudes that induced the last fatigue fracture. If new load magnitudes were selected for the continuation of the dynamic loading, another static-load test was conducted at the revised minimum and maximum loads. After completing the static-load tests, the cyclic loading of the specimen was resumed to induce another fatigue fracture or until the dynamic loading of the specimen was terminated.

2.3.4. Fatigue fractures

Three techniques were used to detect a fatigue fracture in a specimen. One method involved visually inspecting a specimen during the dynamic loading of the specimen. Another technique

involved comparisons of the monitored flexural strains to determine if any of the strains were significantly changing as the number of load cycles increased. A significant change in a strain could indicate the propagation of a fatigue crack. The detection of strain fluctuations at one of the monitored strain gauge locations improved the likelihood that a visual inspection near the same location would reveal the initiation of a fatigue fracture. The third and most common means of identifying that a fatigue fracture occurred involved the activation of a stroke interlock. As previously mentioned, the interlock was set to only allow for a small increase in the amount of deflection of the specimen in a given phase of cyclic loading. Due to difficulties associated with the sensitivity of the interlock mechanism, the displacement variance that was needed to permit for the fatigue testing equipment to operate, without prematurely tripping these interlock devices, caused a fracture crack lengths to be between 1 and 12 in. long when they occurred. Since the load cycles were terminated when the stroke interlock was activated, the number of load cycles that occurred when a fatigue crack was first initiated could not be established. Therefore, for fatigue failures that were detected by this third technique, the number of load cycles that caused the fracture to develop was selected as the number of cycles associated with the activation stroke interlock mechanism.

Each fatigue fracture was examined with a measurement magnifier to determine the length of the crack. This device magnified the viewed region by 30 times its original size and illuminated the area. After a crack was documented, new static-load readings were taken for the minimum and maximum loads that produced the fatigue fracture. After these static tests were conducted, the girder cross section at the fracture location was reinforced to allow for additional dynamic-load testing of other weld details on the same specimen. If a fatigue crack propagated into the web plate of a specimen, the crack tip was located with the aid of the measurement magnifier. To prevent further crack growth, a 1-in. diameter hole was drilled at the end of the fatigue crack through the web plate

of the specimen. The center of the hole was positioned 1/2 in. from the crack tip in the direction of the crack's propagation. The edges of the hole were rubbed smooth with sand paper to remove any potential abrasions that might induce the formation of additional fatigue cracks.

2.3.5. Fatigue fracture reinforcement

Figures 2.15 and 2.16 show the structural steel plates that were used to reinforce a specimen that experienced a fatigue fracture at a new, bottom flange, cover plate and/or at the original, midspan bottom flange splice in a long girder specimen. The cover-plate, repair detail no. 2 shown in Fig. 2.16 was used only once, as a bottom flange reinforcing plate, after fatigue fractures at both the new, bottom flange cover plate no. 2 and original, midspan, bottom flange splice had occurred in the long, exterior girder specimen no. 1. This long repair plate was used in an attempt to reinforce this girder specimen at both locations, so that a fatigue fracture at the new, bottom flange, cover plate no. 1 might be developed. However, due to the high-load magnitudes and the length of this repair detail, the original fatigue fractures continued to propagate. Therefore, this long reinforcing plate was not an effective strengthening method. Figure 2.17 shows a double-angle, web plate reinforcement that was placed horizontally on the web plate of a specimen to prevent a web plate, fatigue crack from occurring or to stop the propagation of an existing, web plate, fatigue crack. The bolts used for these repair details were 1-in. diameter, A325 bolts with hardened nuts and washers. The turn-of-the-nut method was implemented to properly tension the bolts.

Figure 2.18 shows the double-angle, web plate brace that was attached along the bottom of the web plate of a long girder specimen after an 8-ft long section of the bottom flange plate and the lower 3-in. depth of the web plate was removed in an attempt to induce a fatigue fracture at the new, horizontal, web plate attachments. Figure 2.19 shows the portion of a specimen that was removed.

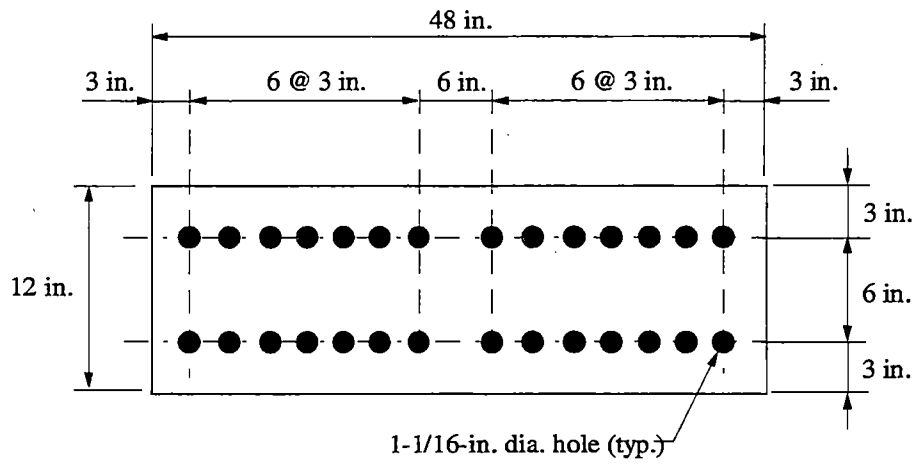


Figure 2.15. Cover-plate repair detail no. 1

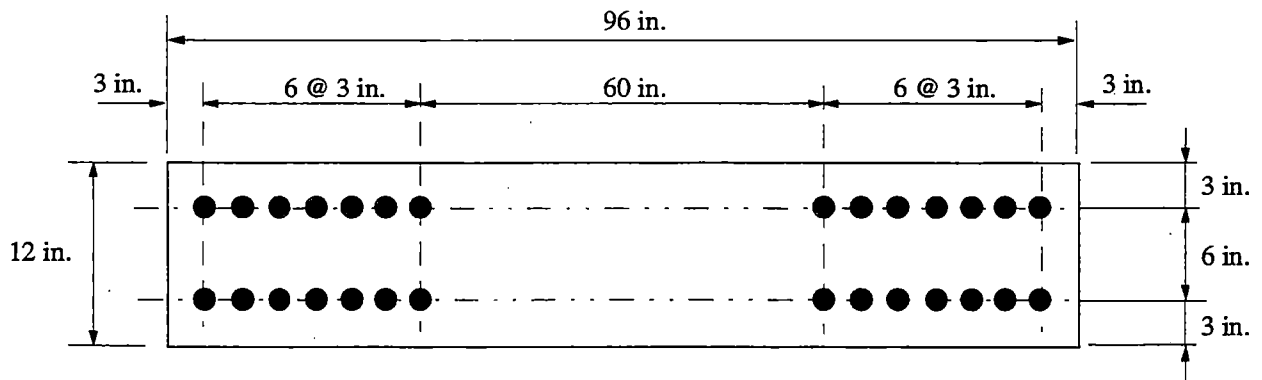


Figure 2.16. Cover-plate repair detail no. 2

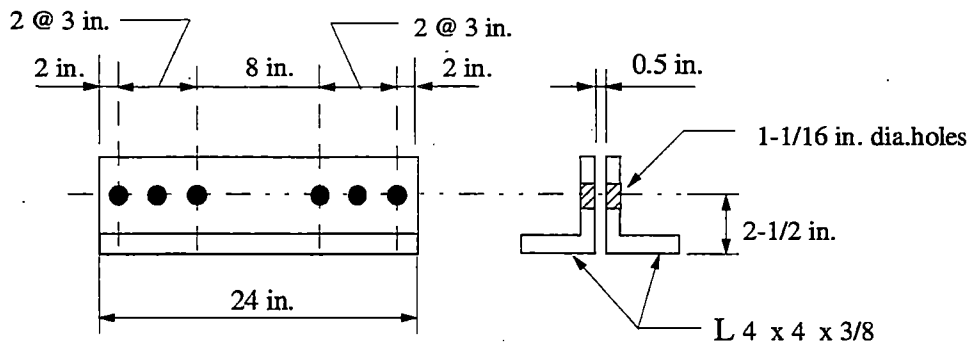


Figure 2.17. Web plate repair detail

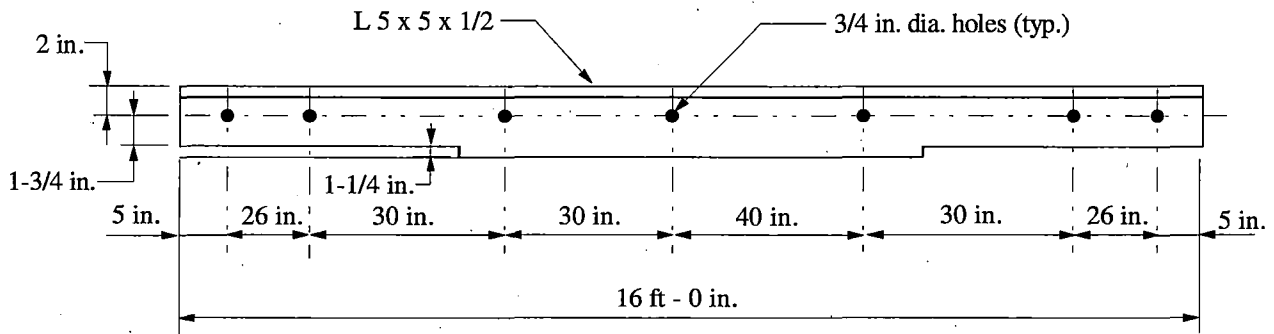


Figure 2.18. Web plate brace for the long girder specimens

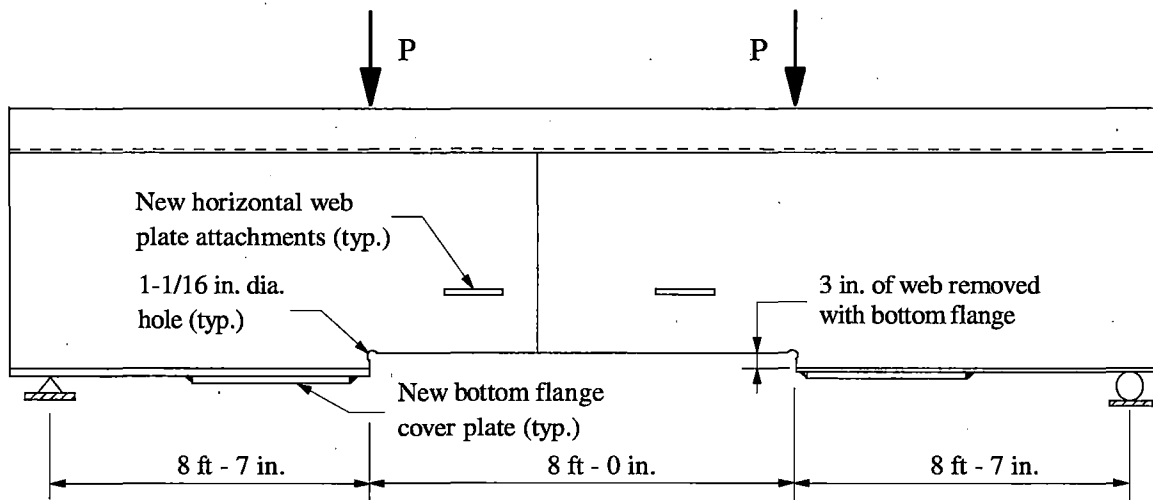


Figure 2.19. Long girder specimen with a portion of the bottom flange and web plate removed

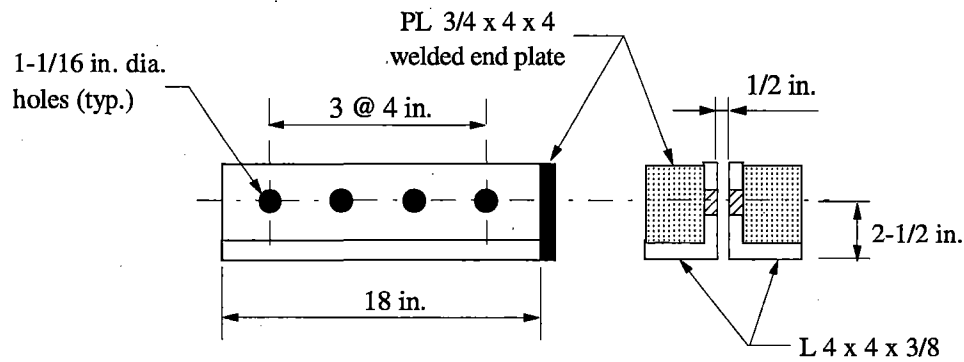


Figure 2.20. Web plate brace at load points

The angle brace was attached along the length of the web plate with 5/8-in. diameter bolts to prevent lateral buckling in the web plate. These bolts, which passed through 3/4-in. diameter holes, were fastened finger-tight to permit slippage between the angle brace and the web plate.

All of the short girder specimens had a slightly warped web plate, which could cause an eccentric loading of these specimens. To prevent vertical buckling of the web plate and to minimize twisting of the top flange plate, the double-angle, web brace shown in Fig. 2.20 was installed under the load points on the short girder specimens. Shim plates were driven between the welded, end plates on these braces and the underside of the top flange plate of these specimens.

CHAPTER 3. EXPERIMENTAL AND ANALYTICAL RESULTS

3.1. Stress Ranges and Events

Four long girder specimens and three short girder specimens were subjected to cyclic loading to induce various stress ranges, SR, in the base and weld metals associated with welded connection details. A total of 17 fatigue fractures occurred at weldments that qualified as Category E details by the Aluminum Association [8]. Ten fractures were in the bottom flange plate for the long and short girder specimens, along the toe of the transverse weld that attached a new, flange cover plate. Four fractures occurred along the new, horizontal web plate attachments on the long girder specimens. Two fractures occurred at the original, midspan, bottom flange plate splice on the long, exterior girder specimens. And, one fracture occurred along the weld of an original, I-shaped, diaphragm connection in the web plate of a long, exterior girder specimen. Secondary fatigue fractures occurred at several holes that were drilled through the web and flange plates. The open holes in the web plate served as crack arresters for previous fatigue fractures. Bolt holes in the web and bottom flange plates were used to attach reinforcement angles and plates that strengthened a girder specimen after a prior fatigue fracture had occurred. A close visual examination of the particular holes that experienced a fatigue fracture revealed that an imperfection along the perimeter of the hole existed at the fracture location.

When a girder specimen was tested, a log book was maintained to chronologically record events relative to the fatigue behavior of the specimen. This information described the experimental, fatigue-life history of the specimen. The date and the number of load cycles were recorded when changes made to a specimen, the test frame and bracing apparatus, and the loading parameters (P_{\min} , P_{\max} , and frequency of loading) and when a fatigue fracture occurred. The log-book information for

a particular specimen was condensed into a tabular format and that information is listed in Tables A1 to A7 of Appendix A.

The test program for each specimen produced a large amount of data in the form of burst-read, data files. These files contain strain, displacement, and load measurements at specific times in the experimental, fatigue-life history of a specimen. While a specimen was being dynamically tested, spreadsheet files were generated to monitor the changes in the magnitude of the longitudinal strain at the gauges that were located near the weldments. Figure 3.1 shows a plot of the strain history for strain gauge nos. 15 and 16 that were located near the bottom flange, cover plate no. 2 on the long, exterior girder specimen no. 1. As the fatigue fracture propagated across the flange width, the measured strain increased at the gauge locations until the fracture grew to a size that caused the deflection of the specimen to activate the hydraulic-ram stroke interlocks, which stopped the testing by shutting off the hydraulic system. The load cycle for which the loading was terminated was chosen as the load cycle for which the fatigue fracture occurred, although the initial fracture may have started long before this load cycle. An examination of the average strains for the two gauge measurements shown in Fig. 3.1 reveals that the bottom flange strains began to increase at about 1,100,000 load cycles, while the testing terminated at about 1,900,000 load cycles.

Figure 3.1 also shows that the measured strains from gauge no. 15 were about 10 to 15 microstrains larger than those measured by gauge no. 16. These strain gauges were symmetrically positioned on the bottom flange plate. The differences in the measure flexural strains were believed to be caused by minor nonsymmetry of the long girder specimen. The longitudinal reinforcement in the concrete slab was not symmetrically positioned across the width of the girder top flange. Also, the web and flange plates on the girder specimen were slightly warped. The girder plates may have been warped during the fabrication, erection, or removal of the bridge girders. Shim plates and

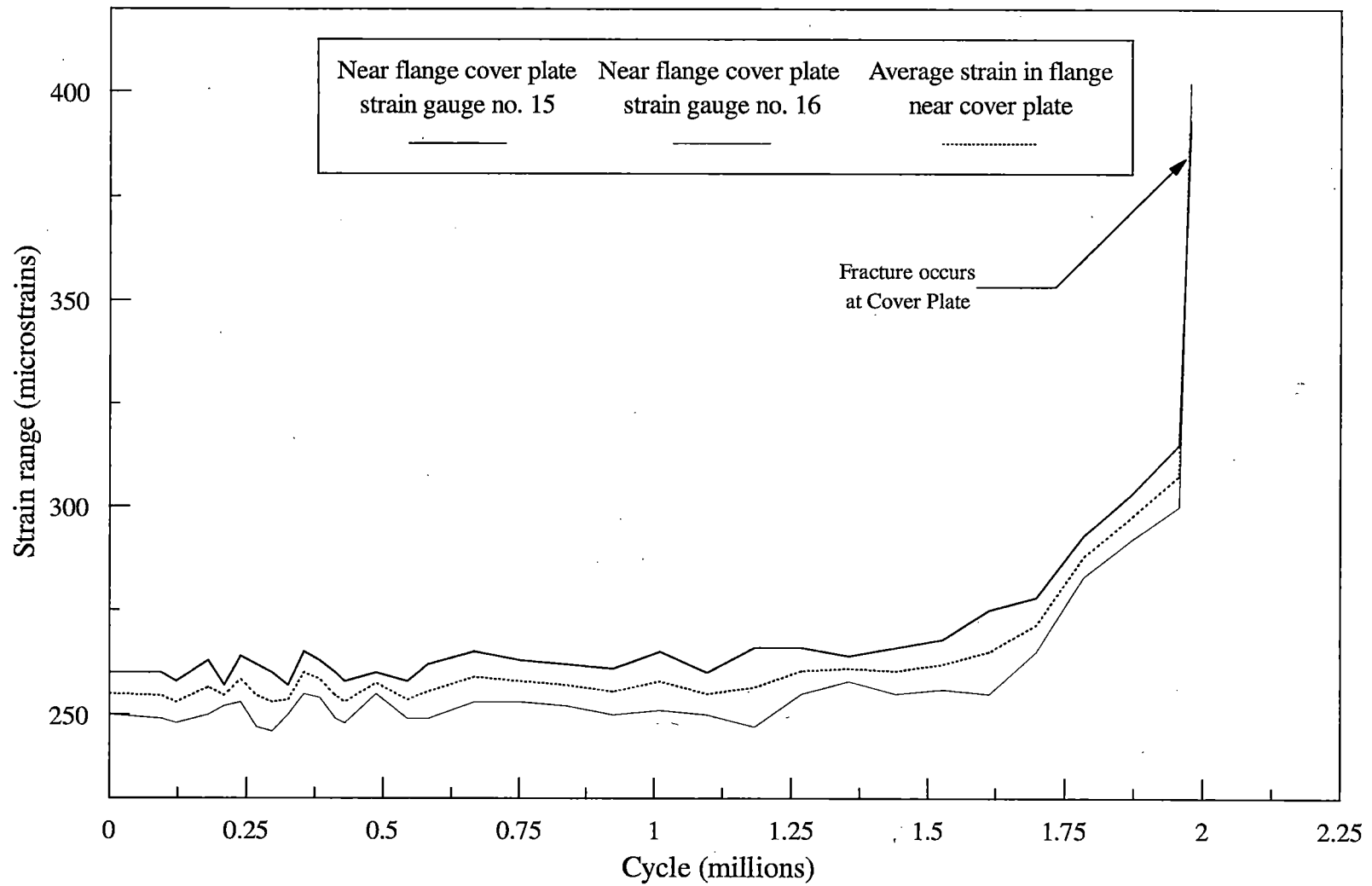


Figure 3.1. Strain history near the flange cover plate no. 2 on the long exterior girder specimen no. 1

bracing at the supports were used in an attempt to eliminate the unsymmetric strain measurements; however, these efforts produced only minimal improvements in the symmetry of the bending strains. Therefore, the average of the two strain gauge readings was used to represent the longitudinal strain in the bottom flange of the girder specimens at these strain gauge locations. The effect of the slightly unsymmetric behavior of the girder specimens on the longitudinal strains in the web plate were considered to be negligible. Therefore, the strains measured by the gauges that were bonded on one side of the web plate established the web plate longitudinal strains at these strain gauge locations.

As discussed in Chapter 2, the voltage output from the strain gauges were monitored in a burst of 60 readings. The burst-read, data files were compiled in spreadsheets, and the strain data was examined to discard any erroneous readings. Figure 3.2 shows the strain data that was recorded from a burst reading of gauge no. 15 on the long, exterior girder specimen no. 1, after the erroneous data points were eliminated. The resulting sinusoidal function is relatively smooth. The dotted line shown in the figure was drawn to represent the expected strain readings in the region where a voltage spike occurred. Similar curves were constructed for the other strain gauge readings. Since the strain data was used to develop the experimental stress ranges at weld locations, the elimination of strain data associated with voltage spikes was necessary to record the appropriate stress history. After the extraneous strain data was removed from the strain record, the experimental strain measurements at specific weld details were computed by averaging the monitored strains from the appropriate gauges. The resulting strain ranges were established and the corresponding stress ranges were evaluated by applying Hooke's Law. The strain and stress ranges for all of the gauge locations, the minimum and maximum hydraulic loads, and the corresponding displacement magnitudes were chronological listed on spreadsheets.

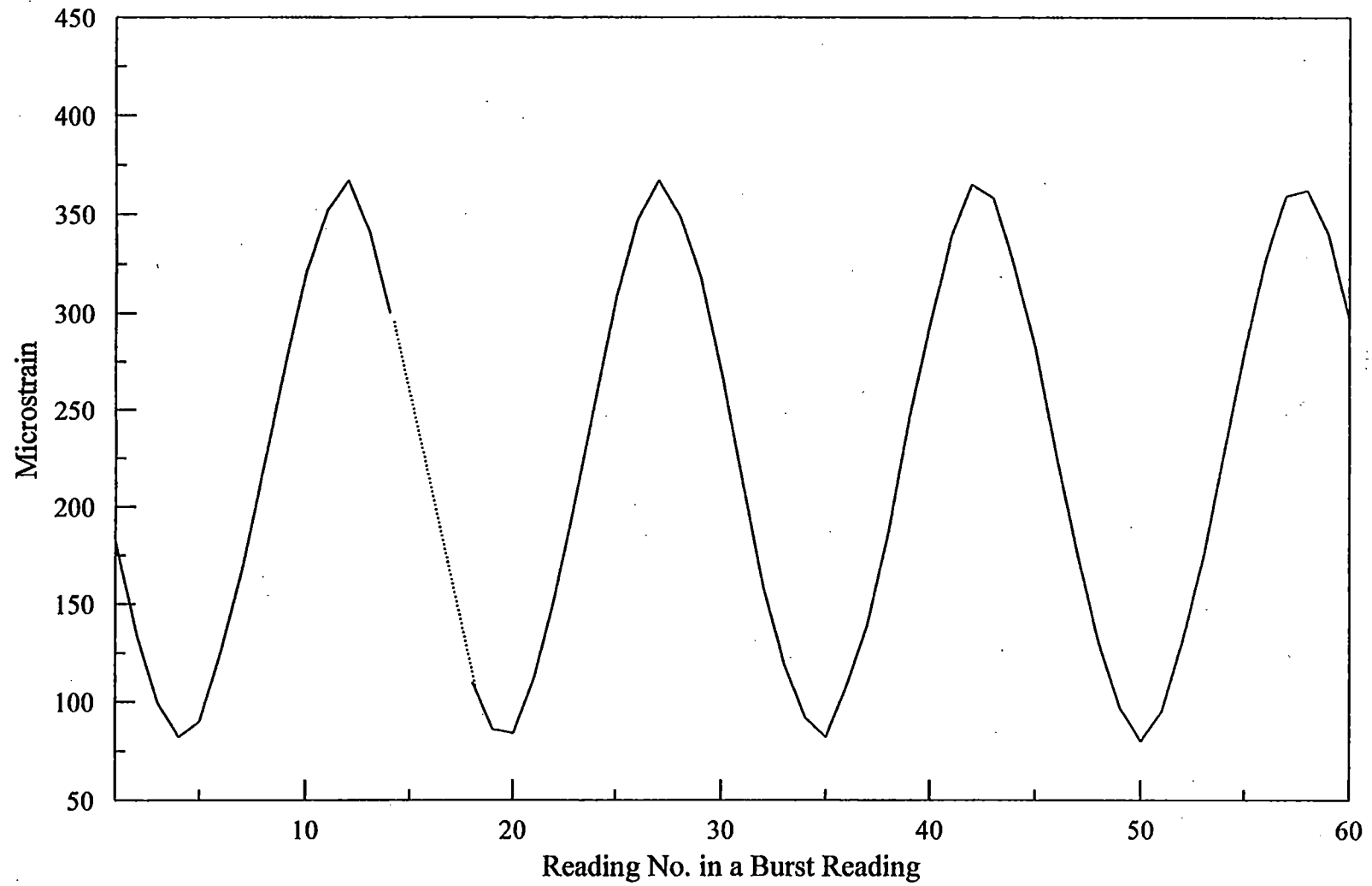


Figure 3.2. Strain readings for strain gauge no. 15 on the long exterior girder specimen no. 1

The measured data from the dynamic-load testing was used to create a stress-history table for each of the girder specimens. These tables contain the theoretical and experimental static and dynamic stress-range data for each specimen that were obtained from the strain-burst readings, which were recorded prior to and after fatigue-life history events. These events included changes in the loading parameters or the discovery of a fatigue fracture. Tables B.1 to B.7 in Appendix B list the stress-history data for the seven girder specimens. Additional information about the fractures or testing events that occurred for the girder specimens is given in Appendix A.

Prior to the fatigue testing of a girder specimen, static loads were applied to a specimen to verify strain linearity and to compare the measured midspan deflection to theoretical values. Graphs of the longitudinal bending strain distribution across the depth of a girder cross section and of the midspan displacement for each of the test specimens are presented in Ref. 27. The strain distribution graphs revealed that a slightly nonlinear strain variation occurred throughout the depth of the long girder specimens, while the short girder specimens exhibited an essentially linear strain distribution. The nonlinear behavior for the long girder specimens was attributed to the close proximity of the original, I-shaped, intermediate diaphragm connection and the new, horizontal, web plate attachments to the vertical alignment of the strain gauges at the instrumented girder cross section, as shown in Fig. 2.11.

3.2. Category E Weld Detail Fractures

3.2.1. Original midspan bottom flange splice

Each of the four long girder specimens had an original, midspan, bottom flange plate splice. Recall that these weldments were made in a fabrication shop prior to the erection of the bridge. The welds at the splice were smooth and without visible imperfections. The fatigue testing of these

specimens induced fractures in the bottom flange plate adjacent to the splice in the two, long, exterior girder specimens. Both fractures occurred through the base metal near the toe of the weld.

Figure 3.3 shows the fatigue fracture that occurred near the bottom flange splice in the long, exterior specimen no. 2 after about 1.06-million load applications. The crack "a" shown in Fig. 3.3a did not extend into the web plate of the specimen. This fatigue fracture propagated over 8 in. across the bottom surface of the bottom flange plate as illustrated by crack "b" in Fig. 3.3b. According to the detail category descriptions given by the Aluminum Association [8], only the tip of this weld is considered to be a Category E detail. The portion of the fillet weld that is parallel to the longitudinal flexural stress direction is classified as a Category B detail, and the portion of the fillet weld that is neither parallel nor perpendicular to the flexural stress direction could be considered to be between a Category B and a Category E detail.

Figure 3.4 is a photograph of the underside of the bottom flange for this long girder specimen at the original, bottom flange splice. The fatigue crack, marked by the black line, extended across the bottom flange width to the hash marks shown at the ends of the black line. The failure started near the apex of the curved edge on the transition plate and propagated in two opposite directions. Figure 3.5 is a photograph of a cut-away view of the interior surface of this same fatigue fracture through the bottom flange plate. The curved portion above the flange plate is the edge of the transition plate. The apex of this transition plate is in vertical alignment with the girder web plate. A close examination of the central region of the fracture surface did not reveal any flaws. The other long, exterior girder specimen experienced an essentially identical fatigue fracture after about 8.64-million load applications.

Although the midspan, bottom flange splices on all of the long girder specimens were similar in quality and geometry, fatigue fractures did not occur at the bottom flange splice on the long,

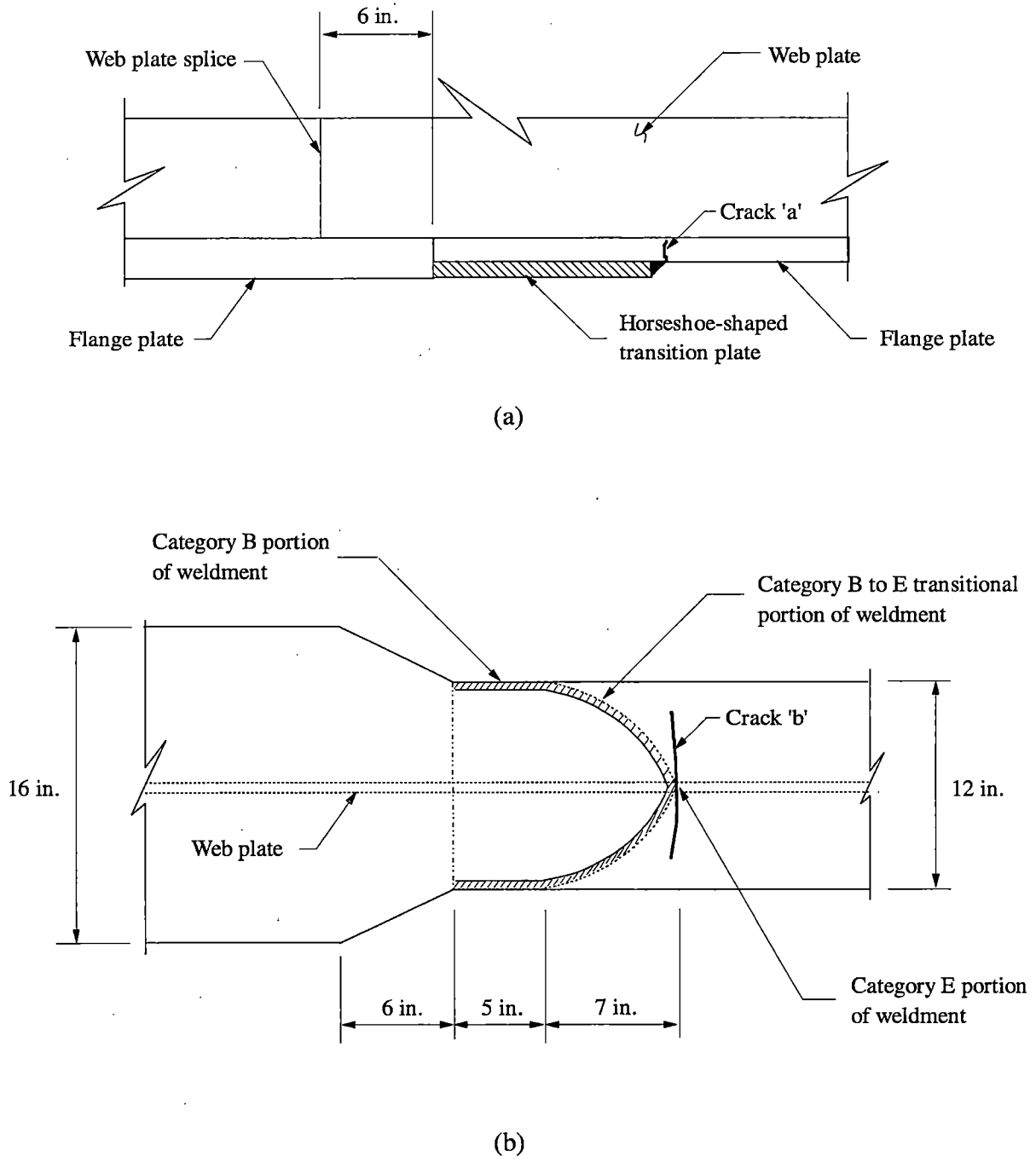


Figure 3.3. Fatigue fracture at the original bottom flange splice in the long exterior girder specimen no. 1: (a) Partial elevation; (b) Underside of the bottom flange

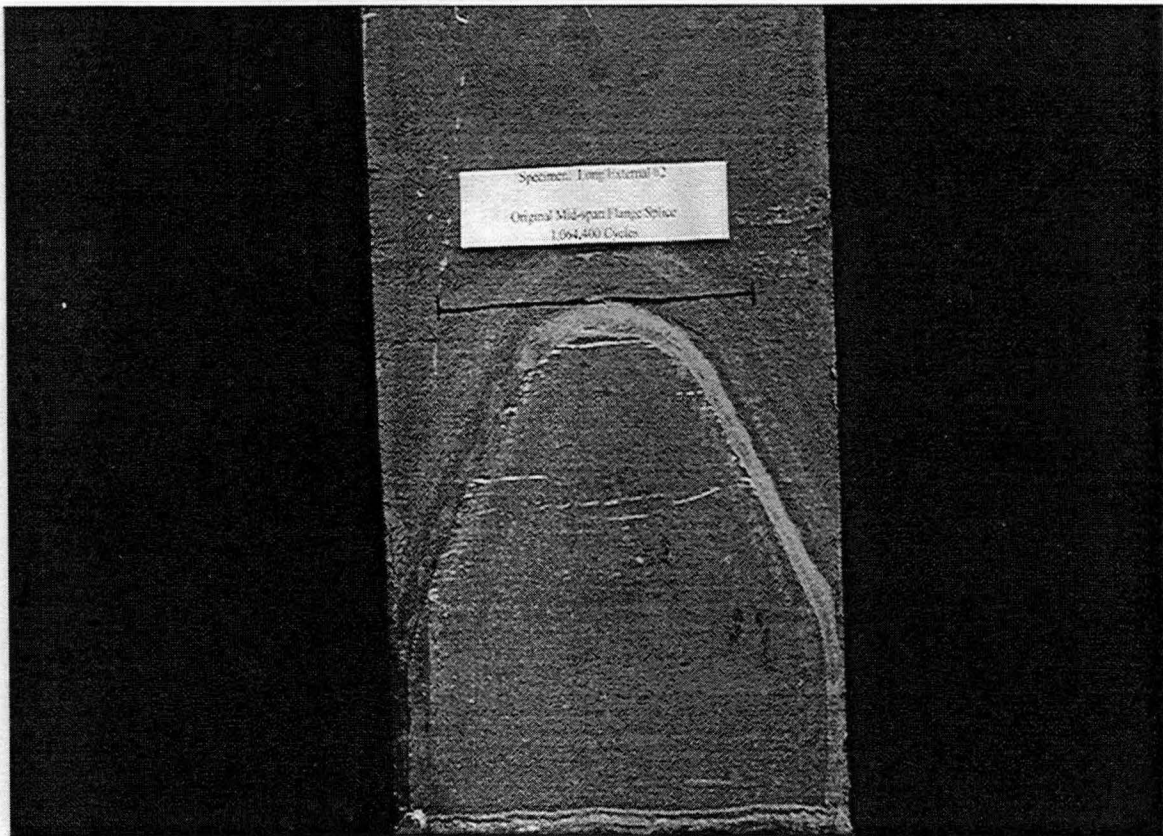


Figure 3.4. Photograph of the fatigue fracture at the original bottom flange splice in the long exterior girder specimen no. 2



Figure 3.5. Photograph of the fatigue surface at the original bottom flange splice in the long exterior girder specimen no. 2

interior girder specimens due to the existence of the original, I-shaped, diaphragm connection that was located on the web plate at a height of 5 in. above the bottom flange splice. A fatigue fracture at the diaphragm weldments in the long, interior girder specimens occurred before a fatigue fracture developed at the original, midspan, bottom flange splice. The failure at the diaphragm connection prevented further testing of these specimens. The dimensions of the fatigue fractures and their location in the base or weld metals that occurred at the original, midspan, bottom flange splice in the long, exterior girder specimens are listed in Table 3.1.

Table 3.1. Original midspan bottom flange splice fatigue fractures

Long exterior girder specimen	Crack length along bottom flange (in.)	Crack length in web (in.)	Weld metal fracture	Base metal fracture
No. 1	11.00	3.38	No	Yes
No. 2	8.25	--	No	Yes

3.2.2. Original I-shaped diaphragm connections

As discussed in Chapter 2, each of the long girder specimens contained an original, intermediate diaphragm, connection. All of the welds between the girder webs and the diaphragm elements had been performed in a fabrication shop, and they appeared to be good quality welds. The exterior girders in the original bridge had I-shaped diaphragms welded directly to the inside face of the web plate, as shown in Fig. 3.6b. The portion of this weld that was across the tip of the diaphragm, bottom flange plate was a Category E weld detail. The interior girders in the original bridge had bracket assemblies whose flange plates passed through slots that were cut in the girder web plate, as shown in Fig. 3.7a. For the slotted web plate, the portion of the weld that was across the thickness of the lower diaphragm plate produced a greater stress riser condition than that which

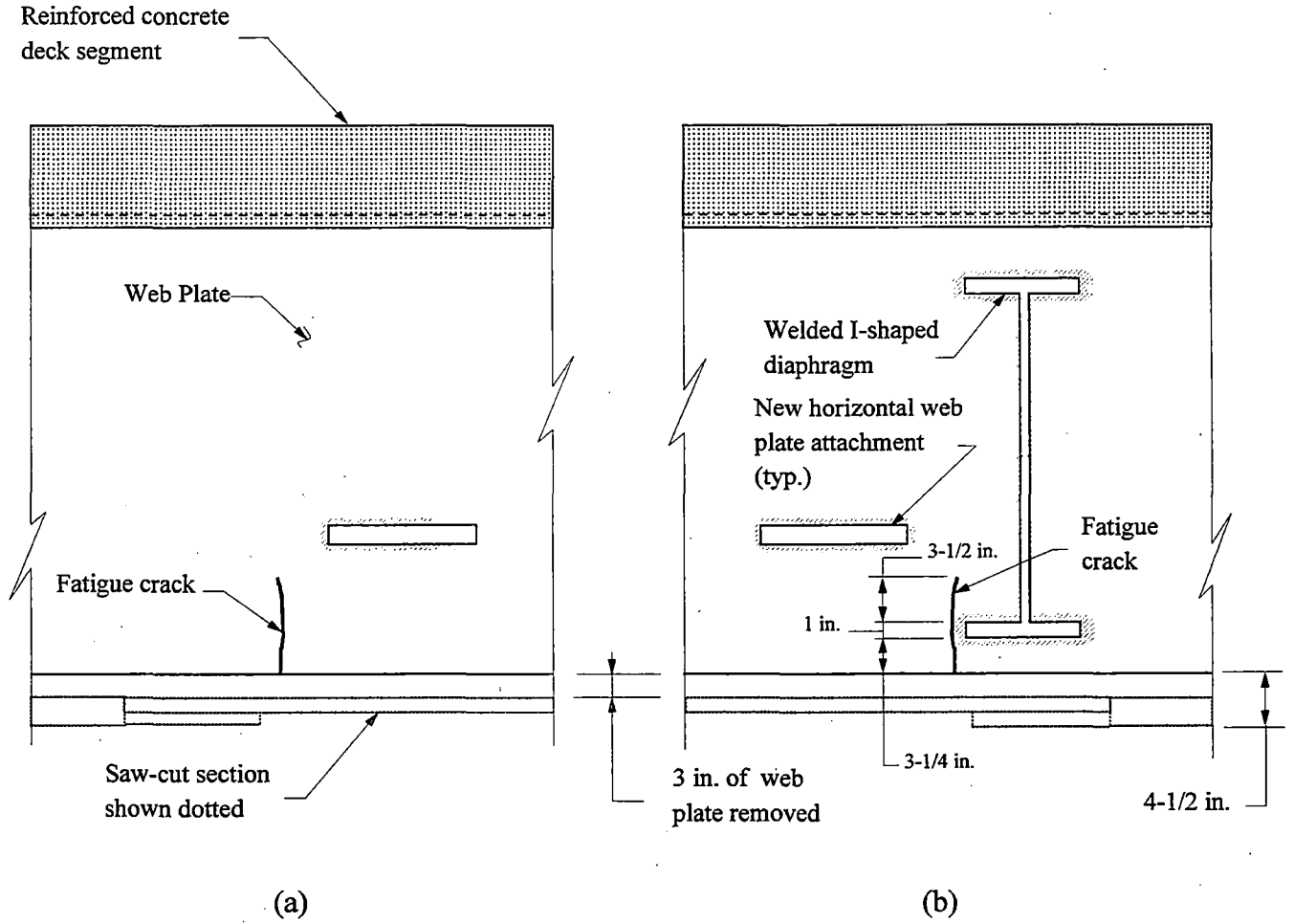


Figure 3.6. Fatigue fracture at the tip of the bottom flange of the I-shaped diaphragm connection on the long exterior girder specimen no 1: (a) Front elevation; (b) Back elevation

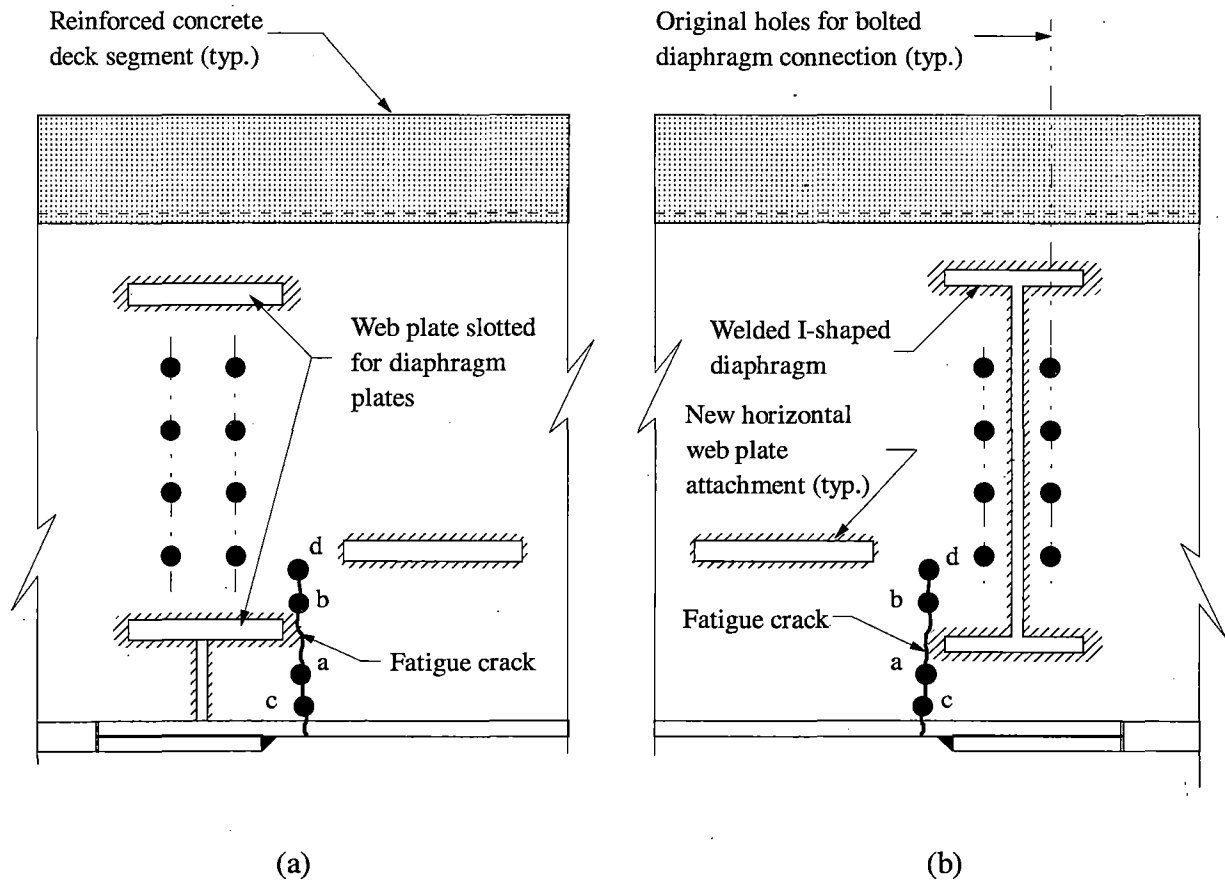


Figure 3.7. Fatigue fracture at the diaphragm connection in the long interior girder specimen no. 1: (a) Front elevation; (b) Back elevation

existed at the same location in the exterior girder specimens. The presence of the girder web plate slot caused this detail to be extremely susceptible to a fatigue fracture. This type of a weld detail has not been addressed by the Aluminum Association design specifications [8].

Three of the four long girder specimens experienced a fatigue fracture at the original, I-shaped, diaphragm connection. The fracture in the long, exterior girder specimen no. 1 occurred after the bottom flange plate and a portion of the girder web plate were removed in an attempt to induce a fatigue fracture at one of the new, horizontal, web plate attachments. Figure 3.6 shows the extent of fatigue crack that developed at the diaphragm location. The fracture occurred through the web plate, base metal at the toe of the weld near the diaphragm, bottom flange tip that was closest to the new, horizontal, web plate attachment. This fracture occurred after an initial application of 8,641,400 load cycles at a nominal-stress range of about 2.5 ksi, an additional application of 818,600 load cycles at a nominal-stress range of about 5.7 ksi, and a further application of 132,500 load cycles with a nominal-stress range of about 8.7 ksi. Due to the similarity between the geometric conditions associated with this fatigue fracture and those corresponding to the new, horizontal, web plate attachments, the diaphragm fracture data for this specimen was included with the data obtained for the new, horizontal, web plate attachments.

Both of the long, interior girder specimens experienced a fatigue fracture in the girder web plate near the diaphragm, lower flange tip that was closest to the new, horizontal, web plate attachment. The extent of the fatigue crack in the long, interior specimen no. 1 is shown in Fig. 3.7. In an attempt to prevent further propagation of the initial fatigue fracture that developed after approximately 2-million load applications, holes "a" and "b" were drilled below and above, respectively, the ends of the initial crack. Due to the location of the fracture, steel reinforcement plates could not be used to strengthen the web plate. After the application of 7.3-million load cycles,

a downward propagation of the fatigue fracture occurred. Hole "c" was drilled in an attempt to arrest further crack propagation in this direction. After 8.1-million cycles, the fatigue crack extended upwards from hole "b". Hole "d" was drilled at the end of this crack extension to permit additional testing of the specimen. However, additional load cycles caused the crack to propagate downward through the bottom flange plate of the specimen and upwards in the web plate. Further repairs on the specimen were not attempted. Therefore, neither the original, midspan, bottom flange splice nor the new, horizontal, web plate attachments on the long, interior girder specimen no. 1 experienced a fatigue fracture. Since the geometrical configuration of the diaphragm connection detail involving the slotted web plate did not match the Category E detail provisions specified by the Aluminum Association [8], this fatigue fracture data was not applied in this study. The dimensions and location with respect to the base or weld metals for the fatigue fractures that occurred at the original, I-shaped, diaphragm connections for the long girder specimens are listed in Table 3.2.

Table 3.2. Original I-shaped diaphragm connection fatigue fractures

Specimen	Crack length above center of connection flange plate (in.)	Crack length below center of connection flange plate (in.)	Weld metal fracture	Base metal fracture
Long exterior girder no. 1	5.25	2.50	No	Yes
Long interior girder no. 1	2.12	1.62	Yes	No
Long interior girder no. 2	2.00	2.25	Yes	No

3.2.3. New bottom flange cover plates

The majority of the fatigue fractures occurred at the new, bottom flange, cover plates. These cover plates were welded at locations outside of the constant-moment regions for the specimens. The appearance of the welds on all specimens was generally consistent; however, they were not as smooth as the original fillet welds that were deposited during the original fabrication of the bridge girders. Some undercutting of the cover plates occurred at the corners of these plates. In addition, the termination point of one weld length and the start of another weld length was often noticeable. The fillet welds that attached the flange cover plates to the girder bottom flange plate involved a Category B weld detail along the flange length, which was parallel to the direction of the longitudinal stress flow, and a Category E weld detail along the ends of the plates, which were perpendicular to the direction of the longitudinal stress flow in the flange.

Figure 3.8 shows the extent of the fatigue fracture that occurred at the toe of the weld for the new, bottom flange, cover plate no. 2 on the short, exterior girder specimen no. 1. This fatigue fracture was developed after approximately 940,000 load applications at a nominal-stress range of 4.85 ksi. The crack extended approximately 8 in. across the bottom flange plate and propagated about 1 in. up into the web plate of the specimen. This type of flange failure was typical for all of the specimens that experienced a fatigue fracture near a bottom flange, cover plate. All of these failures occurred in the heat-affected zone in the flange base metal and were adjacent to the toe of the fillet weld. The dimensions and locations with respect to the base or weld metals for the fatigue fractures that occurred near the new, bottom flange, cover plates for all of the test specimens are listed in Table 3.3. A total of 10 fatigue fractures developed at these details.

After the fatigue tests were completed, the portions of the girder specimens that contained fractures were removed for closer visual examinations. Figure 3.9 is a photograph of the fatigue

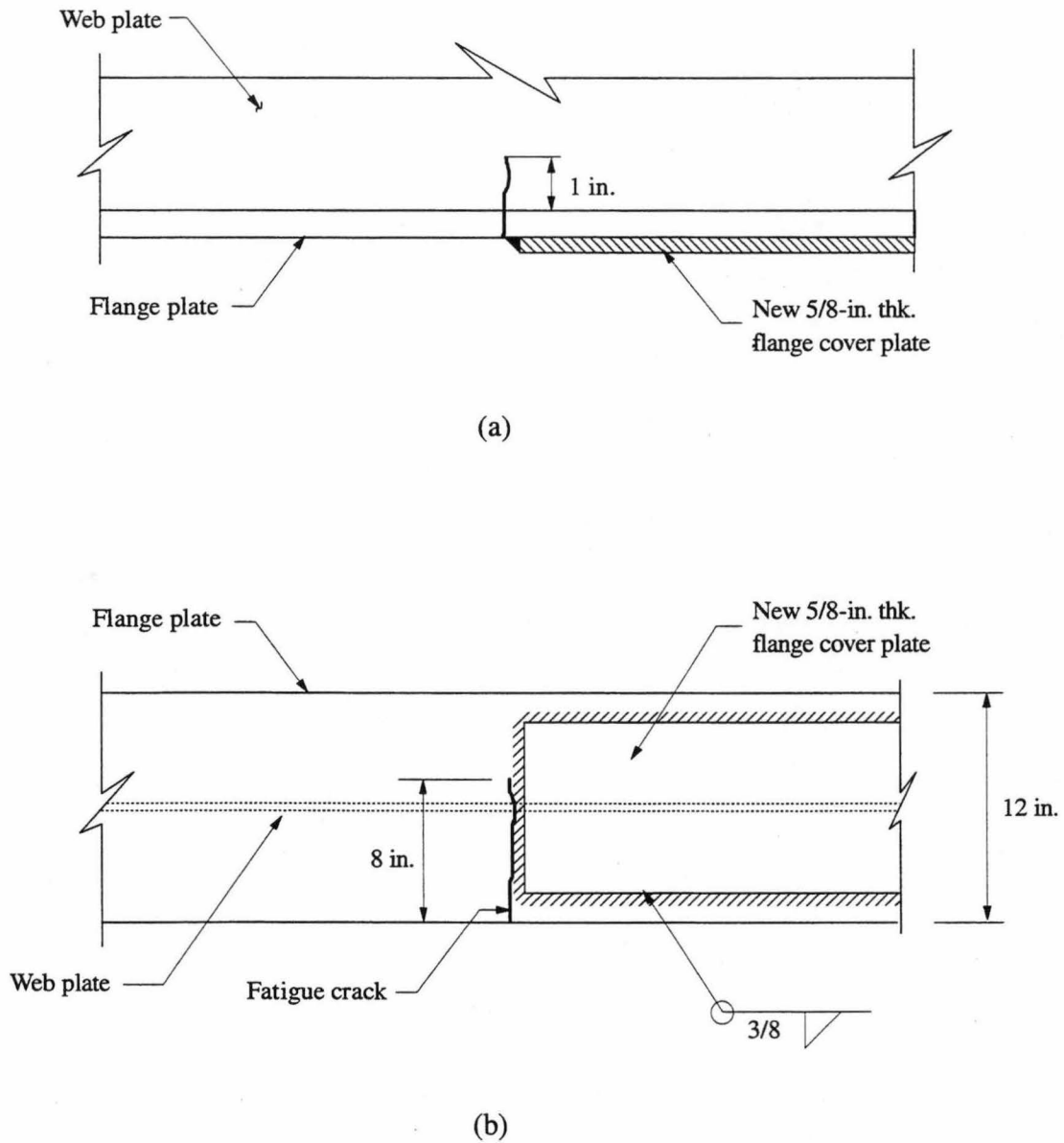


Figure 3.8. Fatigue fracture at the new bottom flange cover plate no. 2 on the short exterior girder specimen no. 1: (a) Partial elevation; (b) Underside of the bottom flange

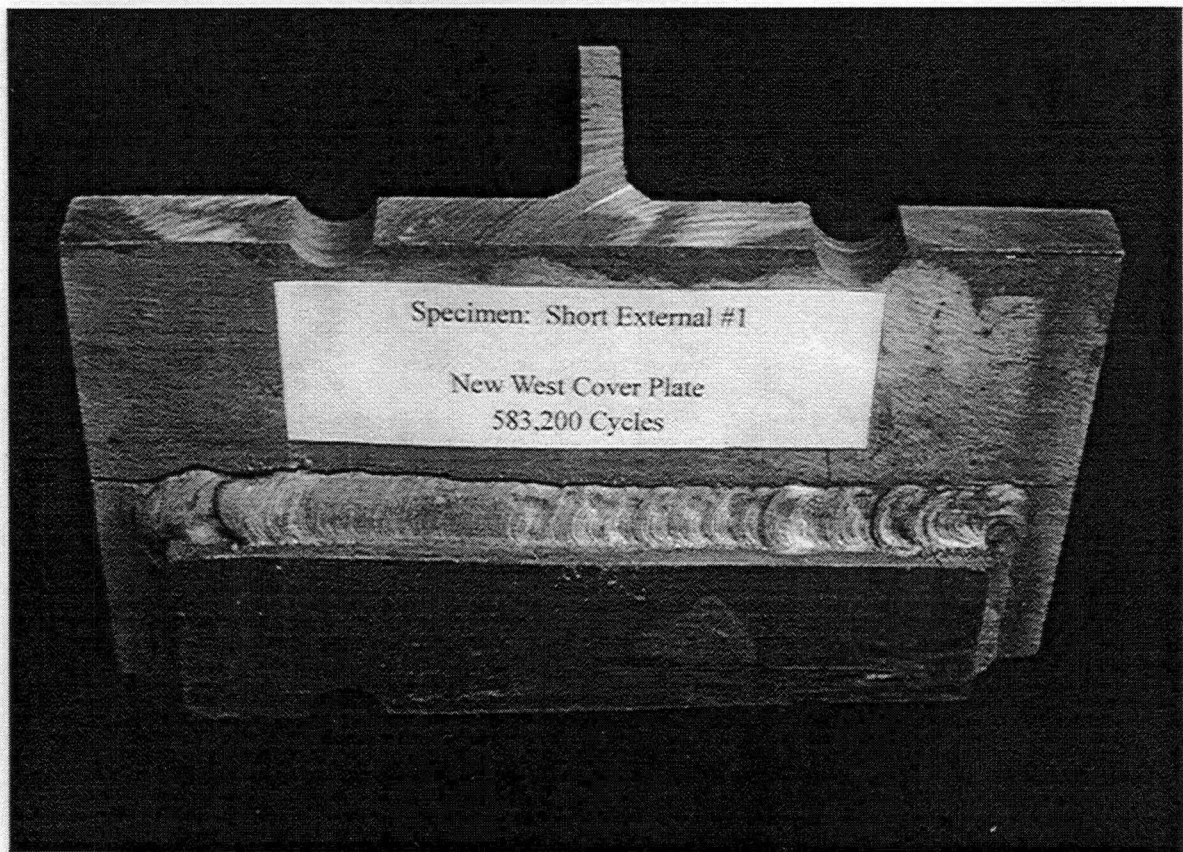


Figure 3.9. Photograph of the fatigue fracture at the new bottom flange cover plate no. 2 on the short exterior girder specimen no. 1

Table 3.3. New bottom flange cover-plate fatigue fractures

Specimen	Cover plate	Crack length across bottom flange (in.)	Crack length in web (in.)	Weld metal fracture	Base metal fracture
Long exterior girder no. 1	No. 2	8.00	1.50	No	Yes
	No. 2	7.00	0.50	No	Yes
Long exterior girder no. 2	No. 2	6.75	0.38	No	Yes
Long interior girder no. 1	No. 2	10.19	---	No	Yes
Long interior girder no. 2	No. 2	6.38	---	No	Yes
Short exterior girder no. 1	No. 1	9.00	1.25	No	Yes
	No. 2	8.00	1.00	No	Yes
Short interior girder no. 1	No. 2	6.50	0.50	No	Yes
	No. 1	10.00	2.75	No	Yes
Short interior girder no. 2	No. 2	7.00	0.50	No	Yes

crack that developed along the toe of the fillet weld between the new, bottom flange, cover plate no. 2 and the bottom flange of the short, exterior girder specimen no. 1. The partial holes shown in the photograph were used to attach a steel reinforcing plate to the specimen after this flange failure had occurred, to permit additional testing of another weld detail. This flange fracture was carefully cut open to expose the interior fracture surfaces. Figure 3.10 is a photograph of the two surfaces along the plane of the fracture. The upper T-shaped portion contains the flange cover plate and the cover plate weld. The lower T-shaped portion was rotated 180° about a horizontal axis so that the left flange tips on both T-shapes are essentially in vertical alignment. A visual examination of the fracture surfaces revealed that the fatigue fracture may have propagated from an overlap in the weld

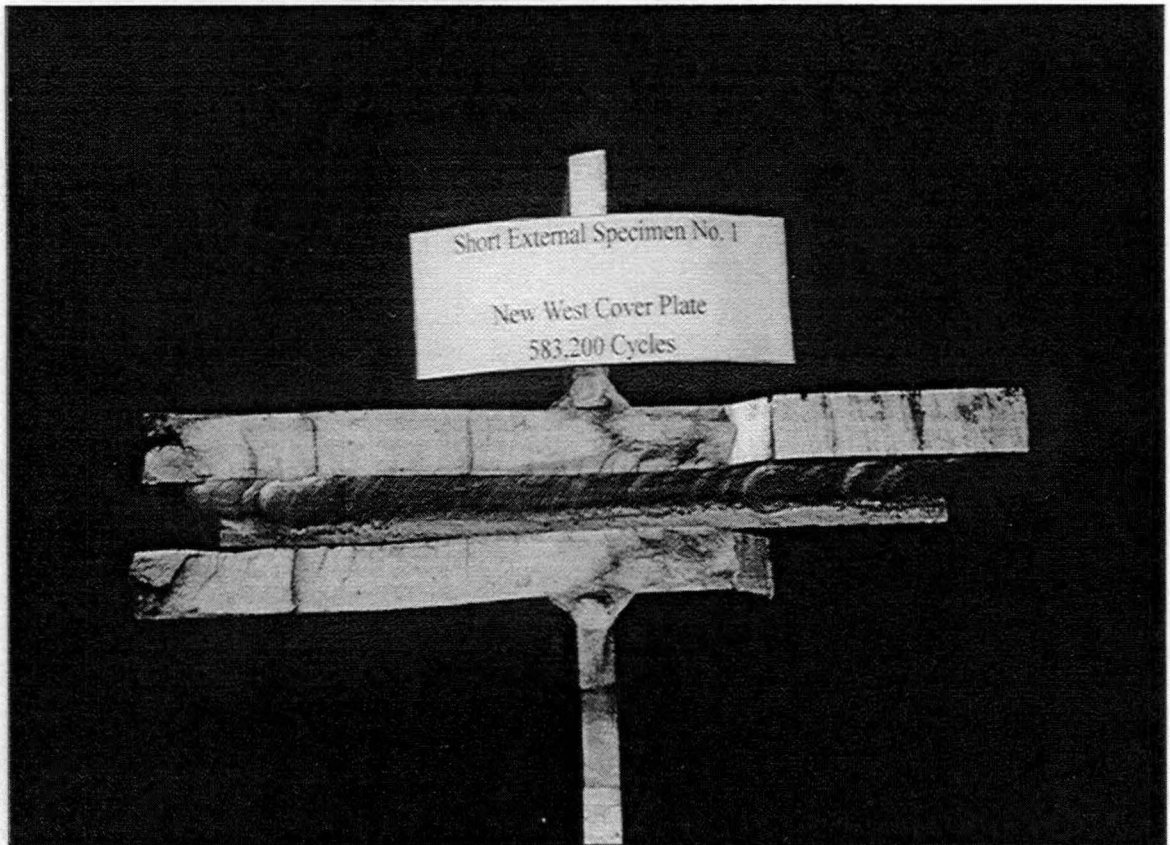


Figure 3.10. Photograph of the fracture surface at the new bottom flange cover plate no. 2 on the short exterior girder specimen no. 1

metal near the end of the cover plate. This type of discontinuity in the weld metal represents an interior flaw that could permit the development of a premature fatigue fracture.

The fatigue fractures near the new, bottom flange, cover plates occurred prior to the formation of the fatigue fractures near the original, midspan, bottom flange splices in three of the four long girder specimens. The nominal-stress range at the Category E portion of the new, bottom flange, cover plate welds was about 88% of the nominal-stress range at the Category E portion of the midspan, bottom flange splice. A comparison of the appearance of the weld along the edge of the new cover plates to that for the original, flange splice revealed that the new weldments were of poorer visual quality than the original weldments. These conditions may have permitted stress raisers to be present on the surface and in the interior of the cover plate welds. As mentioned in Chapter 2, the obvious surface flaws were treated by grinding or rewelding prior to testing, but since fatigue fractures can develop at interior and exterior flaws, such treatments might not have been sufficient to prevent a premature fatigue fracture.

For the short, interior girder specimen no. 1, the fatigue fractures that developed in the girder bottom flange plate adjacent to the weld at both cover plates occurred after 10-million cycles of load application. Several stress-range levels were involved during the testing of this specimen. Initially, a nominal-stress range of 2.3 ksi was induced at the cover plate welds that were closest to the midspan for about 11-million load cycles. Since a fatigue crack had not developed at any point in the specimen, the nominal-stress range was increased to 2.7 ksi at the critical location on the cover plate weld. After about another 0.85-million load cycles were applied at this stress level, a fatigue fracture developed at the bottom flange, cover plate no. 2. After a steel reinforcing plate was bolted to the bottom flange to strengthen the girder at cover plate no. 2, the fatigue loading at the 2.7 ksi nominal-stress level continued until about 16-million load cycles had been applied to the specimen.

To induce a fatigue fracture at the bottom flange, cover plate no. 1, the nominal-stress ratio was increased to 5.0 ksi at the critical section, and the cyclic loading resumed. At about 16.5-million load cycles, the bottom flange of the girder experienced a fatigue fracture at cover plate no. 1. Since this specimen was subjected to variable-amplitude loading, the data from these Category E weld detail fractures were not included in the analysis of data from the constant-amplitude, loading conditions.

3.2.4. New horizontal web plate attachments

The diaphragm connection fatigue fractures in the long, interior girder specimens prevented the fatigue testing of the new, horizontal, web plate attachments in these specimens. Therefore, only the two, long, exterior girder specimens provided fatigue strengths for these weldments. Fatigue fractures occurred at the new, horizontal, web plate attachments on the long, exterior girder specimens prior to the formation of fractures at the intermediate diaphragm connections, even though the nominal-stress range at the web attachments were only about 79% of the stress range that existed at the critical section location for the diaphragm connections. The fillet weld along the ends of the new, horizontal, web plate attachments was a Category E weld detail, while fillet welds along the length of the plate attachments was a Category C weld detail. For these Category E weld details, the quality of the new fillet welds for the web plate attachments must not have been as high as that for the original fillet welds at the intermediate diaphragm connection. Figure 3.11 shows the geometrical configuration and reference dimensions "a", "b", "c", and "d" for the fatigue cracks that developed at the new, horizontal, web plate attachments on the long, exterior girder specimen no. 1. A crack occurred at each end of these plate attachments. Table 3.4 lists the fatigue crack length dimensions above and below the midthickness of the new plate attachment and the location of the fractures with respect to the base or weld metals.

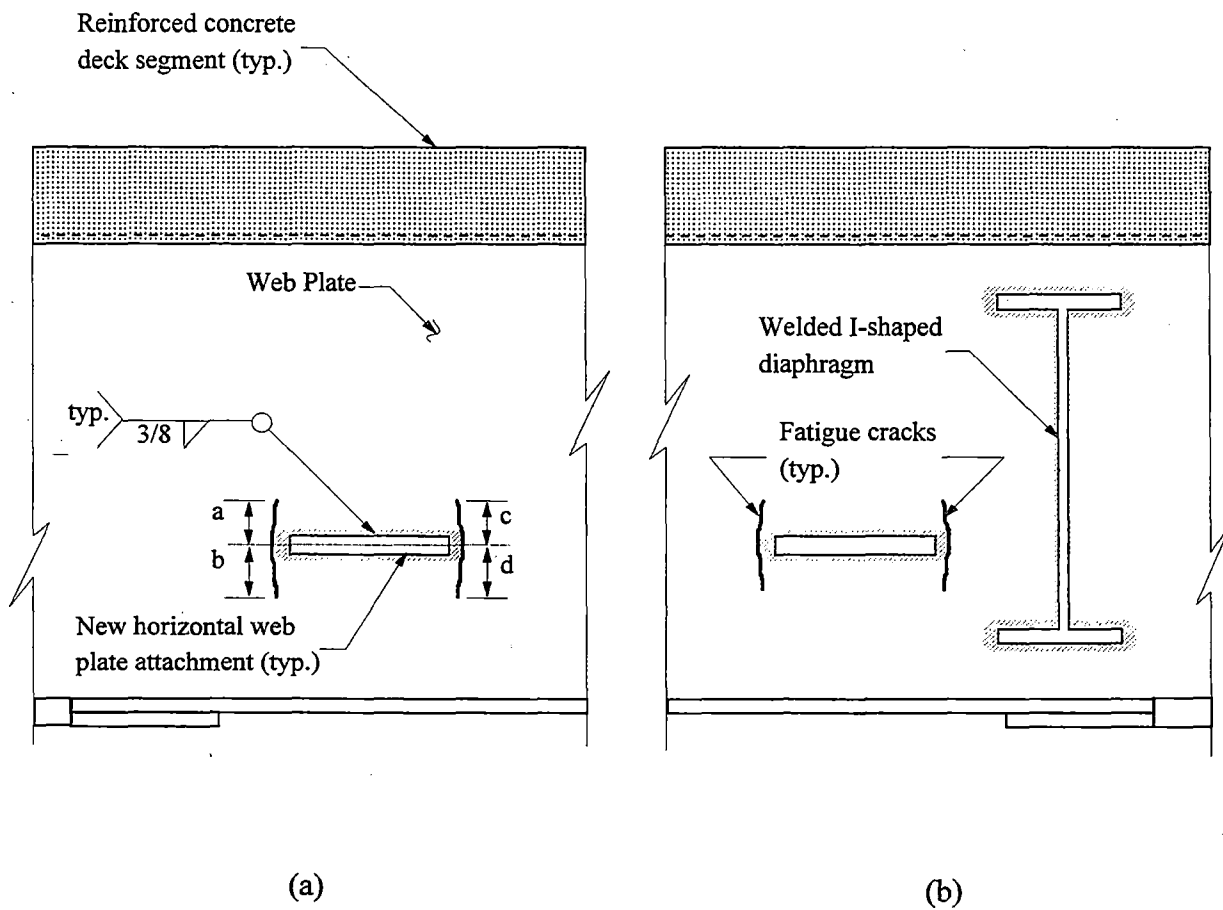


Figure 3.11. Fatigue fracture at the new horizontal web plate attachment no. 1 on the long exterior girder specimen no. 2: (a) Front elevation; (b) Back elevation

Table 3.4. New horizontal web plate attachment fatigue fractures

Long exterior girder specimen	Plate no.	Crack dimensions (in.)		Weld metal fracture	Base metal fracture	Crack dimensions (in.)		Weld metal fracture	Base metal fracture
		"a"	"b"			"c"	"d"		
No. 1	1	0.50	0.50	Yes	Yes	---	---	---	---
No. 1	2	1.25	1.50	Yes	Yes	2.25	2.31	Yes	Yes
No. 2	1	4.00	4.75	Yes	Yes	---	---	---	---
No. 2	2	3.75	4.31	Yes	No	1.00	1.75	Yes	No

Figures 3.12 and 3.13 are photographs of the front and back faces, respectively, of the web plate on long, exterior girder specimen no. 2, that show the fatigue failures at the new, horizontal, web attachments no. 1. These photographs show the web plate attachment orientated in the vertical direction. A visual examination of this fatigue fracture revealed that the crack originated at a point of surface porosity in the weld metal. As discussed in Chapter 2, the web plate attachments were first tack-weld at their ends to the girder web plate before the longitudinal fillet welds were deposited along the plate lengths. Surface porosity is a weld defect that greatly reduces the fatigue life of a weldment [24,32,50]. The fatigue fracture shown in Fig. 3.13 passes through the weld metal, while that same fracture shown in Fig. 3.12 passes through the base metal along the toe of the fillet weld. Except for the new, horizontal, web plate attachment no. 2 in long, exterior girder specimen no. 2, the web plate attachments were accidentally misaligned by approximately 1/4 in. along the length of the specimens. Therefore, a fatigue fracture could propagate through the weld metal on one face of the web plate and through the base metal on the other face of the web plate.

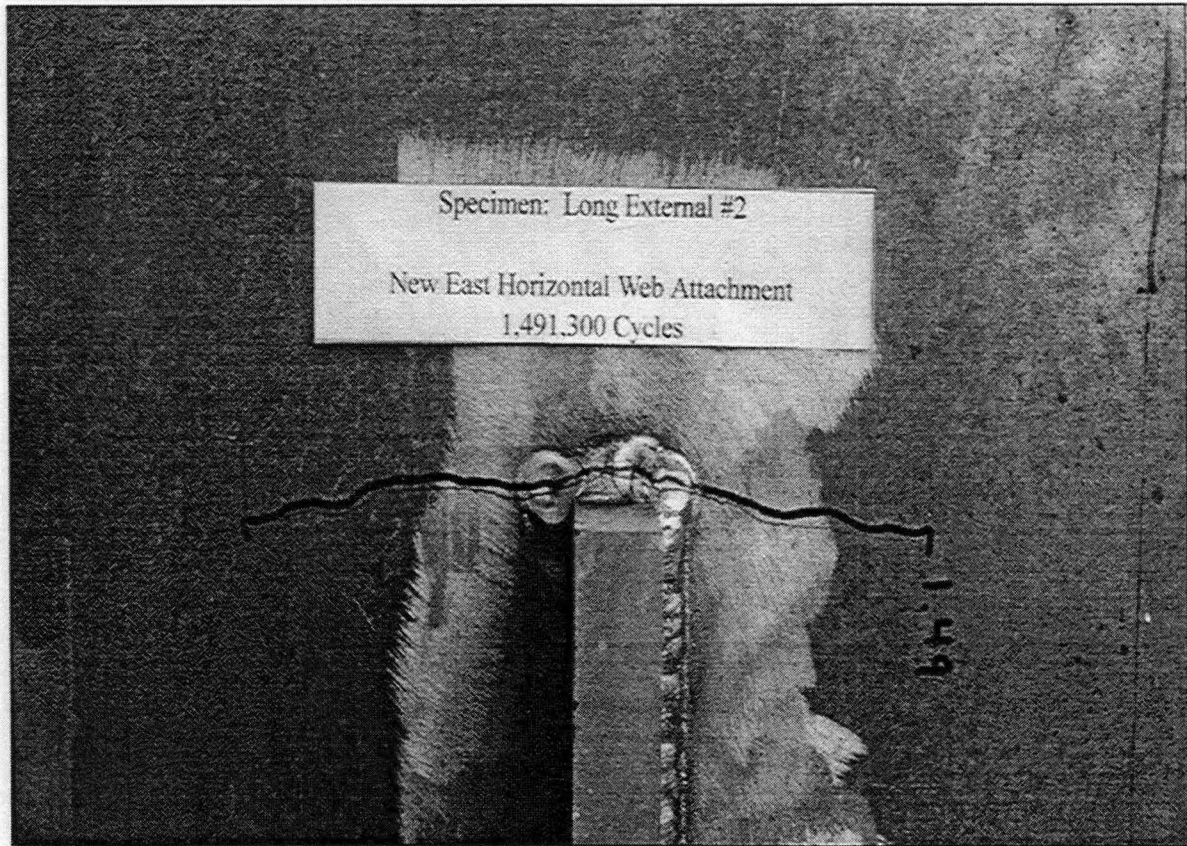


Figure 3.12. Photograph of the fatigue fracture at the new horizontal web plate attachment no. 1 on the front face of the long exterior girder specimen no. 2

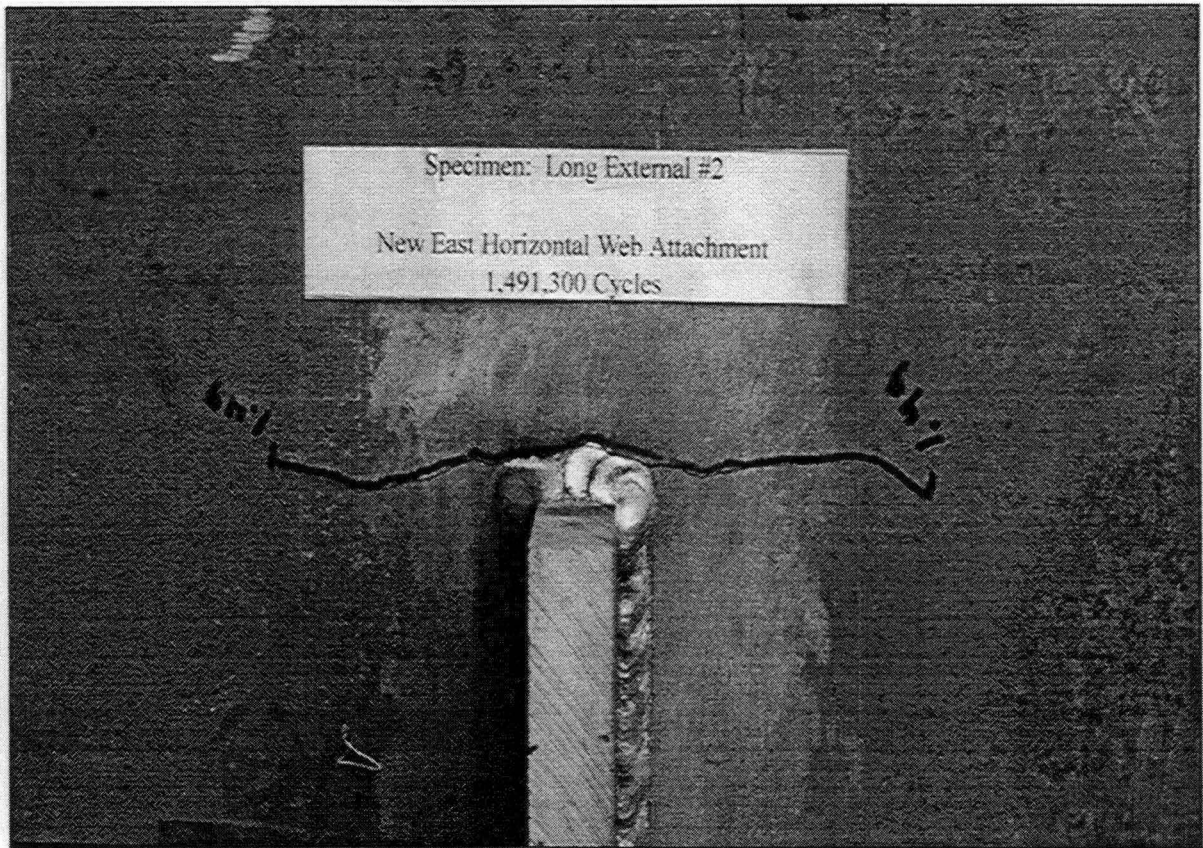


Figure 3.13. Photograph of the fatigue fracture at the new horizontal web plate attachment no. 1 on the back face of the long exterior girder specimen no. 2

3.3. Weldments Not Tested for Fatigue Strength

The scope of this study was limited to the evaluation of fatigue fractures that developed at fillet-welded, Category E details. However, each specimen contained other weld details that were not classified as Category E details. The fatigue strength of these other details could not be evaluated due to the positions of these weldments on the test specimens and due to the damage that each specimen experienced after a fracture developed at a Category E detail. Each of the short girder specimens had four, fillet-welded, partial-height, vertical web stiffeners that qualified as a Category C detail. The load magnitudes, which were applied to the test specimens to induce a fatigue fracture at these web stiffeners, caused the previously developed fatigue fracture at a bottom flange, cover plate to experience crack propagation, regardless of the measures that were implemented to prevent their growth.

The longitudinal welds along the sides of the new, bottom flange cover plates on all of the specimens and the welds along the horseshoe-shaped transition plate at the original, midspan, bottom flange splice that were parallel to the flange tips of the long girder specimens involved Category B details. Fracture fractures at these fillet welds could not be induced due to the large load magnitudes that would have been required to obtain the proper stress range and due to the location of the steel reinforcement plates that were required to strengthen the girder when a nearby Category E weld had previously failed.

Even some of the Category E weld details on the test specimens could not be evaluated for their fatigue strength. In these instances, crack propagation from a previous fatigue fracture prevented additional testing of a specimen. For example, after the original, midspan, bottom flange splice and the new, bottom flange, cover plate no. 2 on the long, exterior girder specimen no. 1 had experienced fatigue fractures, attempts to induce a fatigue fracture at the new, bottom flange, cover

plate no. 1 resulted in the rapid propagation of the fatigue fracture at cover plate no. 2. Attempts to reinforce this girder specimen at cover plate no. 2 were unsuccessful. The dynamic testing of this specimen to induce a fatigue fracture at cover plate no. 1 was terminated after the fatigue fracture at cover plate no. 2 had vertically propagated over 8 in. into the girder web plate.

3.4. Fatigue Fractures at Holes

During the fatigue testing, several fatigue fractures occurred at locations that were not adjacent to a weld. All of these fractures propagated from holes that were drilled in a specimen to allow for the attachment of the steel reinforcement plates, to provide bracing mechanisms, or to provide a crack arrester at the end of a fatigue fracture in the web plate of a specimen. The drilling procedure can produce small nicks and scars around the perimeter surface of a hole. The holes that were drilled through the bottom flange plate of a specimen were made with a magnetic drill that was anchored to a steel plate, which in turn was clamped to the specimen. As long as the core bit for the magnetic drill was sharp, the drilling produced very smooth holes. The holes that were drilled through the web plate of a specimen were made with a hand-held power drill. These holes were often rough. The perimeter surface of these holes were smoothed-out by using a round steel file and sand paper; however, the quality of these holes was not as good as that made with the magnetic drill. When fatigue fractures propagated from holes, these cracks usually occurred in the web plate of a specimen. The damage caused by the fractures in a girder web plate often reduced the cross section of the specimen to an extent that required the termination of the testing for that specimen. In some instances, high-load magnitudes caused a fatigue crack to develop at a bolt hole that was used to attach a steel reinforcement plate to the bottom flange plate of a specimen. The fatigue fractures that developed at holes are described in Appendix A.

3.5. Section Properties and Bending Strains

3.5.1. Neutral axis and moment of inertia

The experimental, longitudinal bending strains were used to calculate the experimental, neutral-axis location, y_{en} , that was measured from the underside of the bottom flange plate of a girder and the experimental, moment of inertia, I_{ex} , with respect to the neutral axis (x-axis) for the girder specimens. Two strain gauges that were in vertical alignment and within the constant-moment region of a test specimen were selected to provide the measured bending strains. The section properties were evaluated as

$$y_{en} = \frac{\epsilon_2 y_1 - \epsilon_1 y_2}{\epsilon_2 - \epsilon_1} \quad (\text{Eq. 3.1})$$

$$I_{ex} = \frac{M(y_n - y_2)}{\epsilon_2 E} \quad (\text{Eq. 3.2})$$

where, ϵ_1 and ϵ_2 = measured bending strains at the strain gauges that were located at heights y_1 and y_2 , respectively, from the bottom of the girder, M = calculated girder bending moment at the gauge positions that was induced by the hydraulic actuators, and E = the modulus of elasticity for the 5083-H113 aluminum alloy, which equals 10,300 ksi. Load and strain values were obtained from a dynamic-burst reading of the instrumentation that was taken early in the dynamic-load testing of each specimen. All of the strains were used with their respective loads to compute the neutral-axis positions and moment of inertia values for a single-burst reading. A statistical analysis was performed on these section properties to determine average y_{en} and I_{ex} -values that were based on the experimental strains for each specimen. A theoretical, neutral-axis location, y_{tn} , and moment of

inertia, I_{xx} , for each girder specimen were determined from the geometrical proportions and the material composition of the individual girder sections by applying engineering mechanics principles. Since the long girder specimens were composite flexural members, the concrete and longitudinal reinforcing bars in a cross section were transformed into an equivalent amount of 5083-H113 aluminum alloy. Table 3.5 lists the theoretical and experimental section properties for the test specimens. For the long girder specimens, the magnitudes of the theoretical and experimental section properties were in relatively good agreement. However, for some of the short girder specimens, significant differences existed between the theoretical and experimental section properties.

Table 3.5. Section properties for the test specimens

Specimen	y_{tn} (in.)	y_{en} (in.)	Diff. (%)	I_{tx} (in. ⁴)	I_{ex} (in. ⁴)	Diff. (%)
Long exterior girder no. 1	31.5	31.3	0.6	17,850	18,100	1.4
Long exterior girder no. 2	31.5	30.8	2.2	17,850	17,450	2.2
Long interior girder no. 1	34.0	32.7	3.8	24,520	24,800	1.1
Long interior girder no. 2	34.0	33.7	0.8	24,520	25,170	2.7
Short exterior girder no. 1	17.8	18.0	1.4	7,070	7,430	5.1
Short interior girder no. 1	17.6	17.3	1.4	9,010	8,980	0.4
Short interior girder no. 2	17.6	16.2	7.7	9,010	8,690	3.6

3.5.2. Strain ranges

Table 3.6 lists the load range; y_{en} , and I_{ex} -values; and the theoretical and experimental strain ranges at the top surface of the bottom flange plate at the end of a bottom flange, cover plate and near the midspan, within the constant-moment region, and the percent difference between these two strain ranges for each specimen. These analytical values were computed by applying engineering mechanics principles, and the experimental strain ranges were determined from the specific strain-gauge measurements. The measured strains were recorded at least 100,000 load cycles before any fatigue fracture had been detected. A comparison of the experimental and theoretical strain ranges for the long girder specimens shows that the experimental strain data related well to the values predicted by theory. A comparison of the experimental and theoretical strain ranges for the short girder specimens consistently showed a significant discrepancy between the predicted and measured strain ranges for the bottom flange, cover plate data, while the strain range differences associated with the gauges that were near the midspan of the specimen were small.

3.6. SN-Relationships

3.6.1. Specimen fatigue strengths

The dynamic loading of a specimen either caused or did not cause a fatigue fracture to develop at a particular weldment. Table 3.7 lists the Category E weld details that developed fatigue fractures in the test specimens during the dynamic loading, the number of load cycles that were applied to cause the fracture, and the nominal and experimental-stress ranges associated with a particular fracture. The experimental stress-range for a fatigue fracture was determined from an evaluation of the strains that were measured over the duration of a particular load range near the weldment. Table 3.8 lists the Category E weld details that did not experience a fatigue fracture after

Table 3.6. Theoretical and experimental strain ranges for the test specimens

Specimen	Load range (kips)	y_{en} (in.)	I_{ex} (in. ⁴)	Strain range at cover plate ^a			Strain range near midspan ^a		
				Theoretical (microstrain)	Experimental (microstrain)	Difference (%)	Theoretical (microstrain)	Experimental (microstrain)	Difference (%)
Long exterior girder no. 1	17.5	31.5	17,850	273	255	6	302	290	4
Long exterior girder no. 2	21.8	31.5	17,850	339	330	3	376	390	4
Long interior girder no. 1	25.2	34.0	24,520	305	283	7	338	342	1
Long interior girder no. 2	25.2	34.0	24,520	305	305	< 1	338	325	4
Short exterior girder no. 1	36.1	17.8	7,070	459	380	17	543	491	10
Short interior girder no. 1	22.2	17.6	9,010	215	145	33	255	235	8
Short interior girder no. 2	27.2	17.6	9,010	264	200	24	313	288	8

^aStrain at the top surface of the bottom flange plate.

being tested at a particular load range for at least 5-million load cycles. The short, interior girder specimen no. 1 was the only test specimen that did not experience a fatigue fracture at a Category E weld detail.

The information given in Tables 3.7 and 3.8 was used to develop two stress-range versus load-cycle relationships (SN-relationships) for the girder specimens. The first SN-relationship that involved the nominal-stress ranges is shown in Fig. 3.14, and the second SN-relationship that involved the experimental-stress ranges is shown in Fig. 3.15. As discussed in Chapter 2, nominal SN-curves are normally used to present fatigue strength relationships. The stress-range and load-cycle data points were plotted on graphs that have logarithmic scales for both axes. The original, bottom flange, splice fractures are shown as solid squares; the new, bottom flange, cover plate fractures are shown as solid circles; and the new, horizontal, web plate fractures are shown as solid diamonds in these figures. The Category E weld details that did not experience a fatigue fracture are shown in Figs. 3.14 and 3.15 as hollow circles with an arrow pointing towards the right, indicating that any potential fatigue fracture for these weld details may occur at a number of load cycles greater than that shown by the data point.

The data for the specimens that experienced a constant-amplitude, cyclic-load, fatigue fracture were statistically analyzed to establish the least-squares-regression line and the lower-bound-strength line shown in Figs. 3.14 and 3.15. A least-squares-regression line, which represents a 50% chance of survival against a fatigue fracture, was obtained by applying a least-squares-linear regression analysis using the Power Regression Method [13] to the fracture data points. A lower-bound-strength line, which is two standard deviations below the least-squares regression line, represents a 95% confidence that 97.5% of the fatigue fractures will occur at stress ranges equal to

Table 3.7. Category E weldments with fatigue fractures

Specimen	Detail	Load cycles (millions)	Nominal stress range (ksi)	Experimental stress range (ksi)
Long exterior girder no. 1	Midspan flange splice	0.64	4.59	4.59
	Cover-plate no. 2 ^a	1.98	2.98	2.74
	Cover-plate no. 2 ^b	1.46	3.07	---
	Horizontal web no. 2	0.13	7.01	6.60
	Horizontal web no. 1	0.14	6.93	6.30
	I-shaped diaphragm	0.13	8.69	9.18
Long exterior girder no. 2	Midspan flange splice	1.06	4.00	4.09
	Cover-plate no. 2	1.31	3.53	3.53
	Horizontal web no. 2	0.18	6.25	5.48
	Horizontal web no. 1	0.18	6.15	5.33
Long interior girder no. 1	Cover-plate no. 2	1.99	3.09	2.72
Long interior girder no. 2	Cover-plate no. 2	1.59	2.98	2.85
Short exterior girder no. 1	Cover-plate no. 1	0.58	4.85	4.04
	Cover-plate no. 2	0.94	4.85	3.93
Short interior girder no. 2	Cover-plate no. 1	9.62	2.80	2.45
^a Failure 7.58 ft from roller support		^b Failure 3.58 ft from roller support		

Table 3.8. Category E weldments without fatigue fractures

Specimen	Detail	Load cycles (millions)	Nominal stress range (ksi)	Experimental stress range (ksi)
Long exterior girder no. 1	Midspan flange splice	8.00	3.20	3.25
	Cover-plate no. 1	8.00	1.66	---
Long interior girder no. 1	Midspan flange splice	8.10	3.60	3.45
	Cover plate no. 1	8.10	2.02	---
	Horizontal web no. 1	8.10	1.33	1.23
	Horizontal web no. 2	8.10	2.25	1.90
Short interior girder no. 1	Cover-plate no. 1	11.00	2.30	1.80
	Cover plate no. 2	5.47	2.70	2.25
Short interior girder no. 2	Cover-plate no. 2	10.55	2.80	2.15

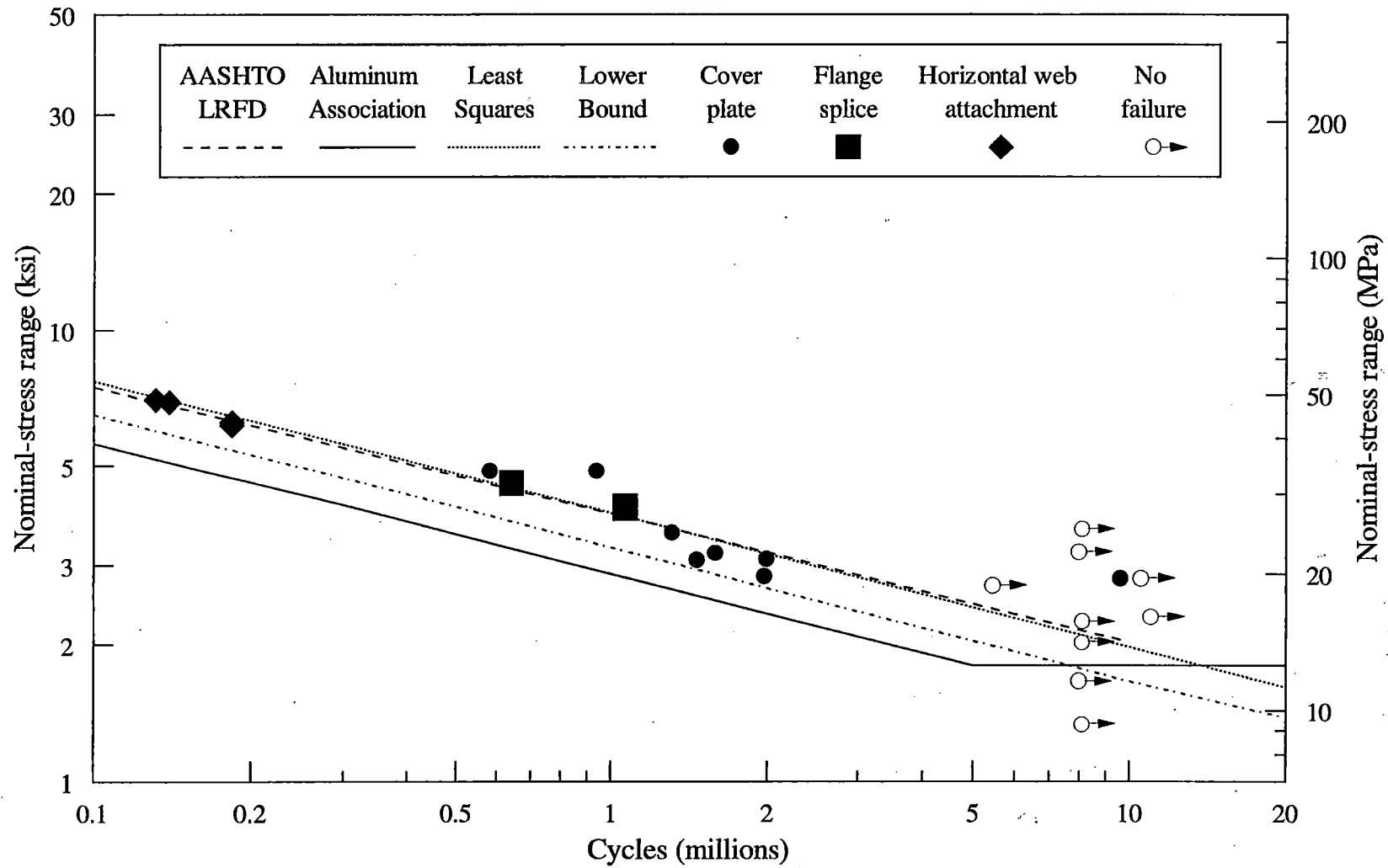


Figure 3.14. Nominal SN-curves for Category E details

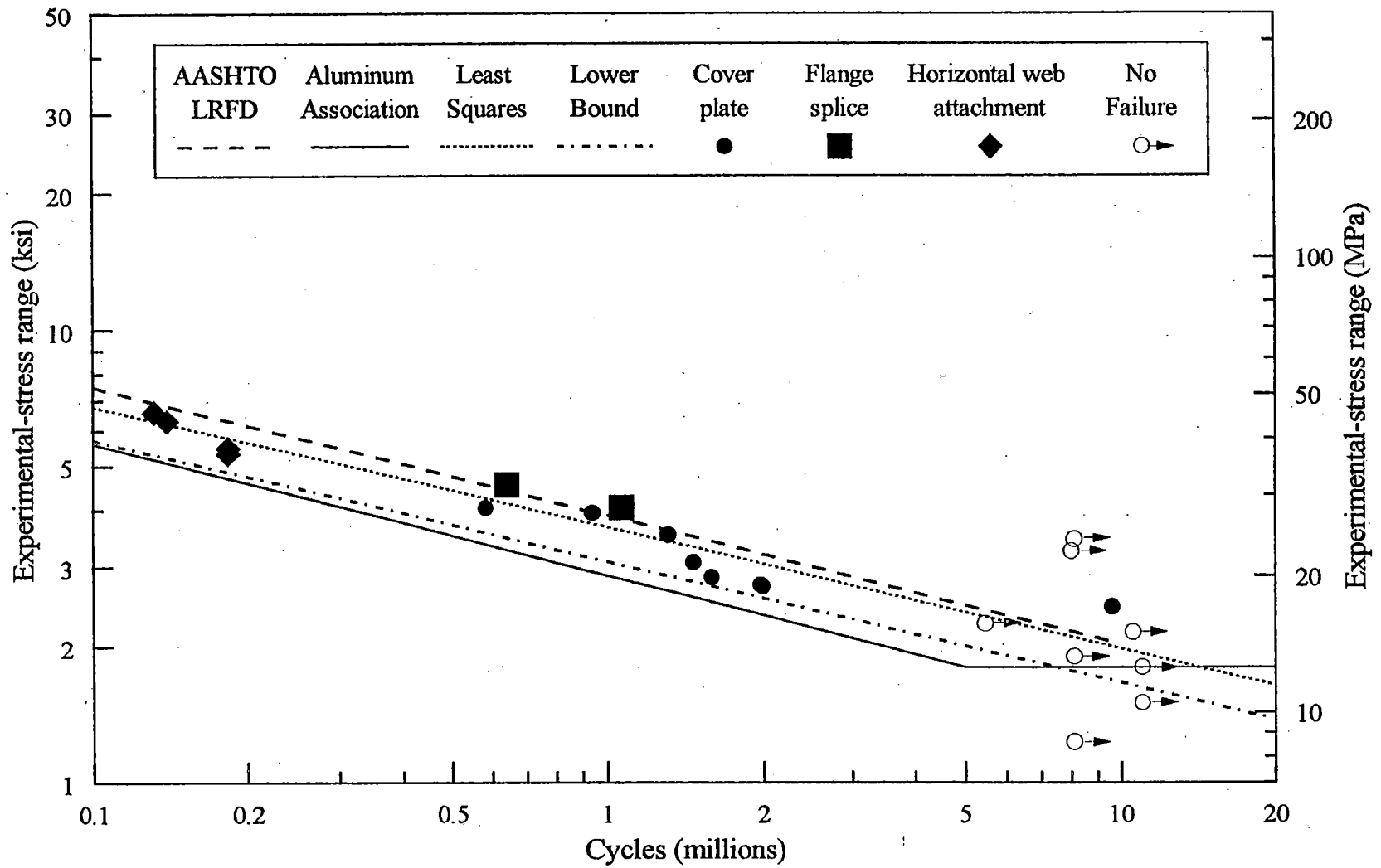


Figure 3.15. Experimental SN-Curves for Category E details

or greater than the stress-range levels associated with this line. None of the SN-data points for the fatigue fractures experienced by the test specimens in this research occurred beneath the lower-bound-strength line.

The heavy dashed line shown in Figs. 3.14 and 3.15 represents the nominal-stress range, fatigue resistance of a member that was developed for the AASHTO-LRFD Specifications [12]. This constant-amplitude, cyclic-load, strength line is given by

$$(\Delta F)_n = \left(\frac{C_1}{N} \right)^{C_2} \geq \frac{1}{2} (\Delta F)_{th} \quad (\text{Eq. 3.3})$$

where, $(\Delta F)_n$ = nominal-stress-range fatigue resistance, C_1 and C_2 are linear-regression-analysis constants associated with a particular weld detail category (for Category E detail weldments: $C_1 = 36.0 \times 10^8$ and $C_2 = 0.237$), N = number of constant-amplitude load-cycles, and $(\Delta F)_{th}$ = constant-amplitude fatigue threshold. For Category E detail weldments, $(\Delta F)_{th} = 2.0$ ksi at 10-million load cycles. Figure 3.14 shows that the least-squares-regression line nearly coincides with the AASHTO-LRFD specification line. The experimental-stress-range, least-squares-regression line shown in Fig. 3.15 is lower than the AASHTO-LRFD specification line.

The solid line shown in Figs. 3.14 and 3.15 represents the allowable-stress range for Category E weldments that was developed by the Aluminum Association [8]. This SN-relationship applies to constant-amplitude, fatigue loading and is defined by

$$S_{rd} = AN^{-1/m} \quad (\text{Eq. 3.4})$$

with $S_{rd} \geq S_{ra}$, where S_{rd} = allowable, fatigue strength, stress range; S_{ra} = induced, service-level, nominal-stress range at the weldment; A = stress-range (y-axis) intercept at $N = 1$; N = number of

constant-amplitude, load cycles; and m = absolute value of the slope of the linear-regression line. For Category E weld details, $A = 160$ ksi and $m = 3.45$ ksi. A constant-amplitude threshold is assumed to exist 5-million load cycles. The Aluminum Association's SN-curve was established at two standard deviations below the least-squares, linear-regression line drawn through the fatigue-fracture data points for the mostly small-size specimens used for their study. The fatigue strength for each of the Category E weld details that experienced a fracture in the ISU research corresponded to strengths greater than the allowable-stress-range limit specified by the Aluminum Association.

3.6.2. SN-curve comparisons

The least-squares, linear-regression lines that were developed from this study and from an investigation of only large-size, Category E weld details (cover-plate fatigue fractures) by Erickson and Kosteas [19] are shown in Fig. 3.16. In their comparison of large and small-size specimens involving transverse, fillet-welds, Erickson and Kosteas noticed a significant reduction in the fatigue strength as the size of the weldment increased. Each linear-regression line corresponds to fatigue tests that were conducted at a specific stress ratio, R . Although some researchers [21,24,34] note that the stress ratio does not have a significant influence on the fatigue life of a structural steel weldment, Erickson and Kosteas [19] and Tomlinson and Wood [55] have stated that the stress ratio affects fatigue life of aluminum weldments. The influence of the stress ratio on fatigue life has not been included in 1994 edition of the Aluminum Association [8] fatigue provisions.

Figure 3.16 shows that the linear-regression line for $R = -1.0$ (full-strain reversal) is significantly higher than the linear-regression lines for $R = 0.05$ and $R = 0.1$. When a full-strain reversal exists, the stress range required to induce a fatigue fracture at a weldment for a specific number of load cycles is larger than that for any other stress ratio. This fact can be explained by realizing that fatigue damage occurs from repetitive tensile strains and that for a full-stress reversal,

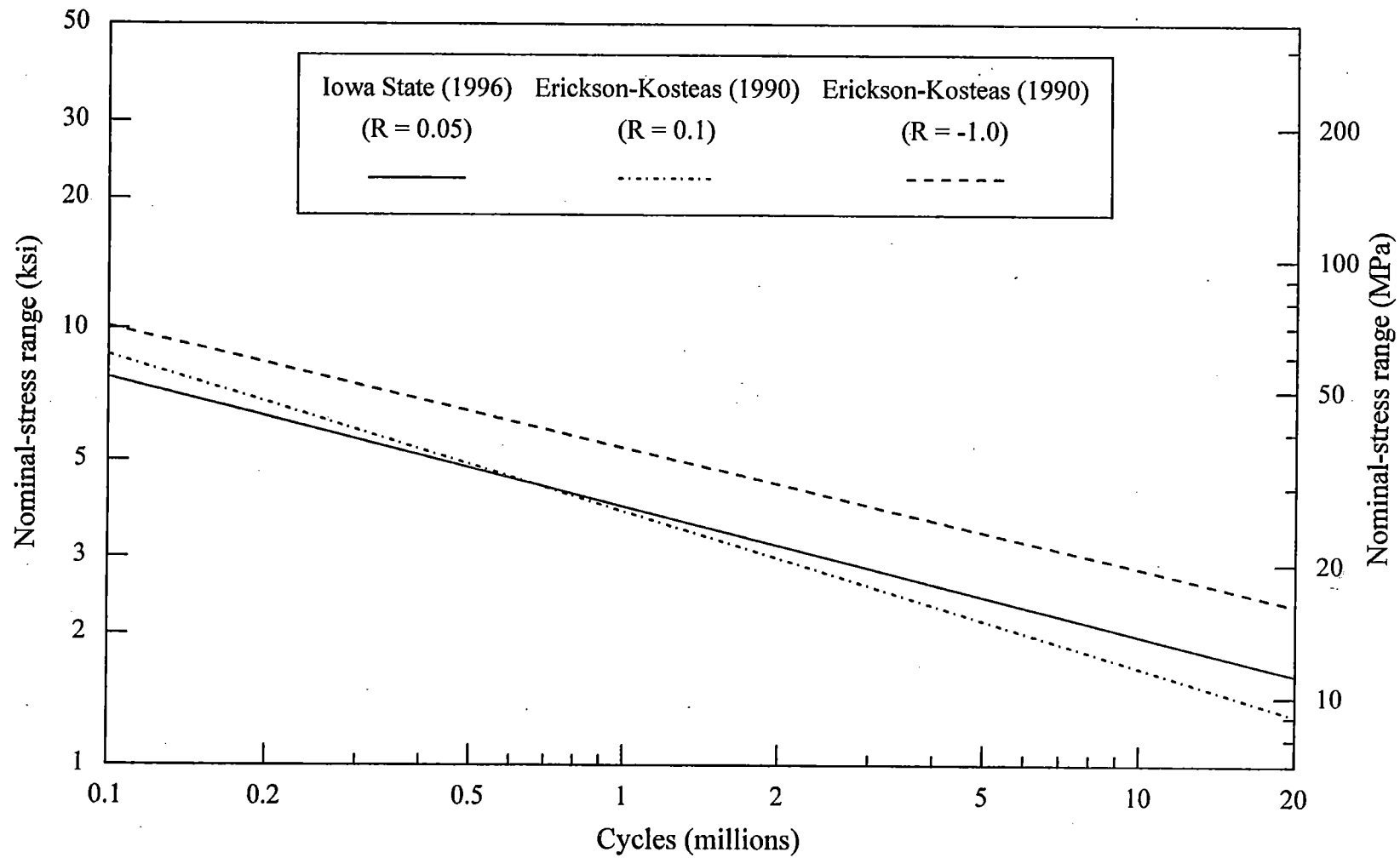


Figure 3.16. SN-curves for transverse-fillet welds on full-size specimens

the compressive portion of the stress range is the same as that for the tensile portion. Therefore, the peak-tensile strain for a negative stress-ratio condition is lower than that for a positive stress-ratio condition. Figure 3.16 shows that the least-squares, linear-regression line for this study, in which $R = 0.05$, is close to the least-squares, linear-regression line by Erickson and Kosteas [19] with $R = 0.1$. The use of similar specimens, weld details, and loading methods attributed to the development of similar SN-curves. The small difference in the two positive stress ratios that existed between the two test programs should not have significantly alter the fatigue behavior of a specimen.

In an attempt to investigate the effects of the size of Category E weld details on their fatigue fracture strength, the fracture results from the ISU, full-size specimens with $R = 0.05$ were combined with the fracture results from the tests by Erickson and Kosteas for their full-size weldments with $R = 0.1$ and -1.0 . These data points were statistically analyzed through a least-squares, linear-regression analysis to obtain a single, linear-regression line for full-size weldments that does not consider the influence of the stress-ratio on the fatigue strength of a specimen. This regression line is shown as the solid line in Fig. 3.17. A data set of fatigue fractures for mostly small-sized, Category E weld details was gathered by representatives of the Aluminum Association from the fatigue test programs of other researchers. These fatigue fractures involved both small-size and full-size weldments; however, the vast majority of those previous tests were conducted using small-size specimens. A linear-regression analysis of these fatigue fracture, SN-data points produced the linear-regression line that is shown as the dotted line in Fig. 3.17. The regression line for the mostly small-size weldments was above the regression line for the full-size weldments; therefore, the scale of an aluminum weldment initially appears to have an influence on the fatigue strength of a structural member. However, these results are not conclusive because the effect of different stress ratios on fatigue strength has not been eliminated. Both regression lines shown in Fig. 3.17 involved a

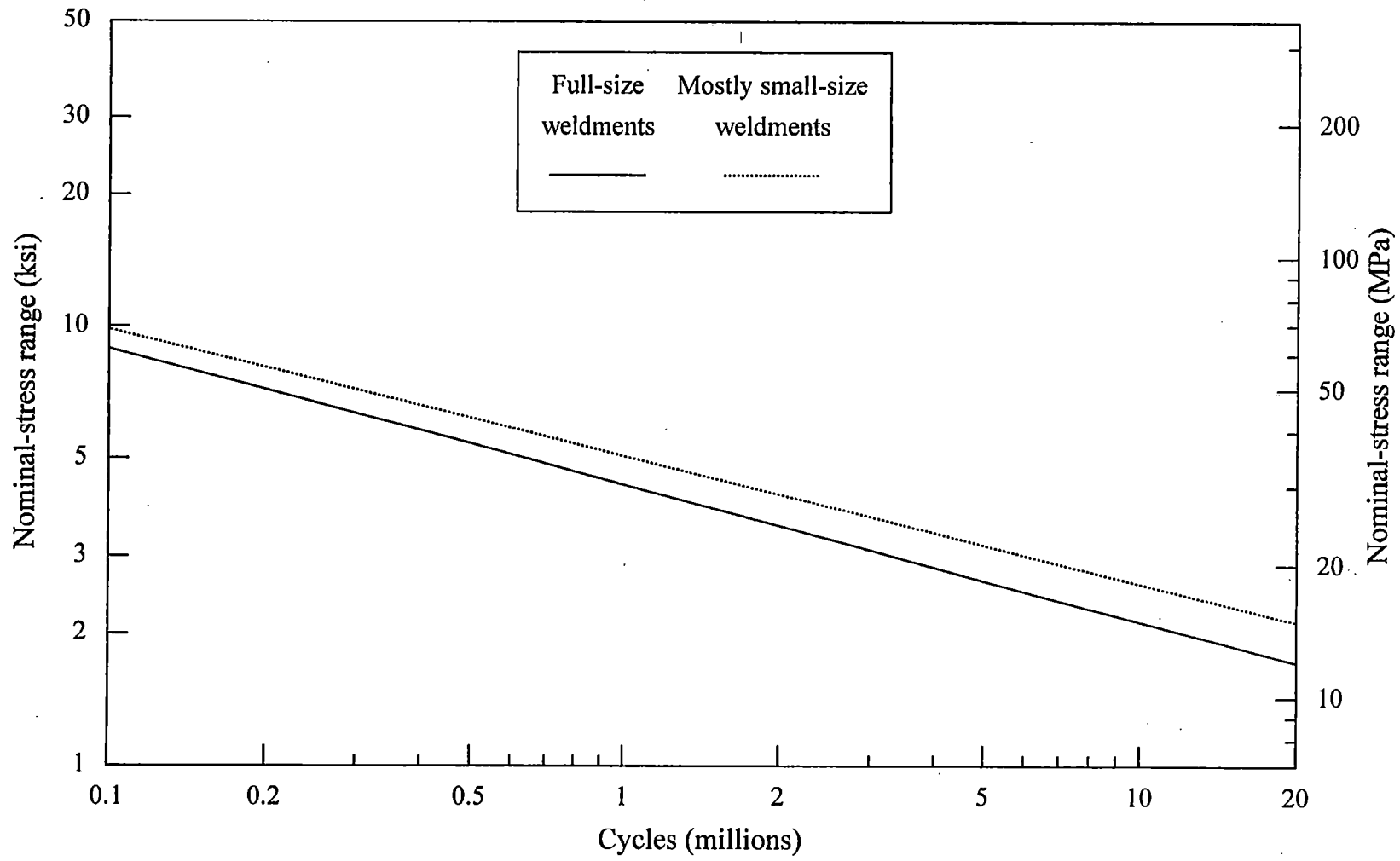


Figure 3.17. SN-curves for small and full-size Category E weldments (R varies)

mixture of test specimens with different stress ratios. One conclusion can be made from an observation of Fig. 3.17. The slopes of the two linear-regression lines are essentially equal. Additional research involving the fatigue strength of Category E weld details should be conducted to isolate the independent effects of the size of a weldment and the stress ratio.

The European Recommendations for Aluminum Alloy Structures (ERAAS) Fatigue Design [20] developed by the European Convention for Constructional Steelwork (ECCS) are similar to the most recent Aluminum Association fatigue provisions [8]. The ECCS structural detail with an F3-Classification is designated as a Category E weld detail by the Aluminum Association. The SN-curve for the ECCS-F3-Classification is also defined by Eq. (3.4), where for an F3-Classification, $A = 574.9$ MPa (83.4 ksi) and $m = 4.32$ MPa (also 4.32 ksi). A constant-amplitude, nominal-stress-range threshold of 16.2 MPa (2.35 ksi) is assumed to exist at 5-million load cycles. Figure 3.18 shows that the SN-curves for ECCS and the Aluminum Association are similar. The database that was used to generate the ERAAS fatigue design curve was not the same as that used to produce the Aluminum Association fatigue provisions, although there is some test data that was included in both databases. The Aluminum Association SN-curve is more conservative than the ECCS SN-curve.

Figure 3.18 also shows the linear-regression, lower-bound, strength line that was established at two standard deviations below the least-squares, linear-regression line for the Category E weld details tested in the ISU research. This lower-bound, strength line is slightly above and nearly parallel to the sloping portion of the Aluminum Association SN-curve, and it crosses the ECCS SN-curve at approximately 700,000 cycles. The fatigue testing conducted during this ISU study did not establish an endurance limit due to the lack of a sufficient number of weld fractures beyond 5-million load cycles. Although slight differences occurred between the lower-bound strength line

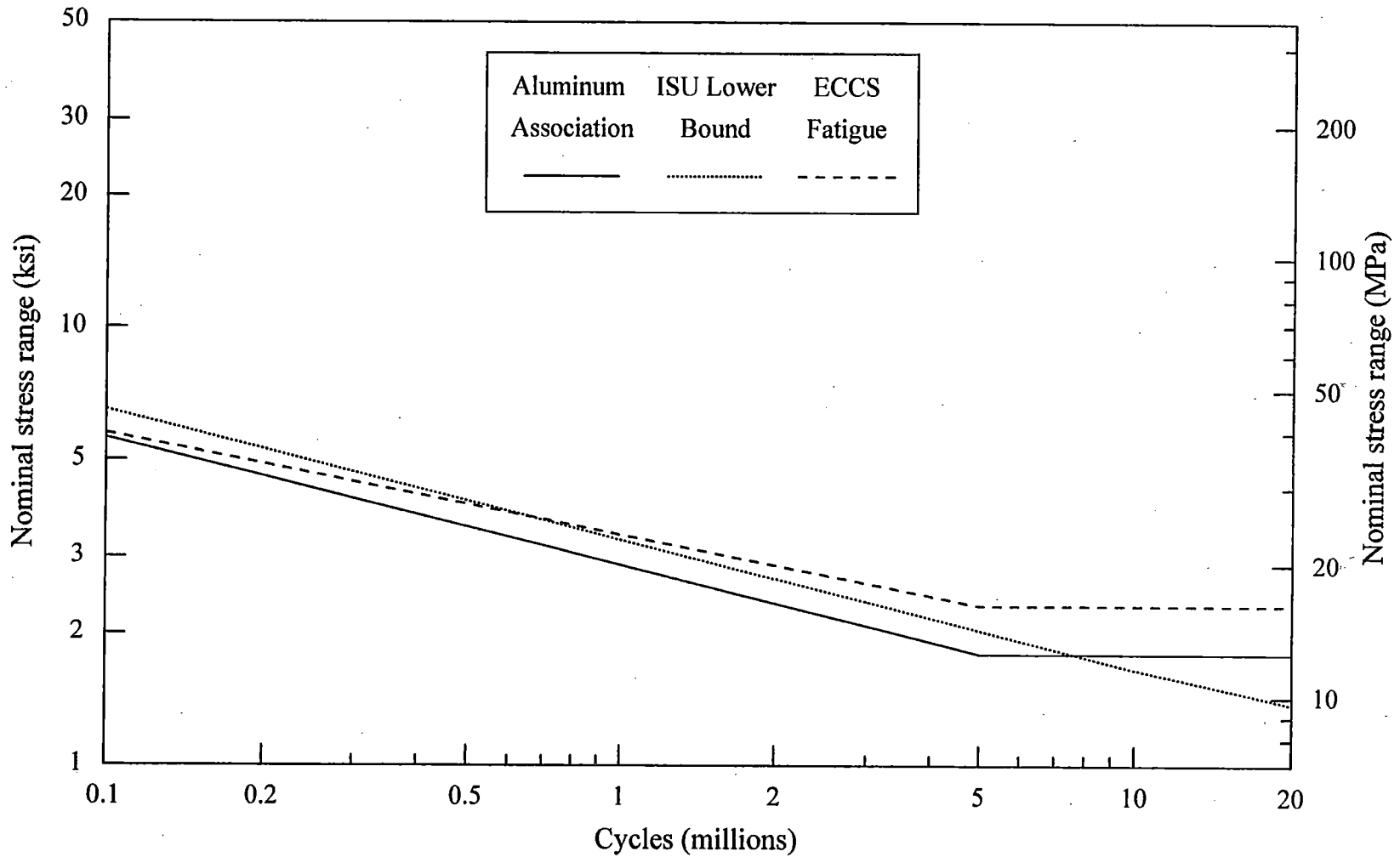


Figure 3.18. Aluminum Association and ECCS SN-Curves for Category E details

generated from this ISU study and the Aluminum Association and ECCS SN-curves, the differences are believed to be attributed to the different fatigue-strength data sets that were used to establish the individual SN-curves.

CHAPTER 4. EPILOGUE

4.1. Summary

The use of aluminum in engineering structures has increased significantly in the past 50 years. Because aluminum alloys possess a natural resistance to corrosion, have yield strengths comparable to commonly used steels such as A36 and A572 Grade 42, and have weights about one-third that of steel, aluminum has become a viable structural material. Since aluminum alloys can be welded; bolted or riveted; and are available in cast, extruded, forged, rolled, and sheet forms, aluminum alloys are as commercially versatile as structural steel. The development of aluminum structural design specifications began in the 1940's and continues to evolve worldwide. Recent improvements to aluminum design specifications have addressed the fatigue behavior of weldments.

In 1994, the Aluminum Association published the sixth edition of the Specifications for Aluminum Structures [8] that established weld detail categories, which linked the geometry and type of weldment to the fatigue life of the structural member. However, a significant portion of this data has been obtained from the fatigue testing of small-size specimens. The relevance of data obtained from small-size specimens compared to data obtained from full-size specimens has been questioned. Research [19] has shown that full-size aluminum weldments tend to experience fatigue fractures with the application of fewer load cycles than small-size specimens of a similar geometry. Fatigue testing of full-size aluminum weldments commonly used in structural applications is essential in order to justify or improve the specification criteria for fatigue design of aluminum structures. Since there is a scarcity of large, welded aluminum structures, and since the cost of fabricating and testing specimens is formidable, few opportunities exist to study the behavior of such components.

Several years ago, engineers from the Iowa Department of Transportation and from the Polk County Engineer's office determined that the 86th Street (Clive Road) overpass of Interstate 80 (I-

80) near Des Moines, Iowa would be redesigned as an interchange. The original overpass was a four-span continuous, welded, I-shaped, aluminum girder bridge that was erected in 1959. The removal of the aluminum girder bridge provided a unique opportunity to perform a static-load test of an aluminum girder bridge and to obtain full-size, aluminum girder section for fatigue testing.

In 1993, and prior to the removal of the bridge, static-load field tests of the bridge were performed by researchers at Iowa State University (ISU). The discussion and results of these tests were reported by Abendroth, Sanders, and Mahadevan [1,2]. The bridge performance had been excellent throughout its 35 years of service.

Eight, approximately 43-ft long, aluminum girder sections were salvaged when the Clive Road Bridge was disassembled. The four girder sections in each 41-ft long end span of the bridge were removed intact. A portion of the nominally 8-in. thick, reinforced concrete, deck section remained attached with shear connectors to the girders. Four of these girders were used for the constant-amplitude, fatigue testing of this study and the other four girders were saved for possible future, variable-amplitude, fatigue testing. Each of the girders that were tested during this research program were cut into two sections. One section, which was approximately 26-ft long, was cut from the end of the girder that was closest to the original bridge-pier location. The remaining section, which was approximately 15-ft long, was the portion of the girder that was closest to the original bridge-abutment location.

The girders had been fabricated from 5083-H113 aluminum alloy plates. This aluminum alloy is favorably suited for use in large, welded, structural applications based on the mechanical and chemical properties of this alloy. The four long girder specimens had an unusual, existing, bottom flange, splice detail that included a transition plate. These specimens also had an existing, I-shaped, diaphragm that was connected near their midlength to the web plate. The bottom flange splice, weld

detail on all of the long girder specimens and the diaphragm connection on the long, exterior girder specimens involved Category E weld details, as classified by the Aluminum Association specifications [8]. The diaphragm connection on the long, interior girder specimens included a slotted-web plate detail. This diaphragm connection did not correspond to any of the weld detail categories specified by the Aluminum Association; however, the effect of the slots in the web plate made this detail more susceptible to a fatigue fracture than a conventional Category E weld detail. The ends of the four, short girder specimens had existing, welded connections that were part of the original bridge fabrication. Along the lengths of these specimens, there were not any existing, weld plate attachments from the original bridge construction.

New 5083-H321 aluminum alloy plates were fillet welded to the girder specimens by a welder, who was certified to weld aluminum. All welds were performed by the Gas Metal Arc Welding procedure, and they were visually inspected for defects by an American Welding Society Certified Welding Inspector. The methods and parameters used to weld the new plates were developed to closely approximate the conditions used in the original welding.

All of the test specimens had two, new, cover plates welded to their bottom flange. Each of the long girder specimens also had two, new pairs of short, horizontal plates welded to their web plate. Each of the short girder specimens also had two new pairs of short, vertical, web stiffener plates welded to their web and bottom flange plates. The transverse fillet welds for the bottom flange, cover plates and the fillet weld across the ends of the horizontal, web plate attachments were Category E weld details. The fillet welds between the vertical, web stiffener plates and the girder bottom flange plate were Category C weld details. These welded attachments reflect the type of connections used in girder construction for which fatigue data is needed.

Loads were applied to the specimens by a pair of 55-kip capacity actuators. The long specimens were supported directly by the test frame, and the load actuators were symmetrically positioned at 4 ft on center over these specimens. The short specimens were supported on fabricated abutments, and the load actuators were symmetrically positioned at 3 ft on center over these test specimens. The portion of the reinforced concrete slab that was attached to the top flange of the girders was removed from the short girder specimens in order to reduce the amount of load that was required to induce the desired stress ranges at the toes of the critical weldments on these specimens. The long girder specimens retained a portion of the original bridge deck.

Instrumentation consisted of electrical-resistance, strain gauges; direct-current, displacement transducers (DCDTs); dial gauges; and load cells. For each specimen a vertical line of strain gauges was positioned in the constant-moment region to observe the strain profile in a cross section of the girder. Strain gauges were also positioned close to the fillet welds that were expected to experience a fatigue fracture during the cyclic loading. These strain gauges were used to observe changes in the longitudinal bending strains prior to the full development of a fatigue fracture at these locations. The DCDTs and dial gauges measured the vertical and lateral motions at the supports and at the midspan of a specimen. When the loads were applied to a specimen, the slightly warped aluminum flange and web plates, which may have been caused by the original welding of the girders and/or the removal of the girders from the bridge structure, induced small lateral displacements and support motion for a specimen.

The voltage outputs of the instrumentation could be measured during the static or dynamic-load tests on a specimen. Each instrumentation device was monitored 300 times per second during a burst reading. These readings were initiated either manually or automatically at a set-time interval.

The experimental measurements were acquired by a data acquisition system and organized by a computer program to obtain the minimum and maximum magnitudes for the measurements.

The minimum and maximum loads that were applied to a girder specimen were established after selecting a desired nominal-stress range at a specific fillet-welded connection. A large stress range would induce a rapid formation of a fatigue fracture, while a very small stress range might not induce a fatigue fracture before 10-million load cycles had been applied. To assist in the determination of a proper stress range, the fatigue provisions of the Aluminum Association specifications [8] and the aluminum fatigue provisions of the AASHTO-LRFD specifications [12] were reviewed. The weld detail that was most susceptible to a fatigue fracture was determined by its stress category designation and its position on the particular test specimen.

Loads were applied to a specimen at a frequency of between 1.0 and 5.0 hertz. Large loads and the corresponding specimen deflections produced large, hydraulic oil flow rates through the actuator servo-valves, which produced the slower load frequencies. During the testing of each specimen, a log book was used to record all events significant to the experimental, fatigue-life history and stress history of a specimen. The fatigue-life history for a specimen included changes that were made to the specimen or testing apparatus, changes that were made in the load magnitudes or frequency, or the occurrence of a fatigue fracture. The stress history of a specimen included the record of the theoretical (nominal) and experimental (measured) stress ranges at each of the weld details.

After a fatigue fracture developed in a specimen, the dimensions of the fracture were recorded and instrumentation measurements for a static-load test that involved the load magnitudes which caused the fracture were taken to note any changes in the static load-behavior of the specimen. If a fatigue fracture occurred in the bottom flange plate of a specimen, the girder was reinforced by

attaching a steel plate that spliced together the two sides of the fractured flange plate. If a fatigue fracture in a bottom flange plate extended upwards into the web plate or if a fracture only occurred within the web plate, holes were drilled at the tips of the fracture in an attempt to arrest further crack propagation at those locations. After a girder was reinforced at a fatigue fracture location, the next aluminum weldment that was considered to be most susceptible to a fatigue fracture on the same test specimen was tested at another specific stress range. This testing procedure continued until a girder specimen could no longer be reinforced or until further testing was not practical.

The strain gauge measurements obtained during the dynamic loading of a specimen were used to calculate the experimental stress-ranges that were induced at the fillet-welded details. The experimental stress-range and number of load cycles that produce a fatigue fracture establish a data point for the fatigue strength behavior of a Category E weld detail. Similar fatigue fracture data points were established for a nominal stress-range and the number of load cycles associated with a fatigue fracture. The nominal stress-range at a fracture point was computed by applying basic engineering mechanics principles. The nominal and experimental fracture data points were independently analyzed by applying linear-regression techniques to establish a least-squares, linear-regression line of stress-range versus load-cycle behavior (SN-curve) for Category E fatigue fractures. A lower-bound-strength line for the fatigue strength of Category E weld details was established at two standard deviations below the regression line for both the nominal and experimental fatigue test results. The nominal, linear-regression line was compared to fatigue fracture results of similar small and full-size Category E weld details of previous researchers. The nominal and experimental, linear-regression and the lower-bound-strength lines were compared to the fatigue provisions specified by AASHTO-LRFD specifications [12] and the Aluminum

Association specification [8], which were formulated from test results that involved many more small-size specimens than full-size specimens.

4.2. Conclusions

The following conclusions were based on the fatigue strength results obtained from the seven girder specimens tested in this ISU study, results and analyses of similar test programs, and available fatigue design provisions from the AASHTO-LRFD specifications [12] and Aluminum Association specifications [8]:

1. The nominal, least-squares, linear-regression, SN-relationship established in this ISU study for the full-size, Category E aluminum weldments that involved a stress ratio, R , equal to 0.05 were similar to that same relationship developed by Erickson and Kosteas when R was equal to 0.10.
2. When the influence of the stress ratio was neglected, full-size, Category E aluminum weldments may experience fatigue fractures at a lower stress range than similar, small-size, aluminum weldments.
3. All of the Category E fatigue fractures that developed in the girder specimens for this ISU study satisfied the allowable stress-range versus load-cycle relationship specified by the fatigue provisions of the Aluminum Association.
4. The least-squares, linear-regression, SN-relationship for the fracture data from this ISU study essentially matched the nominal-strength, SN-curve for Category E aluminum weldments given in the AASHTO-LRFD specification.
5. The SN-curve for the Category E details specified by the Aluminum Association is slightly more conservative than the SN-curve for the F3-structural details specified by the European Convention for Construction Steelworks (ECCS). A Category E weld detail as defined by the Aluminum Association is the same as an F3-structural detail as defined by ECCS. The lower-

bound, strength line developed from fatigue data gathered in this ISU study related better to the SN-curve from the Aluminum Association than to the SN-curve from ECCS.

6. A constant-amplitude, endurance limit for Category E details could not be established for the specimens tested in this ISU study. An insufficient number of fatigue fractures occurred beyond 5-million load cycles. However, since a significant number of the weldments in this ISU study experienced over 5-million load cycles without developing a fatigue fracture, an endurance limit probably exists.
7. Except for the fillet welds associated with the new, horizontal, plate attachments on the web plate of the long girder specimens, the transverse fillet-welded connections that experienced a fatigue fracture always failed in the base metal adjacent to the toe of the weld. The fatigue fractures at the edge of the horizontal plates passed through the web plate base metal on one side of the web plate and through the weld metal on the other side of the web plate, since these horizontal plates were accidentally misaligned along the length of the girder.

4.3. Recommendations

The following recommendations were formulated after evaluating the fatigue strength results of this ISU study, reviewing the available literature concerning fatigue testing of aluminum alloy weldments, and studying the fatigue provisions in the AASHTO-LRFD specifications [12] and Aluminum Association specifications [8]:

1. Additional constant-amplitude, fatigue testing of Category E, transverse, fillet-weld details needs to be conducted to establish the fatigue strength relationship between small-size and full-size weldments.

2. Investigations that address the use of different stress ratios for full-size, aluminum weldments need to be performed to establish the effect that the stress ratio has on the fatigue life of a welded connection.
3. Constant-amplitude, fatigue testing of commonly used welded and bolted aluminum connection configurations, involving detail Categories A through F, for which there is a lack of full-size specimen test data needs to be conducted. These tests will provide some confirmation regarding the adequacy of the current specification, SN-relationships that were established from testing mostly small-size specimens. These additional tests should be designed to determine whether an endurance limit exists for each detail category.
4. More variable-amplitude, fatigue testing of full-size, aluminum specimens with commonly used welded and bolted connections, involving all detail categories, is essential to confirm or modify current specification provisions for this type of loading.

REFERENCES

1. Abendroth, R. E., Sanders, W. W., and Mahadevan, V., "A Continuous Span Aluminum Girder Concrete Deck Bridge," Final Report, Part 1 of 2: Field Performance and Evaluation, Center for Transportation Research and Education, Iowa State University, July 1996.
2. Abendroth, R. E., Sanders, W. W., and Mahadevan, V., "Field Testing of a Continuous Aluminum Girder Highway Bridge," *Proceedings of the Sixth International Conference on Structural Faults and Repair, 1995: Extending the Life of Bridges*, Vol. 1, London, July 3, 1995.
3. Alison, Gordan A., "Evaluation of Seven Aluminum Highway Bridges After Two to Three Decades of Service," *Transportation Research Record*, No. 950, 1984, pp. 123-129.
4. Aluminum Association, Inc., *Aluminum Standards and Data*, Eighth Ed., New York, 1984.
5. Aluminum Association, Inc., *Aluminum Welder's Training Manual*, First Ed., New York, 1972.
6. Aluminum Association, Inc., *Specifications for Aluminum Structures*, Third Ed., New York, 1976.
7. Aluminum Association, Inc., *Specifications for Aluminum Structures*, Fifth Ed., New York, 1986.
8. Aluminum Association, Inc., *Specifications for Aluminum Structures*, Sixth Ed., New York, 1994.
9. Aluminum Company of America, *Welding and Brazing ALCOA Aluminum*, Pittsburgh, Pennsylvania, 1947.
10. American Association of State Highway and Transportation Officials, *Standard Specifications for Highway Bridges*, Fifteenth Ed., Washington, D.C., 1992.
11. American Association of State Highway and Transportation Officials, *Guide Specifications for Aluminum Highway Bridges*, Washington, D.C., 1992.
12. American Association of State Highway and Transportation Officials, *AASHTO LRFD Bridge Design Specifications*, First Ed., Washington, D.C., 1994.
13. American Society for Testing and Materials, "Designation: E 739-80: Standard Practice for Statistical Analysis of Linear or Linearized Stress-Life (S-N) and Strain-Life (ϵ -N) Fatigue Data," *Statistical Analysis of Fatigue Data, ASTM STP 744*, Little/Ekval, Ed., Philadelphia, PA, 1979, pp. 129-137.
14. American Society for Testing and Materials, *Standard Methods of Tension Testing of Metallic Materials (E8-85)*, Philadelphia, PA, ASTM, 1985.

15. Ashton, N. L., "First Welded Aluminum Girder Bridge Spans Interstate Highway in Iowa," *Civil Engineering*, October 1958, pp. 78-80.
16. Ashton, N. L., "Iowa Tries a Welded Aluminum Bridge," *Engineering News Record*, February 20, 1958, pp. 30-32.
17. British Standards Institution, *BS 8118: Structural Use of Aluminum*, London, 1991.
18. Brosilow, R., "What We Have Learned About Fatigue of Welds," *Welding Design & Fabrication*, April 1984, pp. 73-75.
19. Erickson, D. and Kostas, D., "Assessing Transverse Fillet Weld Fatigue Behavior in Aluminum from Full-Size and Small-Specimen Data," *Fatigue and Fracture Testing of Weldments, ASTM STP 1058*, H. I. McHenry and J. M. Potter, Eds., American Society for Testing and Materials, Philadelphia, 1990, pp. 34-46.
20. European Convention for Constructional Steelwork, *European Recommendations for Aluminum Alloy Structures: Fatigue Design*, Document No. 68, First Ed., 1992.
21. Ferry, R. L. and Kissell, J. R., *Aluminum Structures: A Guide to Their Specifications and Design*, John Wiley & Sons, Inc., New York, 1995.
22. Gunn, K. W., and McLester, R., "Fatigue Strength of Welded Joints in Aluminum Alloys," *British Welding Journal*, 9(12), pp. 634-649, 1962.
23. Gurney, T. R., *The Fatigue Strength of Transverse Fillet Welded Joints: A Study of the Influence of Joint Geometry*, Abington Publishing, Cambridge, England, 1991.
24. Gurney, T. R., *Fatigue of Welded Structures*, Second Edition, Cambridge University Press, 1979.
25. Gurney, T. R., "Influence of Artificially Induced Residual Stresses on the Fatigue Strength of Welded Light Alloy Specimens," *British Welding Journal*, 9 (2), Feb. 1962, pp. 90-96.
26. Gurney, T. R., "Influence of Residual Stresses on Fatigue Strength of Plates with Fillet Welded Attachments," *British Welding Journal*, 7 (6), June 1960, pp. 415-431.
27. Hansz, Sean C., "Evaluation of the Fatigue Behavior of Fillet Welds in Full-Size Aluminum Specimens," M.S. Thesis, Iowa State University, Ames, Iowa, 1996.
28. Hartmann, E. C., Holt, M., and Eaton, L. D., "Fatigue Strength Butt Joints in 3/8 in. Thick Aluminum Alloy Plates," *The Welding Journal*, 33 (1), Jan. 1954, pp. 21s-30s.
29. Hartmann, E. C., Holt, M., and Zambocky, A. N., "Static and Fatigue Tests of Arc-Welded Aluminum Alloy 61S-T6 Plate," *The Welding Journal*, Research Supplement, XII, pp. 129s-138s, 1947.

30. Linger, D. A. and Hulsbos, C. L., "Dynamics of Highway Bridges," *Iowa Engineering Equipment Station Bulletin No. 188*, IEES, Ames, Iowa, 1960.
31. Kosteas, D. and Sanders, W., "Redesigning an Aluminum-Concrete Composite Bridge," *Proceedings of the Sixth International Conference on Aluminum Weldments*, Cleveland, Ohio, pp. 125-130, April 1995.
32. Maddox, S. J., Webber, D., "Fatigue Crack Propagation in Aluminum-Zinc-Magnesium Alloy Fillet Welded Joints," *Fatigue Testing of Weldments, ASTM 648*, D. W. Hoepfner, Ed., American Society for Testing and Materials, 1978, pp. 159-184.
33. Mahadevan, V., *Analysis of the Behavior of a Continuous Span Concrete Deck Aluminum Girder Bridge*, M.S. Thesis, Iowa State University, Ames, Iowa, 1995.
34. Mazzolani, F. M., *Aluminum Alloy Structures*, Second Ed., Chapman & Hall, London, 1995.
35. Mindlin, H., "Fatigue of Aluminum-Magnesium Alloys," *Welding Journal*, 42 (6), June 1963, pp. 276s-281s.
36. Miner, M. A., "Cumulative Damage in Fatigue," *Journal of Applied Mechanics*, 12 (3), Sept. 1945, pp. 159-64.
37. Montemarano, T. W. and Wells, M. E., "Improving the Fatigue Performance of Welded Aluminum Alloys," *British Welding Journal*, 59 (6), June 1980, pp. 21-28.
38. Person, N. L., "Fatigue of Aluminum Alloy Welded Joints," *Welding Journal*, 50 (2), Feb. 1971, pp. 77s-86s.
39. Prentzas, E. G., "Experimental Structural Behavior of Iowa's Aluminum Bridge," *The Central Constructor*, October 1958, pp. 15.
40. Radaj, D., *Design and Analysis of Fatigue Resistant Welded Structures*, Halsted Press, New York, 1990.
41. Sanders, W. W., "Fatigue Behavior of Aluminum Alloy Weldments," *WRC Bulletin 171*, Welding Research Council, New York, 1972.
42. Sanders, W. W. and Abendroth, R. E., "Construction and Evaluation of a Continuous Aluminum Girder Highway Bridge," *Proceedings of Sixth International Conference on Aluminum Weldments*, Cleveland, Ohio, pp. 115-124, April 1995.
43. Sanders, W. W. and Day, R. H., "Fatigue Behavior of Aluminum Alloy Weldments," *WRC Bulletin 286*, Welding Research Council, New York, Aug. 1983.
44. Sanders, W. W., Derecho, A. T., and Munse, W. H., "Effect of Exterior Geometry on Fatigue Behavior of Welded Joints," *Welding Journal*, 44 (2), Feb. 1965, pp. 49s-55s.

45. Sanders, W. W. and Gannon, S. M., "Fatigue Behavior of Aluminum Alloy 5083 Butt Welds," *WRC Bulletin 199*, Welding Research Council, New York, 1974.
46. Sanders, W. W. and McDowell, K. A., "Fatigue Behavior of 5000 Series Aluminum Alloy Weldments in Marine Environment," *WRC Bulletin 242*, Welding Research Council, New York, 1978.
47. Sharp, M. L., *Behavior and Design of Aluminum Structures*, McGraw-Hill, 1993.
48. Sharp, M. L. and Nordmark, G. E., "Fatigue Strength of Welded Tubular Aluminum Truss," *Journal of the Structural Division, ASCE*, 103 (ST8), Aug. 1977, pp. 1619-1629.
49. Sharp, M. L., Nordmark, G. E., and Menzemer, C. C., *Fatigue Design of Aluminum Components and Structures*, McGraw-Hill, 1996.
50. Singes, E. G., Baker, R. G., Harrison, J. D., and Burdekin, F. M., "Factors Affecting the Fatigue Strength of Welded High Strength Alloys," *British Welding Journal*, Vol. 14, No. 3, March 1967.
51. Soetens, F., "Connections in Aluminum Alloy Structures," *Aluminum Structures: Advances, Design and Construction*, R. Narayanan, Ed., Elsevier Applied Science, 1987, pp. 105-114.
52. Sutherland, J. G., "Welded Aluminum Fatigue Behavior," *Canadian Metalwork*, 25 (5), May 1962, pp. 33-40.
53. Task Committee on Lightweight Alloys, Committee on Metals, "Suggest Specifications for Structures of Aluminum Alloys 6061-T6 and 6062-T6," *Journal of the Structural Division, American Society of Civil Engineers*, Paper 3341, 88 (ST-6), Dec. 1962, pp. 1-45.
54. Taylor, T. C., "Fatigue Testing of an Al-Mg-Mn Alloy Pressure Vessel," *British Welding Journal*, Feb. 1967, pp. 84-89.
55. Tomlinson, J. E. and Wood, J. L., "Factors Influencing the Fatigue Behavior of Welded Aluminum," *British Welding Journal*, 7 (4), pp. 22-36, 1960.
56. Trinidad, A. A. Jr., "Aluminum Highway Bridges in the USA," *Bridge Management 2*, New York, Bettigole Andrews & Clark Inc.

ACKNOWLEDGMENTS

The research discussed in this report was conducted by the Bridge Engineering Center under the auspices of the Engineering Research Institute (ERI) of Iowa State University (ISU). This investigation was funded through the Center for Transportation Research and Education (formerly the Iowa Transportation Center) at ISU by the Iowa Department of Transportation (Iowa DOT) in cooperation with the Federal Highway Administration. The authors would like to thank William A. Lundquist, Bridge Engineer, and John P. Harkin, Chief Structural Engineer, with the Iowa DOT for their support of the research effort.

We would like to acknowledge Douglas L. Wood, Structures Laboratory Supervisor, Dr. Daniel O. Adams, Department of Aerospace Engineering and Engineering Mechanics, ISU, and all of the other individuals who have provided laboratory assistance and technical advice on this project. During the course of this project, the talents of many other individuals were utilized. We would like to thank Charles Burg and David Rehbein of the United States Department of Energy, Ames Laboratory Technical Services for their welding expertise. We also wish to recognize the following individuals and their companies for their contributions: Don Smart and Steve Ewalt of L-Tec, Bernie Cline of Genex Ltd. Welding Supplies, and Toby Easter of Hobart Welding. Finally, a special thanks to the Iowa DOT for providing Joseph S. Putherickal, Mike Lawzon, and Harold P. Thielen to straighten a damaged aluminum girder section.

The fatigue testing program, including specimen design, was developed with the assistance of Dr. John Fisher and other individuals from the Center for Advanced Testing of Large Structural Systems (ATLAS) at Lehigh University and Dr. Craig Menzemer, University of Akron, formerly with ALCOA Laboratories. Their efforts are gratefully acknowledged.

APPENDIX A. TEST SPECIMEN FATIGUE LIFE HISTORY

This appendix contains a chronological synopsis of the events that occurred during the fatigue testing of the girder specimens. Events such as changes in the load parameters, discovery of fatigue fractures, or other occurrences that might have influenced the specimen response are presented. Tables A.1 through A.7 list the number of load cycles and date (month/day/year) associated with each event for the seven girder specimens. Details concerning the theoretical and experimental stress ranges at specific locations of interest on the girder specimens are presented in Appendix B.

Table A.1. Life history of the long exterior girder specimen no. 1

Cycles	Date	Event
0	03/21/95	Girder was placed and braced in the test frame, and the instrumentation was attached.
93,999	05/05/95	Initial constant-amplitude load cycling and development of the testing methodology ends.
94,000	05/05/95	Final constant-amplitude load cycling initiated. Loading: 3.2 ksi nominal stress range at original bottom flange splice. Maximum Load: 18.54 kips. Minimum Load: 0.93 kips. Load Frequency: 4.0 hertz.
1,977,540	05/11/95	Base metal fatigue fracture occurred across the bottom flange plate at the new bottom flange cover plate no. 2 at the end that was closest to the midspan (inside end). Steel repair plate fastened to bottom flange plate to reinforce girder and stop crack propagation (Fig. 2.15).
1,983,500	05/25/95	Repairs completed and dynamic load testing continued with the same load parameters that were selected to induce a fatigue fracture at the original bottom flange splice detail.
8,000,000	06/12/95	Increased the load parameters in an attempt to induce a fatigue fracture at the original bottom flange splice detail. Loading: 4.5 ksi nominal stress range at the original bottom flange splice detail. Maximum Load: 26.07 kips. Minimum Load: 1.30 kips. Load Frequency: 4.0 hertz.
8,641,400	06/14/95	Base metal fatigue fracture occurred across the bottom flange plate at the apex of the transition plate for the original bottom flange splice. Removed initial bottom flange steel repair plate and attached a different steel repair plate to reinforce the girder at both fracture locations in an attempt to induce a fatigue fracture at the new flange cover plate no. 1 (Fig. 2.16).

Table A.1. (Cont'd)

Cycles	Date	Event
8,641,400	06/23/95	<p>Dynamic load testing resumed. Loading: 4.0 ksi nominal stress range at the inside end of the new bottom flange cover plate no. 1. Maximum Load: 42.66 kips. Minimum Load: 2.13 kips. Load Frequency: 1.0 hertz.</p>
8,809,000	06/25/95	<p>Existing fatigue crack at the inside end of the new bottom flange cover plate no. 2 propagated into the web plate of the girder. Testing stopped to arrest this crack by drilling a hole in the web plate above the crack tip.</p>
8,814,900	06/26/95	<p>Testing stopped to reinforce the test frame by welding bearing stiffeners to the web of each diaphragm that supported an actuator to prevent twisting of the bottom flange plates for the diaphragms in the test frame.</p>
8,814,900	07/04/95	<p>Resumed load cycling; however, changed load parameter. Load frequency increased to 2.0 hertz.</p>
9,460,100	07/10/95	<p>Base metal fatigue fracture occurred across the bottom flange plate at the new bottom flange cover plate no. 2 at the end that was closest to the support (outside end). Previous fatigue crack at the inside end of the new bottom flange cover plate no. 2 propagated further up in the web plate. Drilled a new hole in the web plate above this crack to arrest crack growth. Abandoned efforts to induce a fatigue failure at the new bottom flange cover plate no. 1. A chop-saw was used to remove the girder bottom flange and the bottom 3 in. of the girder web plate between the load points of the specimen in an attempt to induce a fatigue failure at the new horizontal web plate attachments (Fig. 2.19).</p>

Table A.1. (Cont'd)

Cycles	Date	Event
9,460,100 (Cont'd)	07/10/95	<p>Drilled holes at the tips of cracks that were propagating into the web of the girder at the new bottom flange cover plate no. 2 and at the original bottom flange splice.</p> <p>Drilled holes at the intersection of the chop-saw cuts to reduce the stress concentrations at these locations (Fig. 2.19).</p> <p>Attached double angle web plate guide along the length of the specimen at the bottom of the reduced cross section to prevent lateral buckling in the web plate (Fig. 2.18).</p>
9,460,100	07/20/95	<p>Dynamic load testing resumed in an attempt to induce a fatigue fracture at the new horizontal web plate attachments.</p> <p>Loading: 7.0 ksi nominal stress range at new horizontal web plate attachments.</p> <p>Maximum Load: 21.13 kips.</p> <p>Minimum Load: 1.06 kips.</p> <p>Load Frequency: 4.0 hertz.</p>
9,470,700	07/20/95	<p>Testing stopped due to contact of the ends of the double angle bracing member with the bottom flange of the specimen.</p> <p>Double angle brace cut at each end to eliminate contact with the girder bottom flange plate beyond the cut section.</p> <p>Existing fatigue crack at the inside end of the new bottom flange cover plate no. 2 propagated further up into the web plate.</p> <p>Drilled a hole to act as a crack arrester at the new crack tip.</p> <p>Double angle fabricated and fastened to the web plate to splice across the fracture at this location (Fig. 2.17).</p>
9,470,700	07/24/95	Resume dynamic load testing with the same load parameters.
9,487,500	07/24/95	<p>Fatigue crack formed at a burr mark in the drill hole at the intersection point of the chop-saw cuts at the end of the flange removal area that was adjacent to the new bottom flange cover plate no. 2.</p> <p>Fabricated and attached by using the turn-of-the-nut method, a double angle web plate splice to strengthen the girder (Fig. 2.17).</p> <p>Resumed dynamic load testing with the same load parameters.</p>

Table A.1. (Cont'd)

Cycles	Date	Event
9,592,600	07/26/95	<p>Fatigue crack developed through the base metal of the web plate at each end of the new horizontal web plate attachment no. 2.</p> <p>Fatigue crack developed through the base metal of the web plate at the bottom flange tip of the original I-shaped diaphragm that was just above the apex point on the transition plate for the original bottom flange splice. This crack propagated to the bottom of the web plate within the region of the removed girder bottom flange.</p> <p>Resumed dynamic load testing with the same load parameters.</p>
9,597,600	07/26/95	<p>An additional 5,000 load cycles were applied to the girder to observe crack propagation.</p> <p>Fatigue crack observed in the far face of the web plate at both ends of the new horizontal web plate attachment no. 1.</p> <p>Resumed dynamic load testing with the same load parameters.</p>
9,600,000	07/26/95	<p>An additional 2,400 load cycles were applied to the specimen. The fatigue crack at the original I-shaped diaphragm propagated rapidly.</p> <p>The fatigue cracks in the far face of the web plate at the new horizontal web plate attachment no. 1 propagated.</p> <p>End of fatigue testing.</p>

Table A.2. Life history of the long exterior girder specimen no. 2

Cycles	Date	Event
0	08/12/95	Girder was placed and braced in test frame, and the instrumentation was attached.
0	08/16/95	Constant amplitude load cycling initiated. Loading: 4.0 ksi nominal stress range at original bottom flange splice. Maximum Load: 23.14 kips. Minimum Load: 1.16 kips. Load Frequency: 4.0 hertz.
1,064,400	08/20/95	Base metal fatigue fracture occurred across the bottom flange plate at the apex of the transition plate for the original bottom flange splice. Steel splice plate fastened to the bottom flange to reinforce girder and stop crack propagation (Fig. 2.15).
1,064,400	08/23/95	Repairs completed and dynamic load testing continues with the same load parameters in an attempt to induce a fatigue failure at the new bottom flange cover plate no. 2.
1,306,600	08/24/95	Base metal fatigue fracture occurred across the bottom flange plate at the new bottom flange cover plate no. 2 at the end that was closest to the midspan. A chop-saw was used to remove the girder bottom flange and bottom 2-1/2 in. of the girder web plate between the load points of the specimen in an attempt to induce a fatigue fracture at the new horizontal web plate attachments (Fig. 2.19). Drilled holes at the intersection of the chop-saw cuts to reduce the stress concentrations at these locations (Fig. 2.19). Attached double angle web plate guide along the length of the specimen at the bottom of the reduced cross section to prevent lateral buckling of the web plate (Fig. 2.18).

Table A.2. (Cont'd)

Cycles	Date	Event
1,306,600	08/28/95	<p>Change load parameters in an attempt to induce a fatigue failure at the new horizontal web plate attachments.</p> <p>Loading: 6.25 ksi nominal stress range at the new horizontal web plate attachment no. 2.</p> <p>Maximum Load: 18.73 kips.</p> <p>Minimum Load: 0.94 kips.</p> <p>Load Frequency: 4.0 hertz.</p>
1,432,100	08/29/95	<p>Fatigue fracture occurred at the chop-saw intersection point that was closest to the new bottom flange cover plate no. 2.</p> <p>Attached double angle web plate splice using the turn-of-nut method, at each cut intersection point to prevent further crack propagation at these locations (Fig. 2.17).</p> <p>Dynamic load testing resumed with the same load parameters.</p>
1,491,300	08/29/95	<p>Fatigue fracture occurred at the new horizontal web plate attachment nos. 1 and 2 and at the chop-saw intersection point that was closest to the new bottom flange cover plate no. 1. Each fatigue fracture occurred in the base metal adjacent to the welds.</p> <p>End of fatigue testing.</p>

Table A.3. Life history of the long interior girder specimen no. 1

Cycles	Date	Event
0	10/17/95	Girder was placed and braced in test frame, and the instrumentation was attached.
0	10/30/95	Constant-amplitude load cycling initiated. Loading: 3.6 ksi nominal stress range at the original bottom flange splice. Maximum Load: 26.56 kips. Minimum Load: 1.32 kips. Load Frequency: 4.0 hertz.
4,900	10/30/95	Testing stopped due to specimen instability. Adjusted supports and recommenced dynamic load testing with the same load parameters.
1,995,000	11/05/95	Fatigue fracture occurred through the weld metal at the bottom flange tip of the original I-shaped diaphragm that was just above the apex point on the transition plate for the original bottom flange splice. These girder web plate cracks extended above and below the diaphragm bottom flange plate. Drilled holes in the web plate above and below the crack tips to stop crack propagation. Base metal fatigue fracture occurred across the bottom flange plate at the new bottom flange cover plate no. 2 at the end that was closest to the midspan. Steel splice plate fastened to the bottom flange to reinforce the girder and stop crack propagation (Fig. 2.15). Dynamic load testing resumed with the same load parameters.
5,581,400	11/21/95	Testing stopped due to displacement interlock limit violation. No new fatigue cracks were detected, nor were prior cracks propagating. Dynamic loading resumed with the same load parameters..
5,918,600	11/22/95	Testing stopped again due to displacement interlock limit violation. No new fatigue cracks were detected. Dynamic load testing resumed with the same load parameters..

Table A.3. (Cont'd)

Cycles	Date	Event
6,439,500	11/25/95	<p>Fatigue fracture detected at a bolt hole that was drilled through the girder bottom flange plate to attach the steel splice plate at the new bottom flange cover plate no. 2.</p> <p>Girder was reinforced by shifting the steel splice plate 12 in. towards the midspan. Additional bolt holes were drilled through the girder bottom flange plate to accommodate the new position of the splice plate, so that the two fatigue cracks were located between the ends of the splice plate.</p>
6,439,500	11/29/95	Dynamic load testing resumed.
6,519,100	11/29/95	Load frequency reduced to 3.5 hertz.
7,357,000	12/08/95	<p>The fatigue fracture at the original I-shaped diaphragm connection propagated downward from hole that served as a crack arrester.</p> <p>Drilled a new hole in the web plate below the crack tip.</p> <p>Load frequency reduced to 3.0 hertz.</p>
8,103,900	12/11/95	<p>Loading parameters were changed to induce a fatigue fracture at the original bottom flange splice.</p> <p>Loading: 4.0 ksi nominal stress range at the original bottom flange splice</p> <p>Maximum Load: 29.51 kips.</p> <p>Minimum Load: 1.47 kips.</p> <p>Load Frequency: 3.0 hertz.</p>
8,115,000	12/11/95	<p>Fatigue crack at the original I-shaped diaphragm connection propagated upward in the web plate.</p> <p>Hole drilled in the web plate at crack tip to stop further propagation.</p> <p>Dynamic load testing resumed with the same load parameters.</p>

Table A.3. (Cont'd)

Cycles	Date	Event
8,575,400	12/14/95	Fracture at the original I-shaped diaphragm connection propagated downward into the continuous longitudinal fillet weld that connected the web plate to the bottom flange plate of the girder. Could not drill a hole to stop further propagation of this fracture. Dynamic load testing resumed with the same load parameters.
8,708,400	12/15/95	Fatigue crack at the original I-shaped diaphragm connection propagated into the bottom flange plate of the specimen. End of fatigue testing.

Table A.4. Life history of the long interior girder specimen no. 2

Cycles	Date	Event
0	09/--/95	Girder was placed and braced in test frame, and the instrumentation was attached.
0	09/13/95	Constant-amplitude load cycling initiated. Loading: 3.6 ksi nominal stress range at original bottom flange splice. Maximum Load: 26.56 kips. Minimum Load: 1.32 kips. Load Frequency: 4.0 hertz.
1,585,900	09/13/95	Base metal fatigue fracture occurred across the bottom flange plate at the new bottom flange cover plate no. 2 at the end that was closest to the midspan. Steel repair plate fastened to the bottom flange to reinforce the girder and stop crack propagation (Fig. 2.15). Dynamic load testing resumed with the same load parameters.
1,784,300	09/20/95	Fatigue crack occurred through the weld metal at the bottom flange tip of the original I-shaped diaphragm that was just above the apex of the transition plate for the original bottom flange splice. These girder web plate cracks extended above and below the diaphragm flange plate. Drilled holes in the web plate above and below the crack tips to stop crack propagation. Dynamic load testing resumed with the same load parameters.
2,829,300	09/25/95	Fatigue crack at the original I-shaped diaphragm connection propagated upwards in the girder web plate. Drilled hole above the extended crack tip to stop crack propagation. Dynamic load testing resumed with the same load parameters.
4,454,000	10/04/95	Fatigue crack at the original I-shaped diaphragm connection propagated upwards and downwards in the web plate. The bottom crack tip approached the continuous longitudinal fillet weld between the girder web and flange plates. Drilled hole above the upper crack tip in the web plate. Could not drill a hole at the lower crack tip. Dynamic load testing resumed with the same load parameters.
5,096,200	10/06/95	Fatigue crack at the original I-shaped diaphragm connection propagated downward into the bottom flange plate of the girder. End of fatigue testing.

Table A.5. Life history of the short exterior girder specimen no. 1

Cycles	Date	Event
0	01/10/96	Girder prepared for testing: shear studs removed from the top flange plate along the central portion of the span and concrete load pads were cast on the top flange of the girder at the load points. Girder was placed and braced in the test frame, and the instrumentation was attached.
0	01/30/96	Incremental loading performed for preliminary static-strain distribution in specimen. Girder top flange and web plates experienced twisting damage due to instability of a hydraulic actuator on the specimen.
0	02/07/96	Girder repaired by personnel from the Iowa Department of Transportation. A combination of heat treatment and mechanical bending techniques were used to straighten the girder top flange and web plate.
0	02/15/96	Actuator brace fabricated and welded into position to laterally brace the hydraulic rams to the test frame.
0	02/16/96	Constant-amplitude load cycling began. Loading: 5.6 ksi nominal stress range at the new midspan vertical web stiffeners. Maximum Load: 38.02 kips. Minimum Load: 1.09 kips. Load Frequency: 3.0 hertz. Out-of-plane girder web plate bending detected. Testing stopped. Steel web plate stiffener and bearing brace bolted to web of girder directly under the load points (Fig. 2.20).
1,400	02/19/96	Dynamic load testing resumed with the same load parameters.
583,200	02/22/96	Base metal fatigue fracture occurred across the bottom flange plate at the new bottom flange cover plate no. 1 at the end that was closest to the midspan. Attached a steel splice plate to the bottom flange to strengthen the girder (Fig. 2.15). Hole drilled at the crack tip of the portion of this fracture which propagated up into the web plate. Dynamic load testing resumed with the same load parameters.

Table A.5. (Cont'd)

Cycles	Date	Event
938,800	02/24/96	<p>Base metal fatigue fracture occurred across the bottom flange plate at the new bottom flange cover plate no. 2 at the end that was closest to the midspan.</p> <p>Attached a steel splice plate to the bottom flange to strengthen the girder (Fig. 2.15).</p> <p>Fatigue crack at the new bottom flange cover plate no. 1 propagated upwards in the web plate of the specimen.</p> <p>Hole drilled above the crack tip to stop further crack propagation.</p> <p>Dynamic load testing resumed with the same load parameters.</p>
2,202,400	02/29/96	<p>Fatigue fracture occurred in the bottom flange plate at a bolt hole that was used to attach the steel splice plate at the new bottom flange cover plate no. 2. The bolt hole was on the far side of the girder and was the one closest to the midspan.</p> <p>Steel splice plate was repositioned to clear this fracture and the previous fatigue fracture at the new bottom flange cover plate no. 2.</p>
2,202,400	03/05/96	<p>Dynamic load testing resumed with the same load parameters.</p>
2,733,200	03/09/96	<p>Fatigue fracture occurred in the bottom flange plate at a bolt hole that was used to attach the steel splice plate at the new bottom flange cover plate no. 1. The bolt hole was on the near side of the girder and was the one closest to the midspan.</p> <p>End of fatigue testing.</p>

Table A.6. Life history of the short interior girder specimen no. 1

Cycles	Date	Event
0	03/12/96	Girder prepared for testing: shear studs removed from the top flange plate along the central portion of the span and concrete load pads were cast on the top flange of the girder at the load points. Girder was placed and braced in the test frame, and the instrumentation was attached.
0	03/14/96	Constant-amplitude load cycling initiated. Loading: 2.3 ksi nominal stress range at the new bottom flange cover plates at the end that was closest to the midspan. Maximum Load: 23.23 kips. Minimum Load: 1.16 kips. Load Frequency: 4.0 hertz.
61,000	03/14/96	Dynamic load testing stopped due to eccentric loading of the specimen. Realigned the specimen.
61,000	03/17/96	Steel web plate stiffener and bearing brace bolted to the web of the girder directly under the load points (Fig. 2.20). Resumed dynamic load testing with the same load parameters.
405,100	03/20/96	Increased the load frequency to 4.5 Hertz.
820,000	03/21/96	Dynamic load testing stopped to realign the specimen. Increased the load frequency to 5.0 hertz.
11,000,000	04/16/96	Increased the load parameters in an attempt to induce a fatigue fracture at the new bottom flange cover plates. Loading: 2.7 ksi nominal stress range at the new bottom flange cover plates. Maximum Load: 27.27 kips. Minimum Load: 1.36 kips. Loading Frequency: 3.5 hertz.
11,294,000	04/17/96	Increased the load frequency to 4.5 hertz.

Table A.6. (Cont'd)

Cycles	Date	Event
11,850,900	04/19/96	<p>Base metal fatigue fracture occurred across the bottom flange plate at the new bottom flange cover plate no. 2 at the end that was closest to the midspan.</p> <p>Attached a steel repair splice plate to the bottom flange to strengthen the girder (Fig. 2.20).</p> <p>Hole drilled at the crack tip that had propagated up into the web plate.</p> <p>Testing continued with the same load parameters to induce a fracture at the new bottom flange cover plate no. 2.</p>
14,385,200	04/26/96	Increased the load frequency to 5.0 hertz.
16,021,700	05/02/96	<p>Increased the load parameters.</p> <p>Loading: 5.0 ksi nominal stress range at the new bottom flange cover plate no. 2.</p> <p>Maximum Load: 50.5 kips.</p> <p>Minimum Load: 2.53 kips.</p> <p>Load Frequency: 2.75 hertz.</p>
16,197,600	05/03/96	Reduced the load frequency to 2.5 hertz.
16,467,600	05/04/96	<p>Base metal fatigue fracture occurred across the bottom flange plate at the new bottom flange cover plate no. 1 at the end that was closest to the midspan.</p> <p>End of fatigue testing.</p>

Table A.7. Life history of the short interior girder specimen no. 2

Cycles	Date	Event
0	05/--/96	Girder prepared for testing: shear studs removed from the top flange plate along the central portion of the span and concrete load pads were cast on the top flange of the girder at the load points. Girder was placed and braced in test frame, and the instrumentation was attached. Attached web stiffener and bearing brace under the load points (Fig. 2.20).
0	05/20/96	Constant-amplitude load cycling initiated. Loading: 2.8 ksi nominal stress range at the new bottom flange cover plates at the ends that were closest to the midspan. Maximum Load: 28.28 kips. Minimum Load: 1.41 kips. Load Frequency: 4.5 hertz.
4,100	05/20/96	Dynamic testing stopped to realign the girder supports.
4,100	05/21/96	Dynamic load testing resumed with the same load parameters.
773,400	05/22/96	Decreased the load frequency to 4.4 hertz.
985,800	05/23/96	Base metal fatigue crack occurred in the web plate below the bottom diaphragm connection plate at the roller support reaction point for the girder specimen. Drilled holes in the web plate at the crack tips to stop crack propagation. Fabricated web plate stiffeners with bearing brace from double angles to prevent the web plate from rocking lateral (similar to Fig. 2.20). Wedged wooden blocks under the bottom diaphragm connection plate to aid in laterally restraining cracked web plate at the girder reaction point.
985,800	05/24/96	Resumed dynamic loading with the same loading parameters.

Table A.7. (Cont'd)

Cycles	Date	Event
9,615,900	06/17/96	<p>Base metal fatigue fracture occurred across the bottom flange plate at the new bottom flange cover plate no. 1 at the end that was closest to the midspan.</p> <p>Attached a steel splice plate to the bottom flange to strengthen the girder (Fig. 2.15).</p> <p>Resumed testing at the same load parameters, except the load frequency was reduced to 4.0 hertz.</p>
10,545,100	06/19/96	<p>Increased the load parameters to induce a fatigue fracture at the new bottom flange cover plate no. 2 at the end that was closest to the midspan.</p> <p>Loading: 3.1 ksi nominal stress range at the new bottom flange cover plate at the end that was closest to the midspan.</p> <p>Maximum Load: 31.3 kips.</p> <p>Minimum Load: 1.54 kips.</p> <p>Load Frequency: 4.0 hertz.</p>
13,597,500	06/27/96	<p>Fatigue crack in the portion of the web plate just above the roller support for the girder propagated further into the bottom flange and web plates.</p>
14,002,000	07/01/96	<p>End of fatigue testing.</p>

APPENDIX B. TEST SPECIMEN STRESS HISTORY DATA

This appendix contains the load and stress range data for the girder specimens. Tables B.1 through B.7 list the theoretical static, experimental dynamic, and experimental static stress ranges at fatigue fracture locations; corresponding load parameters; and number of load cycles when a particular event occurred during the fatigue testing of the seven girder specimens. The events included changes in the magnitudes or cyclic frequency, initiation or propagation of a fatigue fracture, or addition of reinforcement plates or bracing devices on a specimen.

Table B.1. Stress-range data for the long exterior girder specimen no. 1

Cycle	Load				Stress range							
	range (kips)	max. (kips)	min. (kips)	freq. (hz)	source ^d	fail 1 ^e (ksi)	fail 2 ^f (ksi)	fail 3 ^g (ksi)	fail 4 (ksi)	fail 5 ^h (ksi)	fail 6 ⁱ (ksi)	fail 7 ^j (ksi)
0	17.61	18.54	0.93	---	T	2.98	3.20	1.34	1.61	1.91	2.47	1.02
1st ^a	17.61	18.54	0.93	4.0	D	2.74	3.11	---	---	1.48	---	0.93
1st ^a	17.61	18.54	0.93	---	S	2.81	3.25	---	---	1.66	---	1.00
last ^b	17.61	18.54	0.93	4.0	D	4.10	3.11	---	---	1.48	---	0.93
last ^b	17.61	18.54	0.93	---	S	3.06	3.15	---	---	1.29	---	0.99
1,977,500	17.61	18.54	0.93	---	T	---	3.20	1.34	1.61	1.91	2.47	1.02
1st ^a	17.61	18.54	0.93	4.0	D	---	3.30	---	---	1.17	---	0.97
1st ^a	17.61	18.54	0.93	---	S	---	3.28	---	---	1.15	---	1.00
last ^b	17.61	18.54	0.93	4.0	D	---	3.33	---	---	1.06	---	0.97
last ^b	17.61	18.54	0.93	---	S	---	3.29	---	---	1.15	---	0.96
8,000,000	24.77	26.07	1.30	---	T	---	4.50	1.88	2.27	2.69	3.47	1.44
1st ^a	24.77	26.07	1.30	4.0	D	---	4.59	---	---	1.54	---	1.37
1st ^a	24.77	26.07	1.30	---	S	---	4.53	---	---	1.55	---	1.29
last ^b	24.77	26.07	1.30	4.0	D	---	5.98	---	---	1.70	---	1.37
last ^b	24.77	26.07	1.30	---	S	---	5.82	---	---	1.89	---	1.40
8,641,400	40.53	42.66	2.13	---	T	---	---	3.07	3.71	4.40	5.68	2.36
1st ^a	40.53	42.66	2.13	1.0	D	---	---	---	---	---	---	1.87
1st ^a	40.53	42.66	2.13	---	S	---	---	---	---	---	---	1.86
last ^b	40.53	42.66	2.13	1.0	D	---	---	---	---	---	---	1.92
last ^b	40.53	42.66	2.13	---	S	---	---	---	---	---	---	1.89

Table B.1. (Cont'd)

Cycle	Load				Stress range							
	range (kips)	max. (kips)	min. (kips)	freq. (hz)	source ^d	fail 1 ^e (ksi)	fail 2 ^f (ksi)	fail 3 ^g (ksi)	fail 4 (ksi)	fail 5 ^h (ksi)	fail 6 ⁱ (ksi)	fail 7 ^j (ksi)
8,814,900	40.53	42.66	2.13	---	T	---	---	3.07	3.71	4.40	5.68	2.36
1st ^a	40.53	42.66	2.13	2.0	D	---	---	---	---	---	---	1.77
1st ^a	40.53	42.66	2.13	---	S	---	---	---	---	---	---	1.81
last ^b	40.53	42.66	2.13	2.0	D	---	---	---	---	---	---	1.89
last ^b	40.53	42.66	2.13	---	S	---	---	---	---	---	---	1.87
9,460,000	20.07	21.13	1.06	---	T	---	---	---	8.81	7.01	8.69	6.93
1st ^a	20.07	21.13	1.06	4.0	D	---	---	---	---	6.41	8.91	5.78
1st ^a	20.07	21.13	1.06	---	S	---	---	---	---	6.49	8.62	6.13
last ^b	20.07	21.13	1.06	4.0	D	---	---	---	---	6.60	9.18	6.31
last ^b	20.07	21.13	1.06	---	S	---	---	---	---	6.17	8.49	5.93
9,487,500	20.07	21.13	1.06	---	T	---	---	---	k	7.01	8.69	6.93
1st ^a	20.07	21.13	1.06	4.0	D	---	---	---	---	6.60	9.18	6.31
1st ^a	20.07	21.13	1.06	---	S	---	---	---	---	5.03	8.80	6.11
last ^b	20.07	21.13	1.06	4.0	D	---	---	---	---	6.60	9.18	6.31
last ^b	20.07	21.13	1.06	---	S	---	---	---	---	---	---	6.08

Table B.1. (Cont'd)

Cycle	Load				Stress range								
	range (kips)	max. (kips)	min. (kips)	freq. (hz)	source ^d	fail 1 ^e (ksi)	fail 2 ^f (ksi)	fail 3 ^g (ksi)	fail 4 (ksi)	fail 5 ^h (ksi)	fail 6 ⁱ (ksi)	fail 7 ^j (ksi)	
9,592,600 only ^c only ^c	20.07	21.13	1.06	---	T	----	---	---	---	---	---	8.69	6.93
	20.07	21.13	1.06	4.0	D	---	---	---	---	---	---	---	6.51
	20.07	21.13	1.06	---	S	---	---	---	---	---	---	---	6.10
9,600,000	End of Testing												
^a Reading taken just after listed cycle number ^b Reading taken just before next cycle number ^c Reading taken just before the testing ended ^d T = Theoretical static, D = Experimental dynamic, S = Experimental static ^e Inside end of new bottom flange cover plate no. 2						^f Original bottom flange splice ^g Outside end of new bottom flange cover plate no. 2 ^h New horizontal web plate attachment no. 2 ⁱ Original diaphragm connection ^j New horizontal web plate attachment no. 1 ^k Chop-saw intersection near cover plate no. 1							

Table B.2. Stress-range data for the long exterior girder specimen no. 2

Cycle	Load				Stress range						
	range (kips)	max. (kips)	min. (kips)	freq. (hz)	source ^d	fail 1 ^e (ksi)	fail 2 ^f (ksi)	fail 3 (ksi)	fail 4 ^g (ksi)	fail 5 ^h (ksi)	fail 6 (ksi)
0	21.98	23.14	1.16	---	T	4.00	3.53	3.19	1.32	2.32	1.89
1st ^a	21.98	23.14	1.16	4.0	D	4.09	3.46	---	1.11	1.86	---
1st ^a	21.98	23.14	1.16	---	S	4.50	3.87	---	0.96	1.92	---
last ^b	21.98	23.14	1.16	4.0	D	4.33	3.62	---	1.15	2.03	---
last ^b	21.98	23.14	1.16	---	S	3.51	3.29	---	1.26	2.67	---
1,064,400	21.98	23.14	1.16	---	T	---	3.53	3.19	1.32	2.32	1.89
1st ^a	21.98	23.14	1.16	4.0	D	---	3.62	---	1.11	1.23	---
1st ^a	21.98	23.14	1.16	---	S	---	3.40	---	1.15	1.22	---
last ^b	21.98	23.14	1.16	4.0	D	---	3.75	---	1.14	1.13	---
last ^b	21.98	23.14	1.16	---	S	---	3.80	---	1.05	1.26	---
1,306,600	17.79	18.73	0.94	---	T	---	---	8.02	6.15	6.25	8.09
1st ^a	17.79	18.73	0.94	4.0	D	---	---	---	5.35	5.33	---
1st ^a	17.79	18.73	0.94	---	S	---	---	---	5.74	5.02	---
last ^b	17.79	18.73	0.94	4.0	D	---	---	---	5.48	5.33	---
last ^b	17.79	18.73	0.94	---	S	---	---	---	5.50	5.13	---

Table B.2. (Cont'd)

Cycle	Load				Stress range						
	range (kips)	max. (kips)	min. (kips)	freq. (hz)	source ^d	fail 1 ^e (ksi)	fail 2 ^f (ksi)	fail 3 (ksi)	fail 4 ^g (ksi)	fail 5 ^h (ksi)	fail 6 (ksi)
1,432,100	40.53	42.66	2.13	---	T	---	---	i	6.15	6.25	8.09
1st ^a	40.53	42.66	2.13	4.0	D	---	---	---	5.54	5.27	---
1st ^a	40.53	42.66	2.13	---	S	---	---	---	5.54	5.27	---
last ^{b,c}	40.53	42.66	2.13	4.0	D	---	---	---	6.19	5.88	---
last ^{b,c}	40.53	42.66	2.13	---	S	---	---	---	5.74	5.10	j
1,491,300	End of Testing										
^a Reading taken just after listed cycle number ^b Reading taken just before next cycle number ^c Reading taken just before the testing ended ^d T = Theoretical static, D = Experimental dynamic, S = Experimental static ^e Original bottom flange plate splice						^f Inside end of new bottom flange cover plate no. 2 ^g New horizontal web plate attachment no. 1 ^h New horizontal web plate attachment no. 2 ⁱ Chop-saw intersection near cover plate no. 2 ^j Chop-saw intersection near cover plate no. 1					

Table B.3. Stress-range data for the long interior girder specimen no. 1

Cycle	Load				Stress Range			
	range (kips)	max. (kips)	min. (kips)	freq. (hz)	source ^d	fail 1 ^e (ksi)	fail 2 ^f (ksi)	fail 3 (ksi)
0	25.23	26.56	1.33	---	T	2.88	3.09	3.60
1st ^a	25.23	26.56	1.33	4.0	D	2.24	2.72	---
1st ^a	25.23	26.56	1.33	---	S	---	---	---
last ^b	25.23	26.56	1.33	4.0	D	5.02	3.42	---
last ^b	25.23	26.56	1.33	---	S	---	---	---
1,995,000	25.23	26.56	1.33	---	T	---	---	3.60
1st ^a	25.23	26.56	1.33	4.0	D	---	---	---
1st ^a	25.23	26.56	1.33	---	S	---	---	---
last ^b	25.23	26.56	1.33	4.0	D	---	---	---
last ^b	25.23	26.56	1.33	---	S	---	---	---
6,439,500	25.23	26.56	1.33	---	T	---	---	g
1st ^a	25.23	26.56	1.33	4.0	D	---	---	---
1st ^a	25.23	26.56	1.33	---	S	---	---	---
last ^b	25.23	26.56	1.33	4.0	D	---	---	---
last ^b	25.23	26.56	1.33	---	S	---	---	---
6,519,100	25.23	26.56	1.33	---	T	---	---	---
1st ^a	25.23	26.56	1.33	3.5	D	---	---	---
1st ^a	25.23	26.56	1.33	---	S	---	---	---
last ^b	25.23	26.56	1.33	3.5	D	---	---	---
last ^b	25.23	26.56	1.33	---	S	---	---	---
7,357,000	25.23	26.56	1.33	---	T	---	---	---
1st ^a	25.23	26.56	1.33	3.0	D	---	---	---
1st ^a	25.23	26.56	1.33	---	S	---	---	---
last ^b	25.23	26.56	1.33	3.0	D	---	---	---
last ^b	25.23	26.56	1.33	---	S	---	---	---

Table B.3. (Cont'd)

Cycle	Load				Stress range			
	range (kips)	max. (kips)	min. (kips)	freq. (hz)	source ^d	fail 1 ^e (ksi)	fail 2 ^f (ksi)	fail 3 (ksi)
8,103,900	28.03	29.51	1.48	---	T	---	---	---
1st ^a	28.03	29.51	1.48	3.0	D	---	---	---
1st ^a	28.03	29.51	1.48	---	S	---	---	---
last ^{b,c}	28.03	29.51	1.48	3.0	D	---	---	---
last ^{b,c}	28.03	29.51	1.48	---	S	---	---	---
8,708,400	End of Testing							
^a Reading taken just after listed cycle number ^b Reading taken just before next cycle number ^c Reading taken just before the testing ended ^d T = Theoretical static, D = Experimental dynamic, S = Experimental static					^e Original diaphragm connection ^f Inside end of new flange cover plate no. 2 ^g Burr defect in steel repair plate bolt hole			

Table B.4. Stress-range data for the long interior girder specimen no. 2

Cycle	Load				Stress range		
	range (kips)	max. (kips)	min. (kips)	freq. (hz)	source ^d	fail 1 ^e (ksi)	fail 2 ^f (ksi)
0	17.61	18.54	0.93	---	T	2.98	3.20
1st ^a	17.61	18.54	0.93	4.0	D	2.74	3.11
1st ^a	17.61	18.54	0.93	---	S	2.81	3.25
last ^b	17.61	18.54	0.93	4.0	D	4.10	3.11
last ^b	17.61	18.54	0.93	---	S	3.06	3.15
1,585,900	17.61	18.54	0.93	---	T	---	3.20
1st ^a	17.61	18.54	0.93	4.0	D	---	3.30
1st ^a	17.61	18.54	0.93	---	S	---	3.28
last ^b	17.61	18.54	0.93	4.0	D	---	3.33
last ^b	17.61	18.54	0.93	---	S	---	3.29
1,600,800	24.77	26.07	1.30	---	T	---	4.50
1st ^a	24.77	26.07	1.30	4.0	D	---	4.59
1st ^a	24.77	26.07	1.30	---	S	---	4.53
last ^b	24.77	26.07	1.30	4.0	D	---	5.98
last ^b	24.77	26.07	1.30	---	S	---	5.82
1,783,700	40.53	42.66	2.13	---	T	---	---
1st ^a	40.53	42.66	2.13	1.0	D	---	---
1st ^a	40.53	42.66	2.13	---	S	---	---
last ^{b,c}	40.53	42.66	2.13	1.0	D	---	---
last ^{b,c}	40.53	42.66	2.13	---	S	---	---
5,096,200	End of Testing						
^a Reading taken just after listed cycle number ^d T = Theoretical static, D = Experimental dynamic, ^b Reading taken just before next cycle number S = Experiment static ^c Reading taken just before the testing ended ^e Inside end of new flange cover plate no. 2 ^f Original diaphragm connection							

Table B.5. Stress-range data for the short exterior girder specimen no. 1

Cycle	Load				Stress range				
	range (kips)	max. (kips)	min. (kips)	freq. (hz)	source ^d	fail 1 ^e (ksi)	fail 2 ^f (ksi)	fail 3 (ksi)	fail 4 (ksi)
0	36.12	38.02	1.90	---	T	4.85	4.85	---	---
1st ^a	36.12	38.02	1.90	3.0	D	3.91	3.90	---	---
1st ^a	36.12	38.02	1.90	---	S	3.91	4.70	---	---
last ^b	36.12	38.02	1.90	3.0	D	4.43	3.76	---	---
last ^b	36.12	38.02	1.90	---	S	4.37	3.29	---	---
583,200	36.12	38.02	1.90	---	T	---	4.85	---	---
1st ^a	36.12	38.02	1.90	3.0	D	---	3.79	---	---
1st ^a	36.12	38.02	1.90	---	S	---	3.84	---	---
last ^b	36.12	38.02	1.90	3.0	D	---	4.00	---	---
last ^b	36.12	38.02	1.90	---	S	---	4.44	---	---
938,800	36.12	38.02	1.90	---	T	---	---	---	---
1st ^a	36.12	38.02	1.90	3.0	D	---	---	---	---
1st ^a	36.12	38.02	1.90	---	S	---	---	---	---
last ^b	36.12	38.02	1.90	3.0	D	---	---	---	---
last ^b	36.12	38.02	1.90	---	S	---	---	---	---
2,020,400	36.12	38.02	1.90	---	T	---	---	g	---
1st ^a	36.12	38.02	1.90	3.0	D	---	---	---	---
1st ^a	36.12	38.02	1.90	---	S	---	---	---	---
last ^b	36.12	38.02	1.90	3.0	D	---	---	---	---
last ^b	36.12	38.02	1.90	---	S	---	---	---	---
2,733,200	End of Testing								
^a Reading taken just after listed cycle number					^e Inside end of new flange cover plate no. 2				
^b Reading taken just before next cycle number					^f Inside end of new east cover plate no. 1				
^c Reading taken just before the testing ended					^{g,h} Burr defect in bolt hole				
^d T = Theoretical static, D = Experimental dynamic, S = Experimental static									

Table B.6. Stress-range data for the short interior girder specimen no. 1

Cycle	Load				Stress range		
	range (kips)	max. (kips)	min. (kips)	freq. (hz)	source ^d	fail 1 ^e (ksi)	fail 2 ^f (ksi)
0	22.07	23.23	1.16	---	T	2.30	2.30
1st ^a	22.07	23.23	1.16	4.0	D	1.52	1.81
1st ^a	22.07	23.23	1.16	---	S	1.11	1.22
last ^b	22.07	23.23	1.16	4.0	D	1.49	1.81
last ^b	22.07	23.23	1.16	---	S	1.26	1.86
405,100	22.07	23.23	1.16	---	T	2.30	2.30
1st ^a	22.07	23.23	1.16	4.5	D	1.51	1.82
1st ^a	22.07	23.23	1.16	---	S	---	---
last ^b	22.07	23.23	1.16	4.5	D	1.45	1.82
last ^b	22.07	23.23	1.16	---	S	---	---
820,000	22.07	23.23	1.16	---	T	2.30	2.30
1st ^a	22.07	23.23	1.16	5.0	D	1.52	1.81
1st ^a	22.07	23.23	1.16	---	S	---	---
last ^b	22.07	23.23	1.16	5.0	D	1.36	1.81
last ^b	22.07	23.23	1.16	---	S	---	---
11,000,000	25.91	27.27	1.36	---	T	2.70	2.70
1st ^a	25.91	27.27	1.36	3.5	D	1.32	2.12
1st ^a	25.91	27.27	1.36	---	S	2.29	2.48
last ^b	25.91	27.27	1.36	3.5	D	1.36	2.93
last ^b	25.91	27.27	1.36	---	S	2.29	2.48
11,294,000	25.91	27.27	1.36	---	T	2.70	2.70
1st ^a	25.91	27.27	1.36	4.5	D	1.25	2.15
1st ^a	25.91	27.27	1.36	---	S	---	---
last ^b	25.91	27.27	1.36	4.5	D	---	2.93
last ^b	25.91	27.27	1.36	---	S	---	---
11,850,900	25.91	27.27	1.36	---	T	---	2.70
1st ^a	25.91	27.27	1.36	4.5	D	---	2.25
1st ^a	25.91	27.27	1.36	---	S	---	2.18
last ^b	25.91	27.27	1.36	4.5	D	---	2.15
last ^b	25.91	27.27	1.36	---	S	---	2.09

Table B.6. (Cont'd)

Cycle	Load				Stress range		
	range (kips)	max. (kips)	min. (kips)	freq. (hz)	source ^d	fail 1 ^e (ksi)	fail 2 ^f (ksi)
14,385,200	25.91	27.27	1.36	---	T	---	2.70
1st ^a	25.91	27.27	1.36	5.0	D	---	2.17
1st ^a	25.91	27.27	1.36	---	S	---	---
last ^b	25.91	27.27	1.36	5.0	D	---	2.18
last ^b	25.91	27.27	1.36	---	S	---	---
16,021,700	47.97	50.50	2.53	---	T	---	5.00
1st ^a	47.97	50.50	2.53	2.8	D	---	4.05
1st ^a	47.97	50.50	2.53	---	S	---	4.45
last ^b	47.97	50.50	2.53	2.8	D	---	4.32
last ^b	47.97	50.50	2.53	---	S	---	---
16,197,600	47.97	50.50	2.53	---	T	---	5.00
1st ^a	47.97	50.50	2.53	2.5	D	---	4.89
1st ^a	47.97	50.50	2.53	---	S	---	---
last ^b	47.97	50.50	2.53	2.5	D	---	---
last ^b	47.97	50.50	2.53	---	S	---	---
16,467,600	End of Testing						
^a Reading taken just after listed cycle number				^d T = Theoretical static, D = Experimental dynamic			
^b Reading taken just before next cycle number				S = Experimental static			
^c Reading taken just before the testing ended				^e Inside end of new bottom flange cover plate no. 2			
				^f Inside end of new bottom flange cover plate no. 1			

Table B.7. Stress-range data for the short interior girder specimen no. 2

Cycle	Load				Stress range	
	range (kips)	max. (kips)	min. (kips)	freq. (hz)	source ^d	fail l ^e (ksi)
0	27.19	28.55	1.36	---	T	2.80
1st ^a	27.19	28.55	1.36	4.5	D	2.22
1st ^a	27.19	28.55	1.36	---	S	2.20
last ^b	27.19	28.55	1.36	4.5	D	1.23
last ^b	27.19	28.55	1.36	---	S	2.17
773,400	27.19	28.55	1.36	---	T	2.80
1st ^a	27.19	28.55	1.36	4.4	D	2.27
1st ^a	27.19	28.55	1.36	---	S	2.33
last ^b	27.19	28.55	1.36	4.4	D	2.28
last ^b	27.19	28.55	1.36	---	S	2.33
985,800	27.19	28.55	1.36	---	T	2.80
1st ^a	27.19	28.55	1.36	4.4	D	2.31
1st ^a	27.19	28.55	1.36	---	S	2.44
last ^b	27.19	28.55	1.36	4.4	D	2.84
last ^b	27.19	28.55	1.36	---	S	2.57
9,615,900	27.19	28.55	1.36	---	T	---
1st ^a	27.19	28.55	1.36	4.0	D	---
1st ^a	27.19	28.55	1.36	---	S	---
last ^b	27.19	28.55	1.36	4.0	D	---
last ^b	27.19	28.55	1.36	---	S	---
10,545,100	29.76	31.30	1.54	---	T	---
1st ^a	29.76	31.30	1.54	4.0	D	---
1st ^a	29.76	31.30	1.54	---	S	---
last ^b	29.76	31.30	1.54	4.0	D	---
last ^b	29.76	31.30	1.54	---	S	---
13,597,500	29.76	31.30	1.54	---	T	---
1st ^a	29.76	31.30	1.54	3.0	D	---
1st ^a	29.76	31.30	1.54	---	S	---
last ^b	29.76	31.30	1.54	3.0	D	---
last ^b	29.76	31.30	1.54	---	S	---

14,002,000

End of Testing

^aReading taken just after listed cycle number^dT = Theoretical static, D = Experimental dynamic,^bReading taken just before next cycle number

S = Experimental static

^cReading taken just before the testing ended^eInside end of new bottom flange cover plate no. 1